



Universitetet
i Stavanger

FACULTY OF SCIENCE AND TECHNOLOGY

MASTER'S THESIS

Study programme/specialisation: PETROLEUM TECHNOLOGY	Spring, 2017 Open/ Confidential
Author: HENRIK GRIMSMO BUSENGDAL (signature of author)
Programme coordinator: Supervisor(s): JORUNN HAMRE VRÅLSTAD, JOSTEIN DJUVE, MARTIN FOSSEN*, IVAR ESKERUD SMITH* *SINTEF PETROLEUM AS	
Title of master's thesis: PREDICTION OF DISPERSIONS AND EMULSIONS BY USING LEDAFLOW Q3D	
Credits:	
Keywords: LEDAFLOW Q3D MULTIPHASE FLOW EMULSIONS DISPERSIONS	Number of pages: 139 + supplemental material/other: 12 Stavanger, 15.06.2017 date/year

Acknowledgements

This master thesis, written within the field of petroleum technology, is a culmination of the work to obtain my Master of Science for the Department of Petroleum Engineering at the University of Stavanger. The work has combined the fields of petroleum engineering and computer technology, and I wholeheartedly enjoyed the challenge of examining this topic, given from SINTEF Petroleum.

I would like to extend my gratitude to all of my supervisors. I would first like to recognize Dr. Jorunn Hamre Vrålstad and Dr. Jostein Djuve, my academic supervisors at the University of Stavanger, for their constructive feedback, inspiring comments, patience and editing skills in the completion of this thesis. My sincere gratitude is extended to scientist Martin Fossen and scientist Ivar Eskerud Smith, my academic supervisors at SINTEF Petroleum, for their guidance, background knowledge, and assistance whenever I needed it. I especially appreciate scientist Eskerud Smith's help regarding the solution of the stability problem in LedaFlow Q3D, and by writing helpful Matlab-codes used in the analysing process of the simulation work. Gratitude is also extended to SINTEF scientist Heiner Schümann, for his help in the initial phase of the process, with problem specific knowledge and solutions.

A special thanks also goes to my friends in Trondheim, for opening their home to me and letting me stay at their place, during the weeks I visited SINTEF Petroleum. These visits were of highly importance for the outcome of this thesis, and they would probably not be possible if it had not been for you.

Finally, special recognition goes out to my family, friends, and fellow students, for their encouragement and support during these five years at the University of Stavanger.

"This thesis got my back up against the ropes, and gave me some powerful knock downs, but every time I got up again. I was saved by the bell a couple of times, but I also had good coaching from my ring corner. Eventually I survived the fight, and the result is up to the judges to decide."

Abstract

Topic

Well streams in pipelines are often transported over relatively long distances. The well streams often consist of simultaneous flow of gas, oil and water. Oil and water affect each other by making emulsions, which influence on the fluid properties of the fluid mixture, and further has an impact on flow properties like pressure loss, water holdup and flow regimes. Accurate knowledge of the flow behaviour in a pipeline is crucial to design and optimize production, transportation and processing facilities. The correct design of a pipeline can result in extended lifetime for the oil field, higher economic profitability and optimized production rate.

To extend the knowledge of the well fluids behaviour, there are several experimental techniques available. One is the conventional flow loops, at SINTEF Petroleum laboratories at Tiller, Trondheim. They are accurate testing devices. However, the problem with these flow loops are that they can only test the fluid behaviour inside a pipeline of a certain length. For this reason, SINTEF Petroleum also use the wheel flow simulator, which is a rotating wheel, where the fluids inside “see” an endless pipe through which they flow as a multiphase mixture.

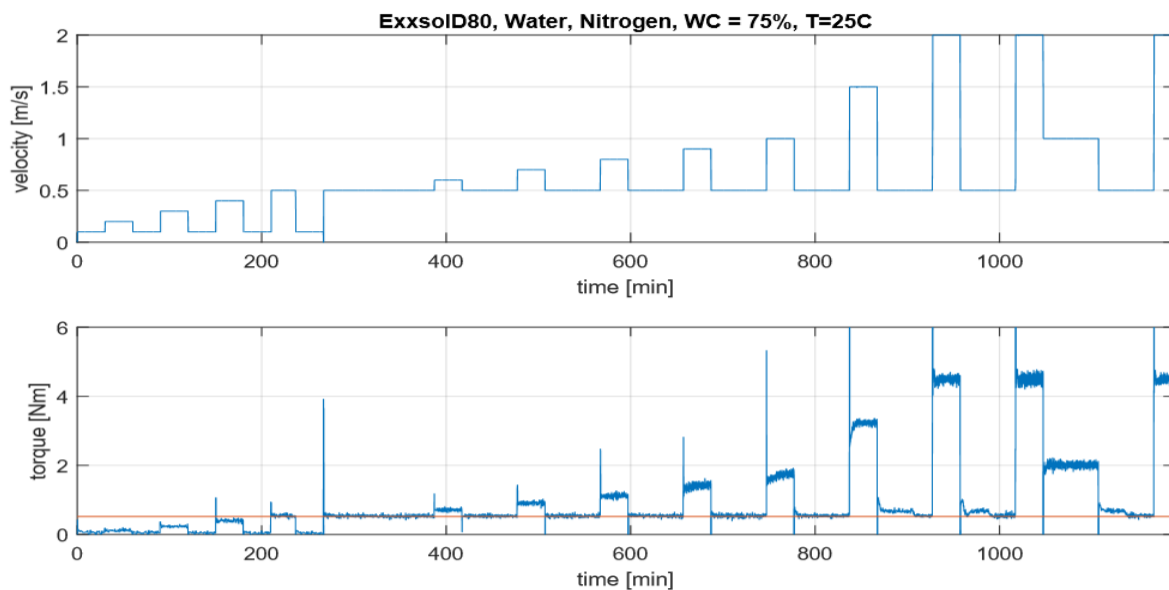
Computer programs simulating the fluid flow, is also an available experimental method to consider. LedaFlow Q3D is a computer program developed by SINTEF, for the purpose to simulate the multiphase fluid mixture in more detail. A special version of LedaFlow Q3D is also available, specially designed to simulate the wheel flow.

Research questions

The research questions are based on how the input parameters in LedaFlow Q3D affect the simulation results. Will it be possible to tune specific simulations to match the results (output of torque) produced from experiments with the wheel flow simulator? Will it be possible to create a blueprint of which input parameters to use for various systems in future simulation work, to match the simulation results with the results produced from experiments with the wheel flow simulator?

Analysis

The simulation work in LedaFlow Q3D will be based on the fluid system from one particular wheel flow experiment, conducted by SINTEF at Tiller, in Trondheim. The fluid system contains 60 % nitrogen, 30 % water (tap water), and 10 % oil (Exxsol D80) by volumes. The initial temperature and pressure was 25 °C and 1 bar. The tested profile of the wheel experiment was a stepwise velocity scan from 0.1 m/s to 2 m/s. However, when simulating in LedaFlow in this thesis, the focus will be on a wheel velocity of 2 m/s, which gave an output of torque equal to approximately 4.5 Nm.



Results

Multiple simulations have been conducted, by systematically adjusting several input parameters. The effect of the input parameters on the simulation results has been investigated, and the acquired knowledge have been used in attempts to tune the simulation cases to match the results produced from experiments with the wheel flow simulator. Some of the simulations was successfully tuned to match with the results from the wheel flow experiment (torque = 4.5 Nm), for a wheel velocity of 2 m/s. However, by using the same input parameters to tune simulations with a wheel velocity of 1 m/s, the simulations failed to match with the results from the wheel flow experiment. These results indicate that it is difficult to create a blueprint for the input parameters. Although some input parameters successfully manage to tune specific simulations to match with the wheel flow experiment, they may not work for various velocities or systems.

Contents

Acknowledgements	2
Abstract	3
Contents	5
List of figures	7
List of tables	10
Abbreviations	11
1 Introduction	12
2 Emulsions	14
2.1 Petroleum emulsions	14
2.2 Types of emulsions	16
2.3 Formation of emulsions	19
2.4 Emulsifying agents	20
2.5 Characteristics and physical properties	25
2.6 The Krieger-Dougherty equation.....	29
2.7 Properties of interfaces	31
2.8 Stability of emulsions.....	33
2.9 Inversion.....	36
2.10 Demulsification.....	39
3 Multiphase flow	41
3.1 Basics about multiphase flow	41
3.2 Flow regimes	42
3.2.1 Flow regimes of liquid-liquid flows.....	42
3.2.2 Flow regimes of gas-liquid flows	45
3.3 Gas-liquid vs. liquid-liquid flows.....	46
3.4 Prediction of multiphase flow behavior	47
3.5 Prediction of oil-water flow characteristics.....	48
3.5.1 Pressure drop.....	48
3.5.2 Water holdup.....	50
3.5.3 Flow pattern identification.....	52
3.5.4 Correlation with the experiment and analysis in this master thesis.....	54
4 CFD modelling	55
4.1 Description of CFD modelling.....	55
4.2 The LedaFlow tool.....	58
4.2.1 Historical background.....	58
4.2.2 Modelling capabilities	58
5 Simulation of the wheel flow simulator in LedaFlow Q3D	61
5.1 Description of the rotating flow wheel simulator	61
5.2 Description of the simulation work in LedaFlow Q3D	64
5.3 Settings in closures Q3D	68
6 Improvement of the LedaFlow Q3D model	80
6.1 Solving the stability problem	80
6.2 Additional problems that was solved.....	84

7 Results and analysis of simulations	85
7.1 Break Up Time Constant and Coalescence Time constant.....	89
7.2 Particle Size Constants, C_1 and C_2	110
7.3 Constant Particle Size, with DPS model turned ON	123
7.4 Constant Particle Size, with DPS model turned OFF	126
7.5 Comparison of various water cuts	129
7.6 Tuning simulation cases with wheel velocity of 1 m/s.....	131
8 Suggestions for future work	133
9 Summary and conclusion	134
10 Bibliography	137
11 Appendix	140
A. Set up guide.....	140
<i>A.1 Creating the case.....</i>	<i>140</i>
<i>A.2 Edit case settings.....</i>	<i>142</i>
<i>A.3 Initializing the case.....</i>	<i>146</i>
B. Run and plot guide.....	149
<i>B.1 Running the case.....</i>	<i>149</i>
<i>B.2 Plotting and visualizing the results.....</i>	<i>150</i>

List of figures

Chapter 2

Figure 2.1: Different kinds of emulsions.....	16
Figure 2.2: Types of emulsions.....	16
Figure 2.3: Water-in-oil emulsion	17
Figure 2.4: Oil-in-water emulsion	18
Figure 2.5: Mechanism of emulsion stabilization	20
Figure 2.6: Surfactants and micelles in an O/W solution	22
Figure 2.7: The association of surfactants in solution, showing the CMC.....	23
Figure 2.8: The solubility-micellization behaviour of surfactants in solution.....	24
Figure 2.9: Surfactant classification	25
Figure 2.10: Droplet size distribution	26
Figure 2.11: Rheology curves.....	27
Figure 2.12: The effect of shear rate and water cut on viscosity of emulsions at 52 °C	28
Figure 2.13: Temperature effect on viscosity (shear rate of 0.1 [1/s]).....	29
Figure 2.14: The relative viscosity of the dispersion as a function of the oil volume fraction.....	30
Figure 2.15: Droplet radius, total area, and total interfacial energy.....	32
Figure 2.16: How to use diagram to find total interfacial energy.....	33
Figure 2.17: Creaming, aggregation, and coalescence in an O/W emulsion	35
Figure 2.18: Effect of brine and pH on emulsion stability.....	36
Figure 2.19: Phase inversion, water fraction vs. viscosity.....	37
Figure 2.20: Examples of the shear-induced inversion of an emulsion.....	38
Figure 2.21: The effect of different repulsive and attractive forces (1 and 2).....	39

Chapter 3

Figure 3.1: Large-scale interface between layers of continuous fluids.....	41
Figure 3.2: Liquid-liquid flow patterns	42
Figure 3.3: Slug/plug flow	43
Figure 3.4: A combination of several flow regimes	44
Figure 3.5: Gas-liquid flow pattern in vertical flow	45
Figure 3.6: Gas-liquid flow pattern in horizontal flow	46
Figure 3.7: Pressure drop vs. flow rate at various water fractions.....	49
Figure 3.8: Water holdup vs. flow rate at various oil fractions.....	50
Figure 3.9: Pressure drop per unit length against oil hold up (heavy oil-water flow)	51
Figure 3.10: Pressure drop per unit length against oil hold up (light oil-water flow)	52
Figure 3.11: Flow pattern comparison of heavy and light oil-water flows	53

Chapter 4

Figure 4.1: The 3-phase system, with 9 associated fields.....	59
Figure 4.2: A quasi-3D mesh for the pipe geometry.....	60

Chapter 5

Figure 5.1: Schematic figure of the wheel flow simulator	61
Figure 5.2: SINTEF wheel flow simulators	62

Figure 5.3: Velocity and torque versus time for the wheel experiment.....	63
Figure 5.4: Colour codes for phase fractions between zero and one	64
Figure 5.5: Initial boundary conditions, and fluid mixing.....	65
Figure 5.6: Coordinate system of the flow wheel.....	66
Figure 5.7: Particle size calculation enabled.....	69
Figure 5.8: Particle size: Variable particle size flag.....	72
Figure 5.9: Emulsion: flag	73
Figure 5.10: Particle size: Constant size	74
Figure 5.11: Particle break up- and coalescence time constants.....	77
Figure 5.12: Default values for the C_1 (left) and C_2 (right) constants	79

Chapter 7

Figure 7.1: Flowchart of test 1 - 4.....	87
Figure 7.2: Flowchart of test 5 - 8.....	88
Figure 7.3: Flowchart of how to influence the value of $t_{rel,km}$	91
Figure 7.4: " t_{kol}/t_{rel} vs. position" for simulation 1.1, 1.9 and 1.10	96
Figure 7.5: " t_{kol}/t_{rel} vs. position" for simulation 2.3 and 2.4.....	97
Figure 7.6: Break up time constant – Torque vs. Time, simulation 1.1 – 1.10	98
Figure 7.7: Break up time constant – Torque vs. Time, simulation 1.11 – 1.13.....	99
Figure 7.8: Break up time constant – Particle size vs. Position.....	100
Figure 7.9: Break up time constant – Viscosity vs. Position	102
Figure 7.10: Coalescence time constant – Torque vs. Time	103
Figure 7.11: " t_{kol}/t_{rel} vs. position" for simulation 2.5 and 2.6.....	104
Figure 7.12: Coalescence time constant – Particle size vs. Position.....	105
Figure 7.13: Coalescence time constant – Viscosity vs. Position	106
Figure 7.14: Particle size constant, C_1 – Torque vs. Time	112
Figure 7.15: Particle size constant, C_1 – Particle size vs. Position (decreasing C_1)	113
Figure 7.16: Particle size constant, C_1 – Particle size vs. Position (increasing C_1)	114
Figure 7.17: Particle size constant, C_1 – Viscosity vs. Position (decreasing C_1).....	115
Figure 7.18: Particle size constant, C_1 – Viscosity vs. Position (increasing C_1).....	116
Figure 7.19: Particle size constant, C_2 – Torque vs. Time	117
Figure 7.20: Particle size constant, C_2 – Particle size vs. Position (decreasing C_2)	118
Figure 7.21: Particle size constant, C_2 – Particle size vs. Position (increasing C_2)	119
Figure 7.22: Particle size constant, C_2 – Viscosity vs. Position (decreasing C_2).....	120
Figure 7.23: Particle size constant, C_2 – Viscosity vs. Position (increasing C_2).....	121
Figure 7.24: Constant particle size (field 4 and 6), DPS model turned ON – Torque vs. Time	124
Figure 7.25: "Particle size vs. Position" & "Viscosity vs. Position," DPS model ON	125
Figure 7.26: Constant particle size (field 4 and 6), DPS model turned OFF – Torque vs. Time ...	127
Figure 7.27: "Particle size vs. Position" & "Viscosity vs. Position," DPS model OFF	128
Figure 7.28: Comparison of water cuts – Torque vs. Time.....	129
Figure 7.29: "Particle size vs. Position" & "Viscosity vs. Position," comparing water cuts	130
Figure 7.30: Final test – Torque vs. Time.....	132

Chapter 9

Figure 9.1: Summary of test 1 - 4.....	135
Figure 9.2: Summary of test 5 - 8.....	136

Appendix

Figure A.1: Overview of overall work window, and “add new case” option menu.....	140
Figure A.2: Wheel case set up helper	141
Figure A.3: Case browser	142
Figure A.4: Case settings menu.....	144
Figure A.5: Numerical Parameters Q3D.....	145
Figure A.6: Closures Q3D	146
Figure A.7: Initialization menu	147
Figure A.8: Patches menu.....	148
Figure A.9: Initializing the case	148
Figure B.1: Status window and simulation running progress	149
Figure B.2: Output information of warnings and errors during simulation run.....	149
Figure B.3: 3D visualization of the mixing of the fluid phases	150
Figure B.4: Visualization options, and selection of which fluid phase to focus on.....	150
Figure B.5: Graph Setup.....	151

List of tables

Chapter 2

Table 2.1: Examples of emulsions in the Petroleum industry.....	15
Table 2.2: Typical CMC values	23

Chapter 3

Table 3.1: Gas-liquid vs liquid-liquid flows.	47
--	----

Chapter 5

Table 5.1: Fluid properties of the wheel experiment	64
Table 5.2: Constant settings in Closures Q3D	69

Chapter 7

Table 7.1: Settings in closures Q3D.....	85
Table 7.2: Standard input parameters for all simulations.....	86
Table 7.3: Input values for "break up time constant."	92
Table 7.4: Input values for "coalescence time constant."	93
Table 7.5: Input values for "particle size constant, C ₁ ."	111
Table 7.6: Input values for "particle size constant, C ₂ ."	111
Table 7.7: Input values for "constant particle size" - DPS model "on."	124
Table 7.8: Input values for "constant particle size" - DPS model "off."	126
Table 7.9: Phase fractions for simulation 1.1 and simulation 7.1.....	129
Table 7.10: Final test, with wheel velocity 1 m/s.....	131

Appendix

Table A.1: PVT settings.....	143
Table A.2: Numerical input settings	144
Table A.3: Input parameters to initialize the case	147

Abbreviations

EOR	Enhanced oil recovery
CFD	Computational fluid dynamics
1D	One-dimensional
3D	Three-dimensional
Q3D	Quasi three dimensional
CMC	Critical micelle concentration
DLVO theory	Derjaguin, Landau, Verwey and Overbeck theory.
CAC	Critical aggregation concentration
PIP	Phase Inversion Point
O/W	Oil-in-water emulsion
W/O	Water-in-oil emulsion
O/W/O	Oil-in-water-in-oil emulsion (multiple or complex emulsion)
W/O/W	Water-in-oil-in-water emulsion (multiple or complex emulsion)
G/W	Gas-in-water dispersion
G/O	Gas-in-oil dispersion
W/G	Water-in-gas dispersion
O/G	Oil-in-gas dispersion
LSI	Large scale interface
H_w	Water holdup
V_{sw}	Superficial water velocity
V_{so}	Superficial oil velocity
CAE	Computer aided engineering
CAD	Computer aided design
GUI	Graphical user interface
R&D	Research and development
LDHI	Low-dosage hydrate inhibitors
PVT	Pressure volume temperature
CFL	Courant-Friedrichs-Lewy
DPS	Dynamic particle size
FOU scheme	First order upwind scheme

1 Introduction

The simultaneous flow of gas, oil and water in pipelines is a common occurrence in the petroleum industry, and can cause significant flow assurance problems during production. Increased offshore oil and gas exploration and production have resulted in transportation of well fluids in pipelines over relatively long distances. Often, the fluid from the well contains water, which is already present within the reservoir, or injected during enhanced oil recovery operations (EOR). Water fraction often increase during the producing life of a well [1][2].

Accurate knowledge of behaviour of oil and water flow in a pipeline is crucial to design/optimization of production, transportation, and processing facilities. Oil and water affect each other by making emulsions, which influence on the fluid properties of the fluid mixture, and further has an impact on flow properties like pressure loss, water holdup, and flow regimes. Chapter 2 will explain some properties of emulsions, and Chapter 3 will present information about the multiphase flow together with the flow properties just mentioned.

The correct design of a pipeline can result in an extended lifetime for the oil field, higher economic profitability, and optimized production rate. When the design and production of the fields infrastructure with associated pipelines is completed, it is not only complicated, but also expensive to change the construction. Research in this field has been taking place for decades, and it is still necessary to improve production techniques and make things cheaper. Many researchers have attempted to generalize the liquid-liquid or two phase flow system through mechanical models and developed means for predicting the flow patterns, pressure drop, and water holdups. At Tiller, in Trondheim, SINTEF Petroleum has several kinds of flow loops, and a wheel flow simulator (explained in chapter 5), available to perform experiments on two-phase and three-phase flow mixtures. The last 15 years, SINTEF have also been working on the development of LedaFlow, which can be used to model multiphase flow systems on computers.

There are two methods available to model the multiphase flow. For a straight pipe with constant mass flow rate, it is possible to assume steady-state, solve a momentum balance, and then find pressure loss and phase holdups. The other option is to perform a dynamic simulation, as in this thesis.

There are many available computational fluid dynamics (CFD) codes, that can provide an accurate prediction of the well stream using a three-dimensional grid. Nevertheless, it could take many years to simulate a 50-mile long pipeline with these tools, which is impractical and inconvenient. Therefore, the petroleum industry use one dimensional (1D) models instead, like the Leda 1D model. Leda Q3D, the code used in this thesis, is something in between a CFD code and the Leda 1D code. It is unpractical to simulate the entire pipeline with Leda Q3D, for the same reason as with a CFD code. It is time consuming to produce the simulation results. Nevertheless, the Leda Q3D code is useful when trying to get detailed information about phenomena that one tries to simulate with the 1D code. This knowledge can possibly be used in further work, by improving the 1D models, e.g. by answering how fast emulsions are made under certain conditions, how stable these emulsions are, how the viscosity evolves, or how important droplet size distribution in emulsions are for the results of the simulations. More information about CFD codes, and LedaFlow will be presented in chapter 4 and chapter 5.

The work in this thesis will include several simulations using LedaFlow Q3D. By systematically changing the input parameters in the simulations, the aim is to better understand how these input parameters affect the simulation results. Hopefully this knowledge will make it possible to tune specific simulations in LedaFlow Q3D to be more or less identical with the results produced from the wheel flow simulator, and to better understand which physical processes that are important in the formation of emulsions. This will make it possible to use the results from LedaFlow Q3D as input values, or as additional information, in the one dimensional models.

2 Emulsions

2.1 Petroleum emulsions

By mixing two immiscible fluids in a container, then shaking the container, examination will reveal that one of the two phases has become a collection of droplets dispersed in the other phase. A colloidal system or colloidal dispersion has been created, which is a heterogeneous system that is made up of a dispersed phase and a continuous phase. The dispersed phase is often referred to as the internal phase, and the continuous phase as the external phase. I.e. in case of dust, the solid particles are the dispersed phase, and the air is the continuous phase [3][4].

Emulsions are a special kind of colloidal dispersion. One in which a liquid is dispersed in a continuous liquid phase, and the dispersion is stabilised due to surfactants, solid particles or other mechanisms, often referred to as emulsifying agents. Petroleum emulsions of any significant stability contain oil, water, and at least one emulsifying agent. The amount of water that emulsifies with crude oil varies widely from field to field. It can be less than 1 % and sometimes larger than 80 % [4][5].

Emulsions occur in almost all phases of oil production and processing, i.e. inside reservoirs, wellbores, wellheads, wet crude handling facilities, gas/oil separation plants, and during transportation through pipelines, crude storage, and processing [5].

As shown in table 2.1, some petroleum emulsions may be desirable and others may not. The water that is co-produced together with the crude oil creates several problems, and usually increases the unit cost of the oil production. The produced water must be separated from the oil, treated, and disposed off properly. All these steps increase costs. Emulsions can be difficult to treat and may cause several operational problems in crude handling facilities and gas/oil separating plants [5].

Occurrence	Usual type of emulsion
UNDESIRABLE EMULSIONS	
Well-head emulsions	W/O
Fuel oil emulsions (marine)	W/O
Oil sand flotation process, froth	W/O or O/W
Oil sand flotation process, diluted froth	O/W/O
Oil spill mousse emulsions	W/O
Tanker bilge emulsions	O/W
DESIRABLE EMULSIONS	
Heavy oil pipeline emulsion	O/W
Oil sand flotation process, slurry	O/W
Emulsion drilling fluid, oil-emulsion mud	O/W
Emulsion drilling fluid, oil-base mud	W/O
Asphalt emulsion	O/W
Enhanced oil recovery in situ emulsions	O/W

Table 2.1: Examples of emulsions in the Petroleum industry [4].

Although, petroleum emulsions might be desirable in some situations. Oil based drilling fluid is an example of a desirable petroleum emulsion. Here a stable emulsion (usually oil dispersed in water) lubricate the drill bit and carry cuttings up to the surface. Other emulsions are made to reduce viscosity to increase the ability to flow. Emulsions of asphalt are both less viscous than the original asphalt and stable so that they can be transported and handled. Another example of emulsions that are made for lower viscosity with good stability are those made from heavy oils. They are intended for economic pipeline transportation over long distances. In these emulsions, the heavy oil is dispersed as droplets in the continuous water phase, which means that mostly water is in contact with the pipe wall, resulting in less friction and pressure drop [4].

2.2 Types of emulsions

Produced oilfield emulsions can be classified into three broad groups:

- Oil-in-water (O/W).
- Water-in-oil (W/O).
- Multiple or complex emulsions (O/W/O or W/O/W) [10].

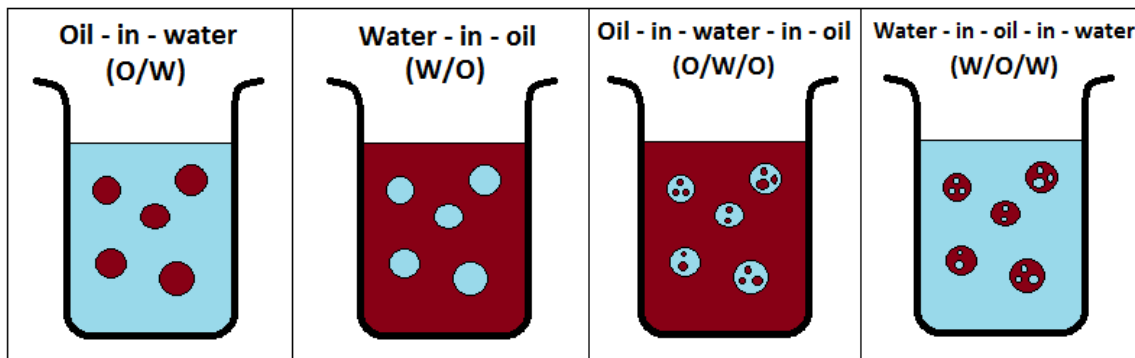


Figure 2.1: Different kinds of emulsions.

W/O emulsions consist of water droplets dispersed in a continuous oil phase, and O/W emulsions consist of oil droplets dispersed in a continuous water phase. In the oil industry, W/O emulsions are more common, therefore, the O/W emulsions are sometimes referred to as “reverse” emulsions. Multiple emulsions are more complex and consist of tiny droplets suspended in bigger droplets that are suspended in a continuous phase. Figure 2.1 and figure 2.2 illustrates the different kinds of emulsions. From left to right, in both figures, there is examples of O/W emulsion, W/O emulsion, and then examples of multiple- or complex emulsions. The multiple emulsion, illustrated in figure 2.2, is an W/O/W emulsion. The droplet sizes in figure 2.1 have been greatly exaggerated for illustration purposes [5].

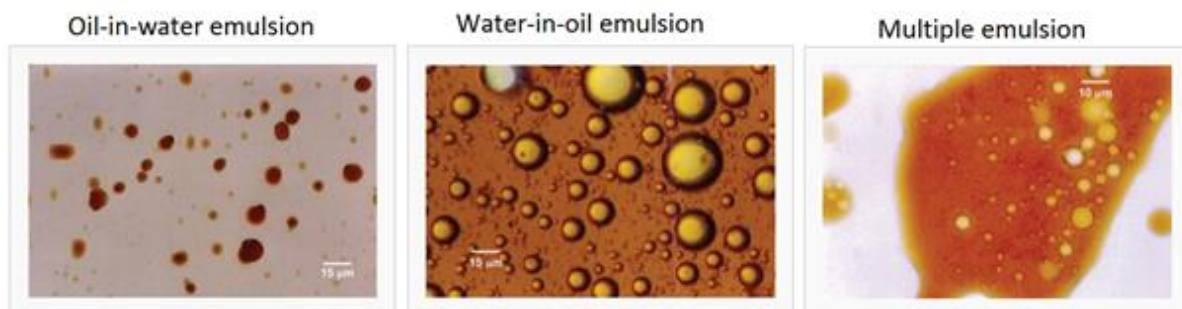


Figure 2.2: Types of emulsions [5].

Given the oil and water phases, the type of emulsion formed depends on several factors. As a rule of thumb, when the volume fraction of one phase is very small compared with the other, the phase that has the smaller fraction is the dispersed phase and the other is the continuous phase. When the volume-phase ratio is close to one (a 50:50 ratio), then other factors determine the type of emulsion formed [5].

Bancroft's rule states that "the liquid in which the emulsifying agent is most soluble becomes the continuous phase." The theory is based on the belief that if an emulsifying agent is preferentially wetted by one of the phases, then more of the agent can be accommodated at the interface if the interface is convex towards that phase, i.e. if that phase is the continuous phase [4].

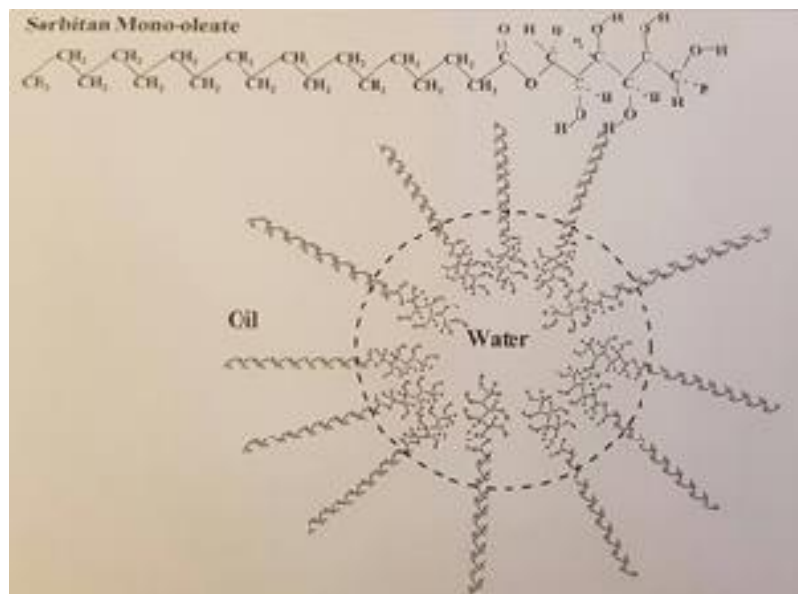


Figure 2.3: Water-in-oil emulsion [6].

W/O and O/W emulsions represent symmetrically inverted images of the interface. Emulsifying agents (surfactant molecules) with strong polar group interaction tend to form W/O emulsions, whereas molecules with weaker polar group interactions tend to form O/W emulsions. More detailed explanation of emulsifying agents and surfactant-chemistry will be presented later in this chapter. Figure 2.3 and figure 2.4 shows examples of W/O and O/W mixtures [6].

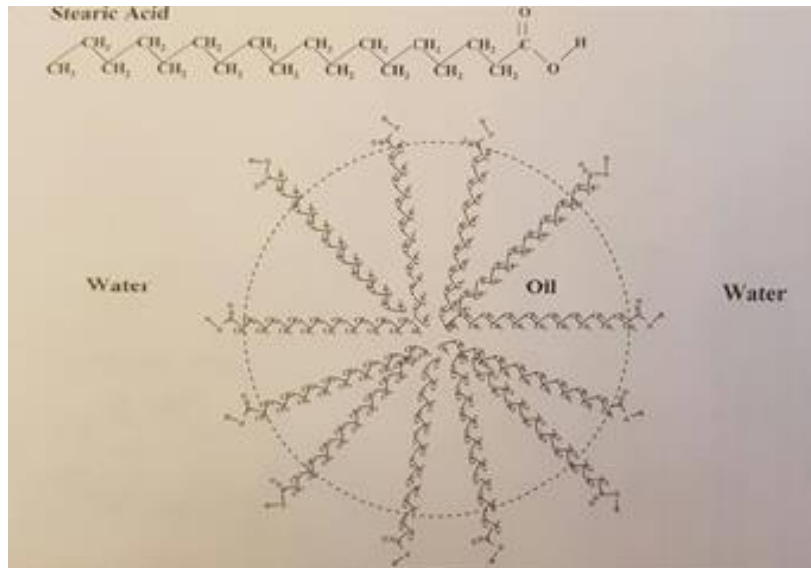


Figure 2.4: Oil-in-water emulsion [6].

Since Graham invented the term “colloid” in 1861, one has distinguished between two very different types of colloidal dispersions. They can be subdivided into lyophobic and lyophilic colloids (if the dispersion medium is aqueous then the terms hydrophobic and hydrophilic, respectively, are used). Lyophilic colloids form spontaneously when two phases are brought together, because the dispersion is thermodynamically more stable than the original separated state. Lyophobic colloids, which include all petroleum emulsions other than microemulsions, are not formed spontaneously when the phases are brought together, because they are unstable compared with the separated states. However, these dispersions can be created by other means, and need emulsifying agents to form a stable emulsion [4].

Emulsions are also classified by the size of the droplets in the continuous phase. Dispersed droplets smaller than 100 nm are referred to as microemulsions, and dispersed droplets larger than 100 nm are referred to as macroemulsions. Most petroleum emulsions are macroemulsions. Emulsions of this kind are normally thermodynamically unstable, i.e. the two phases will separate over time because of a tendency for the emulsion to reduce its interfacial energy by coalescence and separation. However, droplet coalescence can be reduced or even eliminated through several stabilization mechanisms [5][7].

Interfacial tension, interfacial energy, and stabilizing mechanisms will be further explained later in this chapter.

In contrast to the macroemulsions, the microemulsions form spontaneously when two immiscible phases are brought together because of their extremely low interfacial energy. Droplets of this size scatter little light, and the emulsion appear to be transparent. These microemulsions are considered thermodynamically stable, and do not break on centrifuging [4][5].

2.3 Formation of emulsions

The amount of mixing and the presence of emulsifier are critical for the formation of an emulsion. Petroleum emulsions form when oil and water come into contact with each other, when there is sufficient mixing, and when an emulsifying agent or emulsifier is present. During crude oil production, there are several sources of mixing, including [5]:

- Flow through reservoir rock.
- Flow through tubing, flow lines and production headers.
- Flow through valves, fittings and chokes.
- Flow through surface equipment.

In general, the greater the mixing, the smaller the droplets dispersed in the continuous phase, and consequently a tighter emulsion [5].

The second factor important in emulsion formation is the presence of an emulsifier. The presence, amount and nature of the emulsifier determines, to a large extent, the type and “tightness” of an emulsion. Crude oils contain natural emulsifiers. Nevertheless, there are different types of crudes with different amounts of natural emulsifiers. The emulsifying tendencies vary widely. Crude with a small amount of emulsifier forms a less stable emulsion and separates relative easily. Other crudes contain the right type and amount of emulsifier, which lead to a very stable or tight emulsion [5].

2.4 Emulsifying agents

As already mentioned, produced oilfield emulsions contain oil, water and an emulsifying agent. Emulsifiers stabilize emulsions and include surface active agents and finely divided solids [5].

Surfactants and solid particles

Surface active agents (surfactants) are compounds that are partly soluble in both water and oil. They have a hydrophobic part that has an affinity for oil and a hydrophilic part that has an affinity for water. The energetically most favourable orientation for these molecules is at the oil/water interphase, where they form interfacial films, so that each part of the molecule can reside in the solvent for which it has the greatest affinity. The interfacial films often provide the stabilizing influence in emulsions because they can both lower interfacial tension and increase the interfacial viscosity. Figure 2.5 illustrates an example of the mechanism of emulsion stabilization [4][5].

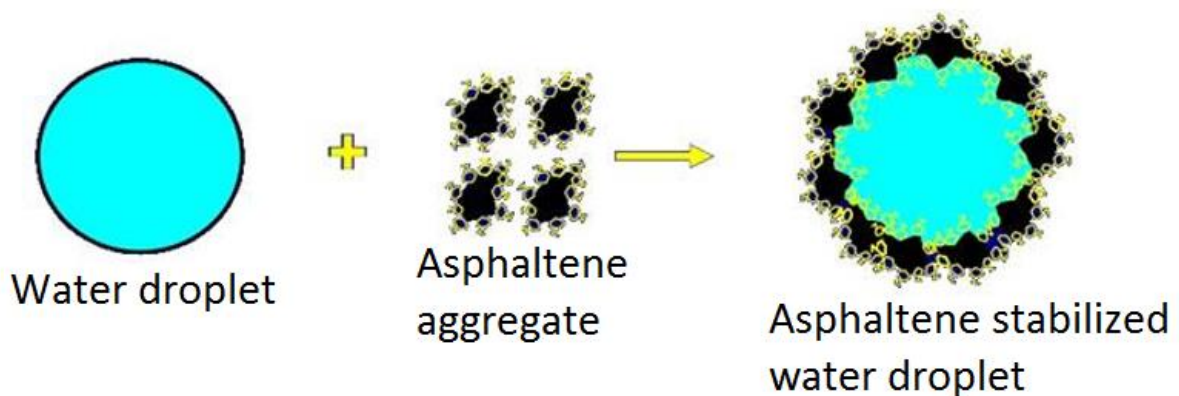


Figure 2.5: Mechanism of emulsion stabilization [7].

Increasing interfacial viscosity provides a mechanical resistance to coalescence. Lowering the interfacial tension promotes dispersion, and thereby makes it easier to create smaller droplets. A consequence of surfactant adsorption at an interface is that it provides an expanding force acting against the normal interfacial tension. If π is this expanding pressure (surface pressure), then we get equation 2.1 [4].

(eq. 2.1)

$$\gamma = \gamma_i - \pi$$

γ : New interfacial tension, after reduction due to expanding interfacial pressure.

γ_i : Initial interfacial tension.

π : Expanding interfacial pressure.

Thus, surfactants tend to lower interfacial tension, and hence help the dispersion and emulsification process to happen more easily, because only a minor increase in total interfacial energy is required [4].

Naturally occurring emulsifiers in the crude oil include asphaltenes and resins, organic acids, and bases. Other surfactants that may be present are from the chemicals injected into the formation or wellbores, e.g. drilling fluids, stimulation chemicals, corrosion inhibitors, scale inhibitors, wax, and asphaltene control agents [5].

Fine solids can act as mechanical stabilizers. These particles, which must be smaller than emulsion droplets, collect at the oil/water interface and are wetted by both oil and water. The effectiveness of these solids in stabilizing emulsion droplets depends on factors such as particle size, interparticle interactions and wettability of the particles. Finely divided solids found in oil production include clay particles, sand, silt, asphaltenes and waxes, corrosion products, shale particles, mineral scale and drilling muds [5].

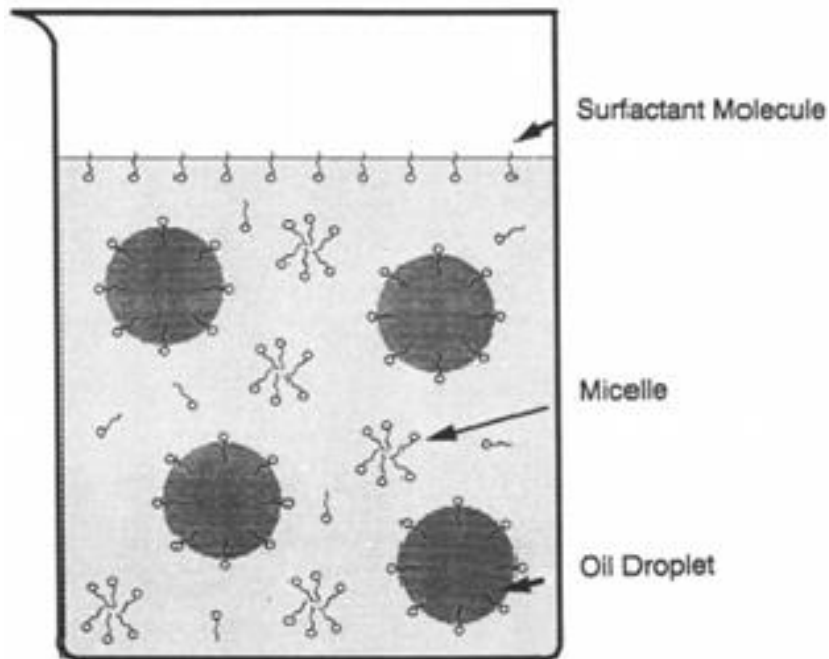


Figure 2.6: Surfactants and micelles in an O/W solution [4].

Micelles

In normal aqueous solutions, dilute concentrations of surfactant act as normal electrolytes, but at higher concentrations very different behaviour occur. This behaviour can be explained in terms of organized aggregates called micelles in which the lipophilic parts of the surfactants associate in the interior part of the aggregate and leave the hydrophilic parts to face the aqueous medium. Consequently, the micelles will not stabilize the emulsion droplets like the monomer surfactant molecules.

Figure 2.6 illustrates surfactants associations in an O/W emulsion, with both monomer surfactant molecules and micelle aggregates. The size of the surfactant molecules and the oil droplets has been greatly exaggerated for the purposes of illustration [4].

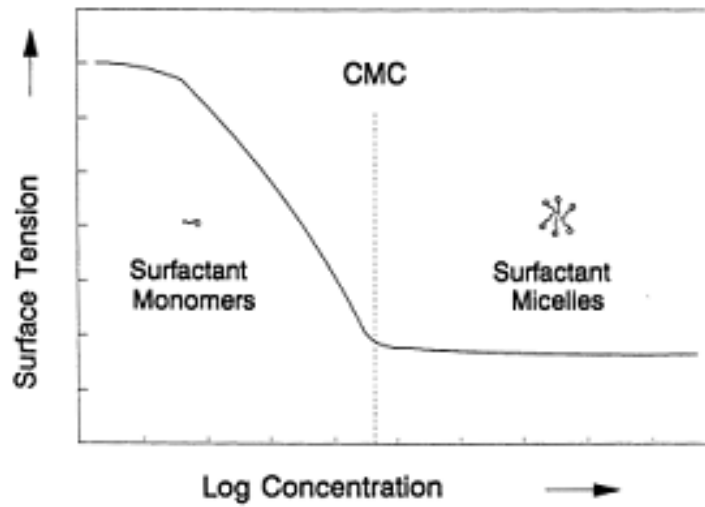


Figure 2.7: The association of surfactants in solution, showing the CMC [4].

The concentration at which micelle formation becomes significant is called the critical micelle concentration (CMC). The CMC is dependent on the property of the surfactant and several other factors, because the micellization is opposed by thermal and electrostatic forces. A low CMC is favoured by increasing the molecular mass of the lipophilic part of the molecule, lowering the temperature and adding electrolyte. Some typical values for low electrolyte concentrations at room temperature are presented in table 2.2. Figure 2.7 shows how the concentration of surfactants monomers affects the surface tension, until the concentration reaches CMC [4].

Surfactant class	CMC [mol/l]
Nonionic	$10^{-5} - 10^{-4}$
Anionic	$10^{-3} - 10^{-2}$
Amphoteric	$10^{-3} - 10^{-1}$

Table 2.2: Typical CMC values [4].

The solubility of micelle-forming surfactants show a strong increase above a certain temperature, termed the Krafft point (T_k), illustrated in figure 2.8. The sudden increase in surfactant solubility is explained by the fact that the monomer surfactants have limited solubility, whereas the micelles are very soluble. Below the Krafft point the solubility of the surfactant is too low for micellization. As temperature increases towards the Krafft point, the solubility increases until the CMC is reached. At this temperature, a relatively large amount of surfactant can be dispersed in micelles, and solubility increases greatly. Above the Krafft point the CMC determines the surfactant monomer concentration. Consequently, maximum reduction in surface or interfacial tension occurs at this surfactant concentration [4].

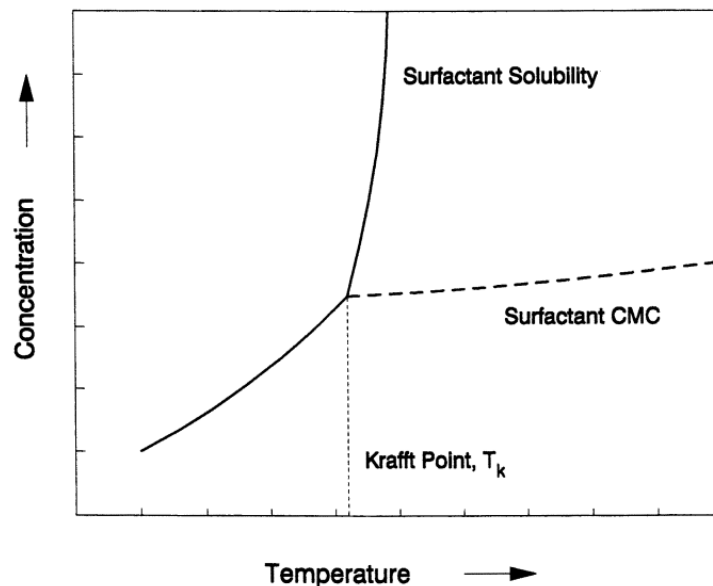


Figure 2.8: The solubility-micellization behaviour of surfactants in solution [4].

Classification of surfactants

The “tail” of most surfactants are fairly similar, consisting of a hydrocarbon chain. Surfactant molecules have either one or two tails. Those with two tails are said to be double-chained. Most commonly, surfactants are classified according to their polar head group. This is illustrated in figure 2.9. A nonionic surfactant has no charged groups in its head. The head of an ionic surfactant carries a net negative charge (anionic), or a net positive charge (cationic). If a surfactant contains a head with two oppositely charged groups, it is termed amphoteric [8].

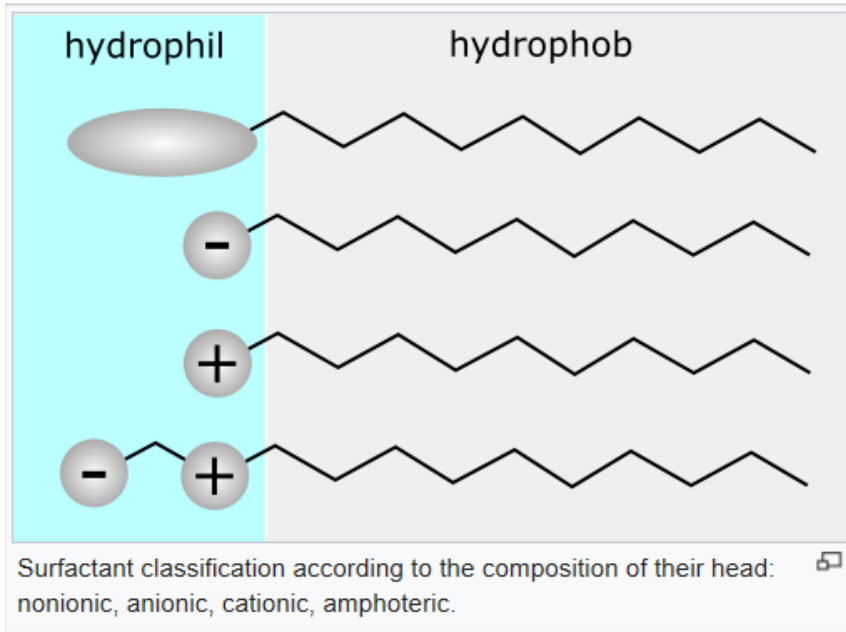


Figure 2.9: Surfactant classification [8].

2.5 Characteristics and physical properties

Droplet size

Colloidal droplets in colloidal dispersions are between 10^{-3} μm and 1 μm in diameter, but emulsion droplets may be even larger. In fact, produced oilfield emulsions generally have droplet diameters that exceed 0.1 μm and may be larger than 100 μm [4][5].

As already mentioned, one can distinguish between macroemulsions (size >100 nm) and microemulsions (size <100 nm). Petroleum emulsions are normally macroemulsions, but there will always be a distribution of the droplet sizes. Figure 2.10 shows the droplet size distribution of typical petroleum emulsions. The droplets size distribution in an emulsion depends on several factors including the [4][5][7]:

- Interfacial tension.
- Shear.
- Nature and amount of emulsifying agents.
- Presence of solids.
- Bulk properties of oil and water.

Droplet size distribution in an emulsion determines, to a certain extent, the stability of the emulsion. As a rule of thumb, the smaller the average size of the dispersed droplets, the tighter and more stable the emulsion becomes [5].

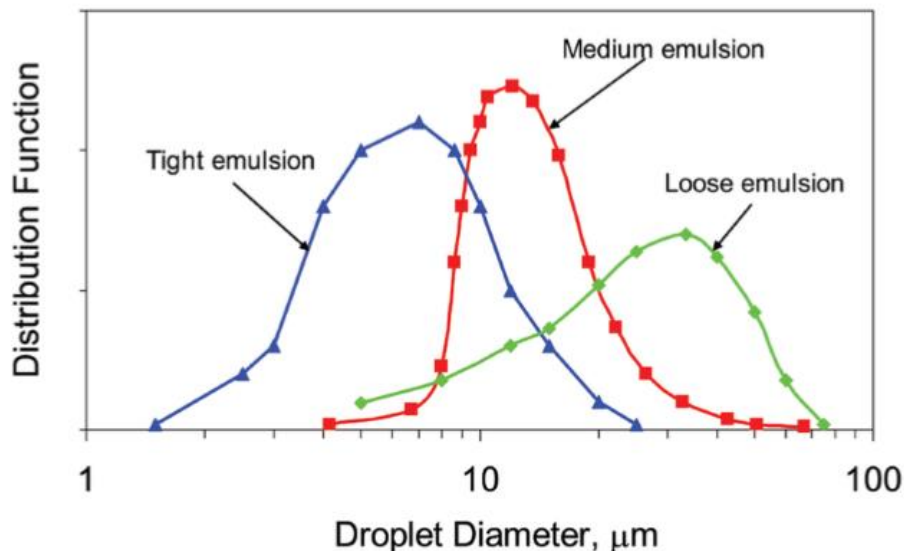


Figure 2.10: Droplet size distribution [5].

By comparing several emulsions, a droplet size distribution weighted toward the smaller sizes will usually represent the most stable emulsion. The droplet size also has an important influence on the viscosity. Considering repulsion forces like electrostatic and steric interaction between the droplets, the emulsion viscosity will be higher when droplets are smaller. The viscosity will also be higher when the droplet sizes are relatively homogenous, i.e. when the droplet size distribution is narrow rather than wide [4].

Rheology

High viscosity might be the reason that an emulsion is troublesome, e.g. it can result in a resistance to flow that must be dealt with. To describe the viscosity of the emulsion we need to consider if the emulsion is a Newtonian or non-Newtonian fluid. A convenient way to summarize the flow properties of fluids is by plotting flow curves of shear stress versus shear rate. These curves can be categorized into several rheological classifications. Figure 2.11 gives a presentation of some of these rheological classifications [4].

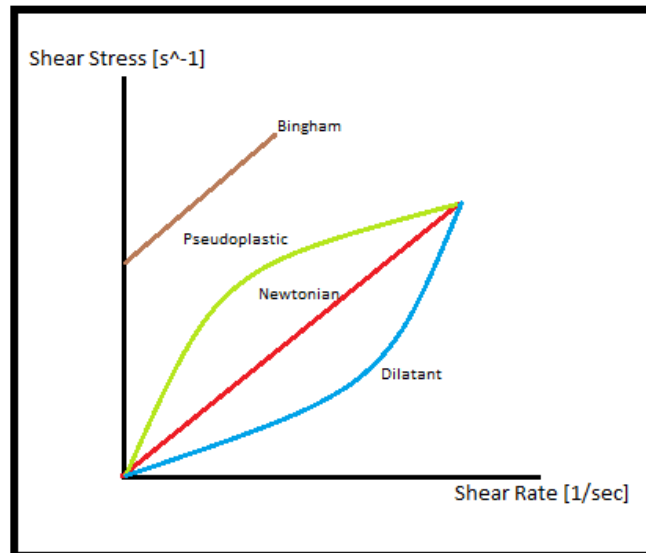


Figure 2.11: Rheology curves.

The rheological properties of an emulsion are very important, and depends on several factors like the [5]:

- Viscosities of oil and water.
- Volume fraction of water dispersed.
- Droplet-size distribution.
- Temperature.
- Shear rate.
- Number of solids present.

A fluid is considered non-Newtonian when its viscosity is a function of shear rate. At a certain volume fraction of the water phase (water cut), oilfield emulsions behave as shear-thinning or pseudoplastic fluids (i.e., as shear rate increases, viscosity decreases). Figure 2.12 shows an example of the viscosities of tight emulsions at 52 °C at different water cuts. The constant values of viscosity for all shear rates, or a slope of zero, indicate that the emulsions exhibit Newtonian behavior up to a content of 40 %. At water cuts greater than 40 %, the slope of the curves deviate from zero, which indicate non-Newtonian behavior. The non-Newtonian behavior is pseudoplastic or shear thinning behavior [5].

An interesting phenomenon is observed in figure 2.12 at 80 % water cut. Up to a water cut of 80 %, the emulsion is a W/O emulsion. At 80 % water cut, the emulsion “inverts” to an O/W emulsion, and the water, which was the dispersed phase, now becomes the continuous phase. This phenomenon is called “phase inversion,” and will be further explained later in this chapter. In this particular case, the phase inversion took place at 80 % water cut, but emulsions can “invert” at other water cuts [5].

The phase inversion phenomenon is illustrated more informative in figure 2.13, when the graph is a function of apparent viscosity versus water cut.

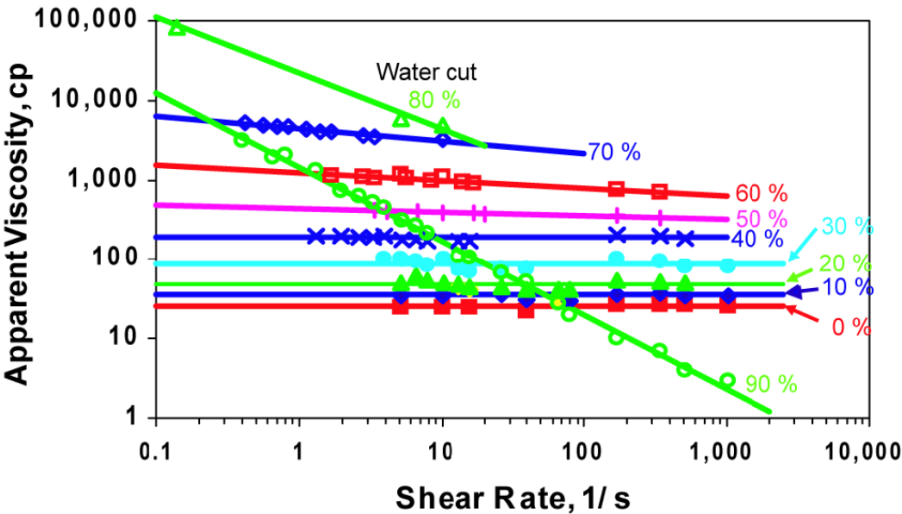


Figure 2.12: The effect of shear rate and water cut on viscosity of emulsions at 52 °C [5].

Figure 2.13 also shows the effect of temperature on emulsion viscosity. Emulsion viscosity decreases with increasing temperature [5].

The previous discussion about rheology has dealt with the bulk viscosity of the emulsion. A closely related and important property is the interfacial viscosity, in the oil-water interface region. As mentioned previously, emulsions form rigid interfacial films encapsulating the dispersed droplets. These interfacial films stabilize an emulsion by lowering the interfacial tension, and increasing interfacial viscosity which result in suppressing the rate of oil film drainage during the coalescence of dispersed droplets (thereby reducing the rate of emulsion breakdown) [4][5].

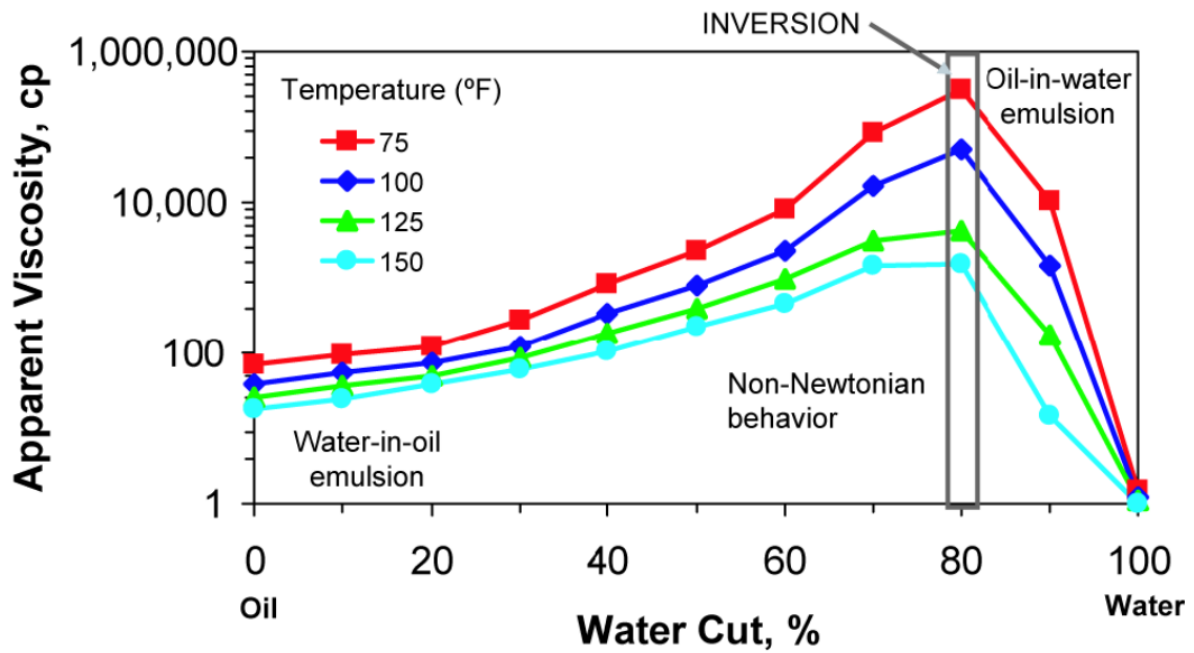


Figure 2.13: Temperature effect on viscosity (shear rate of 0.1 [1/s]) [5].

2.6 The Krieger-Dougherty equation

The Krieger-Dougherty equation can be used to model the suspension viscosity η (viscosity of the entire mix of dispersed and continuous phase), and to evaluate aggregation phenomena, illustrated in equation 2.2 [9][10][11].

(eq. 2.2)

$$\eta_r = \frac{\eta}{\eta_c} = \left(1 - \frac{\phi}{\phi_M}\right)^{-[\eta]\phi_M}$$

η_r : The relative viscosity [cP].

η : The intrinsic viscosity of the suspension [cP].

η_c : The viscosity of the continuous fluid phase [cP].

ϕ : The volume concentration of dispersion droplets in the continuous phase.

ϕ_M : The maximum packing.

Formally the equation models the dependence on particle volume fraction, ϕ , and the maximum volume fraction, ϕ_M (also referred to as the maximum packing). This equation shows that there is an increase in viscosity of the medium when particles are added, and the increase depends on the concentration of the particles [9].

Note that in the simulations with LedaFlow Q3D in this thesis, the default value in LedaFlow of the maximum volume fraction was used ($\phi_M=1$). This value for the maximum volume fraction is very high, and in reality this value would be closer to approximately 0.77.

Figure 2.14 illustrate the concentration dependence of the relative viscosity by plotting the viscosity at two shear stresses (0.2 Pa and 2 Pa) as a function of the oil volume fraction [10].

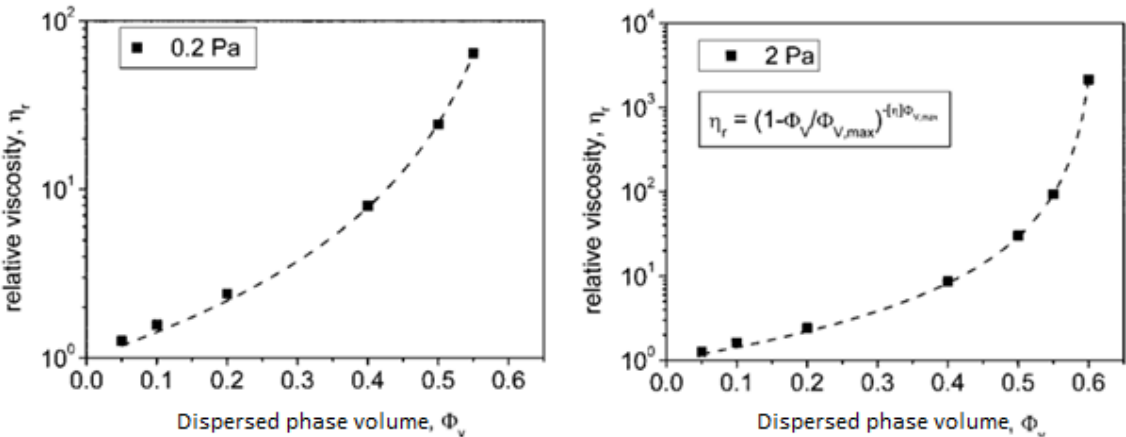


Figure 2. 14: The relative viscosity of the dispersion as a function of the oil volume fraction [10].

An intrinsic viscosity value of 2.5 cP is expected for suspensions of spherical particles, or an emulsion with non-deformed droplets [9][10].

Therefore, if the viscosity of the dispersed phase and the concentration of the aggregates are known, and the maximum packing of the particles is determined, then the viscosity of the emulsion can be calculated.

2.7 Properties of interfaces

In simple two-phase colloidal systems, a thin intermediate region, known as the interface, lies between the internal (dispersed) and the external phase (continuous phase). Emulsified droplets have large interfacial area, and even a modest interfacial energy per unit area can become a considerable total interfacial energy. Figure 2.15 illustrates the interaction between the droplet radius, total area and total interfacial energy. The figure in this example show the total area and energy changes involved in emulsifying 1 barrel of oil into water by dispersing into progressively finer droplets. The total area increases by a factor of two each time a droplet is subdivided into drops of half the previous radius. This example represents emulsion droplets with interfacial tension of 35 mN/m, and the total interfacial energy is consequently calculated by multiplying the interfacial tension by the total interfacial area [4].

To achieve emulsification an energy equivalent to the total interfacial energy has to be added to the system, for example by mechanical shear force. Another alternative is to use surfactant chemistry to lower the interfacial free energy, or interfacial tension.

Interfacial tension is the force per unit length around a surface, or the free energy required to create new surface area. Unit for interfacial tension are millinewtons per meter (mN/m). Equation 2.3 shows the relation between interfacial tension (γ , mN/m), interfacial total area (A , m²) and interfacial energy (E , Nm) [4].

(eq. 2.3)

$$E = \gamma * A$$

E : Interfacial energy [Nm].

γ : Interfacial tension [mN/m].

A : Total area [m²].

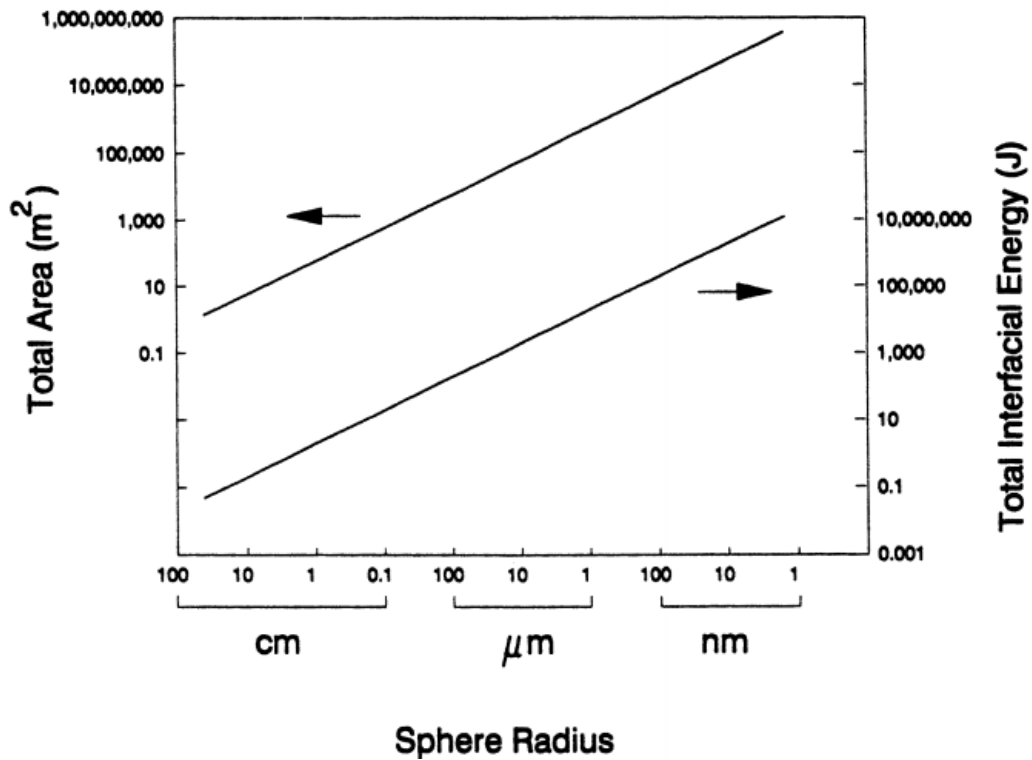


Figure 2.15: Droplet radius, total area, and total interfacial energy [4].

Figure 2.16 illustrates how to use the diagram to find the total interfacial energy related to total interfacial area. Draw a horizontal line from a given value for total area, until it reaches the first sloping line (which represent the relation between total area and sphere radius). Then draw a vertical line down, until it reaches the second sloping line (which represent the relation between sphere radius and total interfacial energy). Finally draw a horizontal line until it reaches the axis for the total interfacial energy. By adding surfactants to lower the interfacial tension of the emulsion droplets, consequently the angle of the sloping lines in the diagram will decrease.

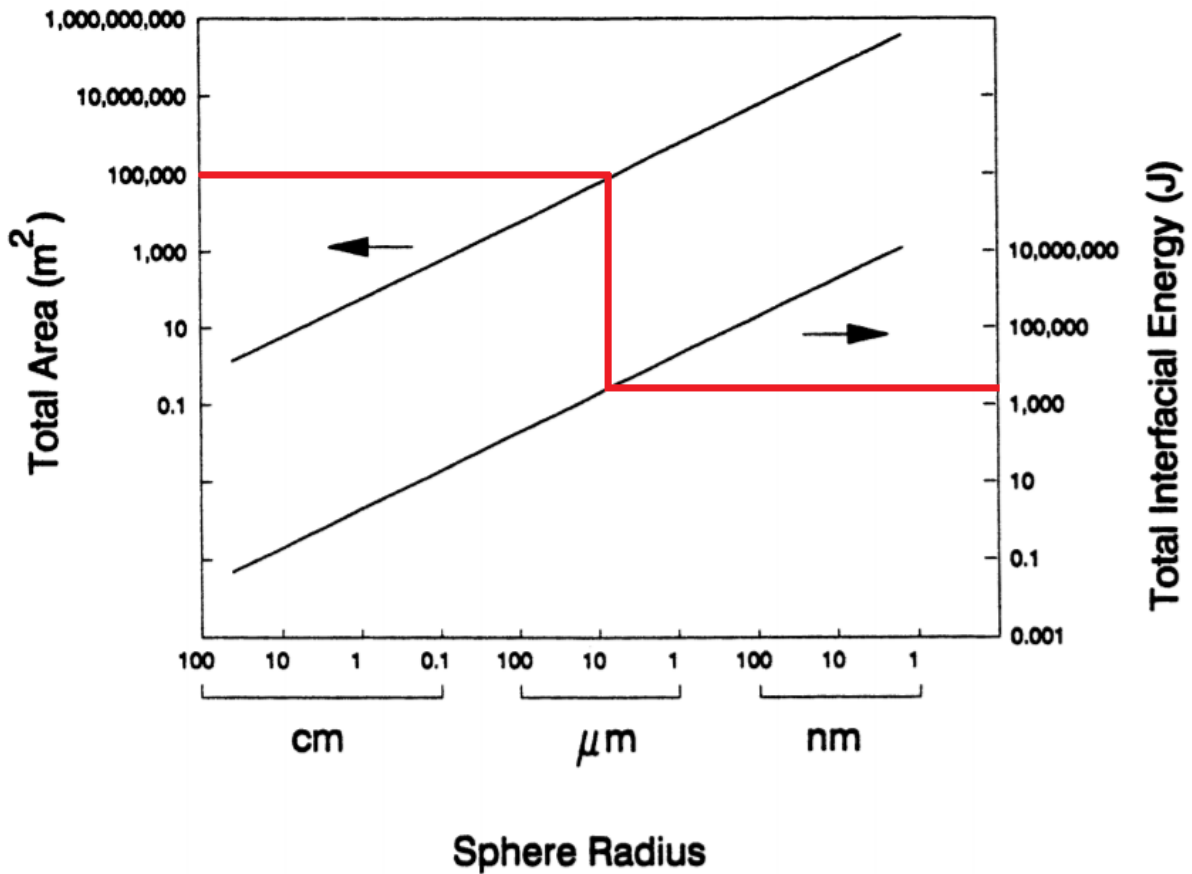


Figure 2.16: How to use diagram to find total interfacial energy [4].

2.8 Stability of emulsions

From a thermodynamic point of view, an emulsion is an unstable system because there is a natural tendency for a liquid/liquid system to separate and reduce its interfacial area and, hence, its interfacial energy. However, most emulsions demonstrate kinetic stability, i.e. they are stable over a period of time. Petroleum emulsions are classified based on their degree of kinetic stability. Loose emulsions separate in a few minutes, medium emulsions separate in tens of minutes and tight emulsions separate (sometimes only partially) in hours or days, or sometimes even longer (figure 2.10) [12].

Stabilizing mechanisms

The tendencies to form stable or unstable emulsions vary a lot among different kinds of crude oils. Emulsions of any significant stability contain at least one emulsifying agent. The emulsifying agent may lower interfacial tension and thereby make it easier to create small droplets, and stabilize the small droplets to prevent them from coalescing into

larger droplets, or even separate out as a bulk phase. Just straightforward casual mixing of the components seldom produces emulsions that persists for any length of time. The emulsifying agents suppress the mechanisms that would otherwise break down the emulsion. Such mechanisms include i.a.; sedimentation, creaming, aggregation, and coalescence. Creaming, aggregation, and coalescence is illustrated in figure 2.17 (sedimentation is not included in the figure, but is the opposite of creaming) [4][12].

- *Sedimentation and creaming* results from external forces, usually gravitational or centrifugal. The emulsion droplets rise to the top (creaming), if their density is lower than the continuous phase, or sink to the bottom (sedimentation), if their density is larger than the continuous phase [13].
- *Aggregation* (also referred to as flocculation or coagulation) is when two or more droplets collide and stick together, with virtually no change in total surface area. The surface charge influence the distribution of nearby ions in the polar medium. Ions of opposite charge (counter-ions) are attracted to the surface, and ions of like charge (co-ions) are repelled from the surface. In other words, the main cause of repulsive forces are electrostatic repulsion between like-charged emulsion droplets, and the main cause of attractive forces are the Van der Waals forces between opposite-charged emulsion droplets. When the droplets collide and stick together, they retain their identity but lose their kinetic independence, because the aggregate moves as a single unit. Aggregation may further lead to coalescence and the formation of a larger droplets [4][13].
- In *coalescence*, the original species lose their identity and become part of a new species. In other words, two or more droplets fuse together to form a single larger unit with a reduced total surface area. This may continue until the phases separates [4].

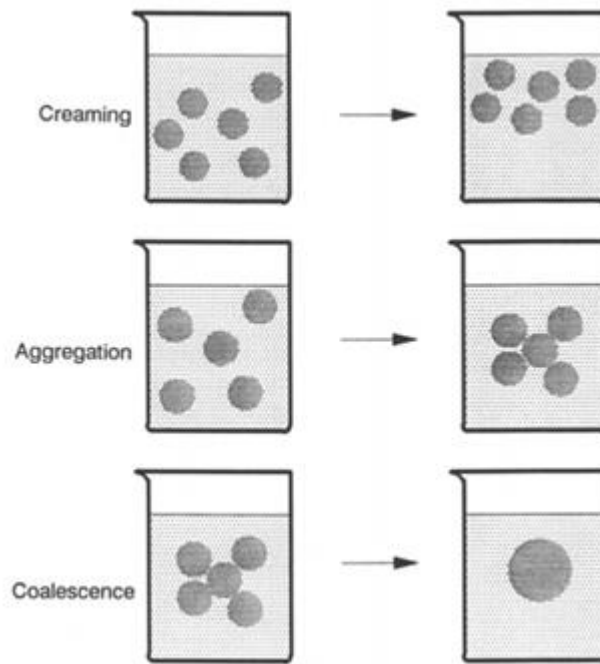


Figure 2.17: Creaming, aggregation, and coalescence in an O/W emulsion [4].

Petroleum emulsions are stabilized by films that form around the dispersed droplets. As already mentioned, these films result from adsorption of emulsifying agents (surfactants or solid particles). They enhance the stability of an emulsion by increasing the interfacial viscosity, and suppressing the coalescence process by providing a mechanical barrier to coalescence. Clearly interfacial films are primarily responsible for emulsion stability. Factors that affect interfacial films area [13]:

- *Heavy polar fractions in the crude oil.* These compounds are the main constituents of the interfacial films surrounding the water droplets that give emulsions their stability [13].
- *Solids, including organic (asphaltenes, waxes) and inorganic (clays, scales, corrosion products, etc.) materials.* Fine solid particles form rigid films that can inhibit the coalescence of emulsion droplets. Solid particles may be electrically charged, which also enhance the stability of the emulsion because of repulsion forces between the dispersed droplets [13].
- *Temperature.* Temperature affect stability of the emulsion by affecting the physical properties of oil, water, interfacial films, and surfactant solubility's in the oil and water phases. Perhaps the most important effect of temperature is on the

viscosity of emulsions because viscosity decreases with increasing temperatures (see figure 2.13). Other examples include; temperature increases the thermal energy of the droplets and, therefore, increases the frequency of drop collisions. It also reduces interfacial viscosity, which results in a faster film-drainage rate and faster drop coalescence [13].

- *Droplet size and droplet size distribution.* Emulsions that have smaller droplets will generally be more stable [13].
- *pH of the brine, and brine composition.* The pH of the water affects the rigidity of the interfacial films, and the specific ions present in the brine can also influence interfacial film behaviour. Figure 2.18 illustrates the effect of brine and pH on emulsion stability [13].

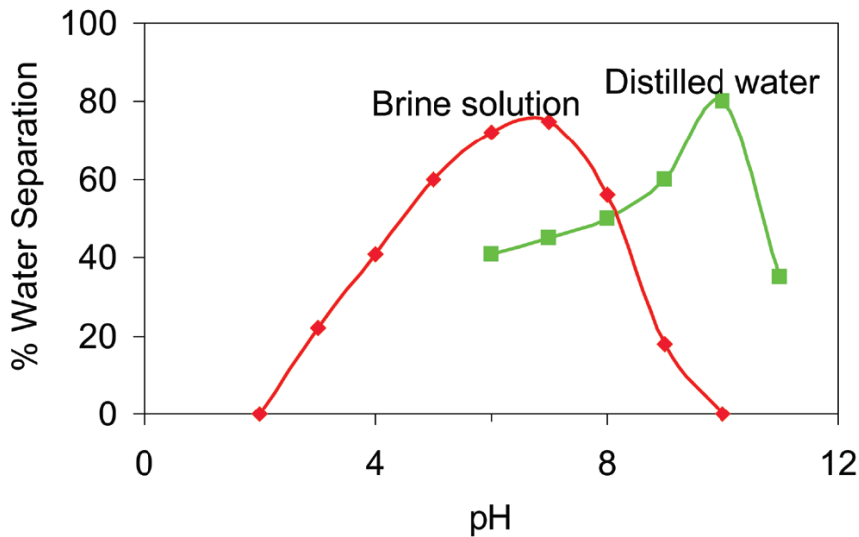


Figure 2.18: Effect of brine and pH on emulsion stability [13].

2.9 Inversion

Phase inversion, in oil-water emulsion systems, refers to a phenomenon where, with a small change in the operational condition, dispersions of oil drops in water becomes dispersions of water drops in oil, or vice versa. This transition is usually associated with an abrupt change in the rates of momentum, heat and mass transfer between the continuous and dispersed phases and between the dispersion and the system solid boundaries. Since the rheological characteristics of the dispersion, and the associated

pressure drop, change abruptly and significantly at, or near, the phase inversion point (PIP), the PIP is a major factor to be considered in the design of oil-water transportation pipelines. PIP is usually defined as the critical volume fraction (critical water fraction or critical oil fraction) of the dispersed phase above which this phase will become the continuous phase. For example, the corrosion of the pipe is determined to a large extent by the identity of the phase that wets it. If avoiding corrosion is of high importance, it might be clever to design the pipe to induce W/O emulsions, where the oil phase wets the pipe wall. In other situations, reducing pressure drop might be of higher importance. By inducing O/W emulsions, where water wets the pipe wall, the friction on the pipe wall will be reduced, and consequently the pressure drop will be less as well [1].

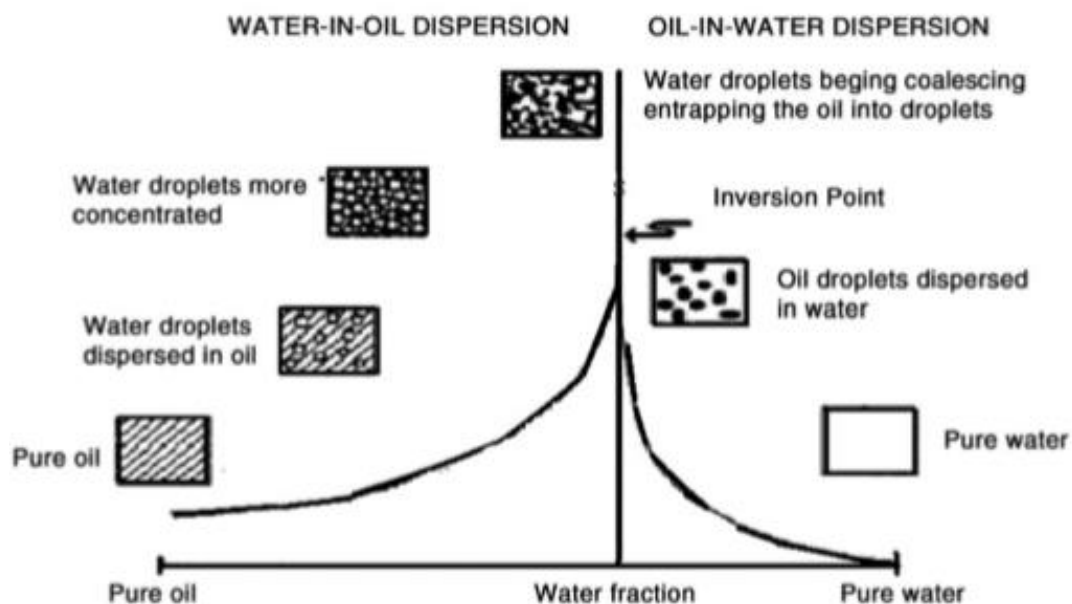


Figure 2.19: Phase inversion, water fraction vs. viscosity [1].

Figure 2.19 illustrates the phase inversion process. As the water fraction increase, the water droplets become more concentrated and start to coalesce. At the PIP the water become the continuous phase, and the inversion occurs at the maximum apparent viscosity. Once past the PIP, the apparent viscosity drops significantly due to the water becoming the continuous phase. The significant reduction of viscosity results in a dramatically reduction of pressure drop as well [1].

In the region near the inversion point, multiple emulsions may be encountered. The process is not always exactly reversible. That is, hysteresis may occur if the inversion point is approached from different sides of the composition scale. Figure 2.20 shows the irreversible inversion of an emulsion brought about by the application of shear. The figure illustrates how inversion occurs when shear rate increases, simultaneously as the viscosity decreases. Nevertheless, the emulsion stays the same without any reversible process when shear rate decreases to initial value [4].

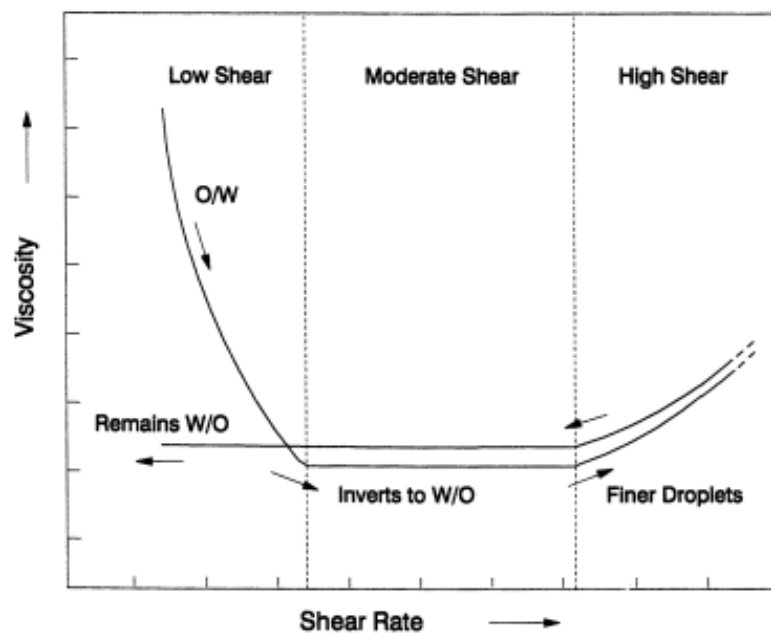


Figure 2.20: Example of the shear-induced inversion of an emulsion [4].

The first contribution of phase inversion modelling was registered at the beginning of the 20th century when Ostwald (1910) assumed that the dispersion phase volume fraction could not exceed the relative volume occupied by the closed-packed sphere configuration, which is about 0.74 for monodispersed rigid spheres. Otherwise, phase inversion would occur. This essentially mechanistic model has the virtue of acknowledging the hysteresis phenomenon, but it does not take into account any surfactant effects, which are known to be of considerable importance in most practical cases. Because of surfactants, the inversion point can occur at a wide range of volume fractions [1].

2.10 Demulsification

Demulsification (emulsion breaking) involves two steps. First, agglomeration of droplets must occur. Then, the agglomerated droplets must coalesce. Only after these two steps can complete phase separation occur. A W/O petroleum emulsion from a production well might contain up to 60 – 70 % water. Some of this will readily settle out. The rest requires specific emulsion treatment. In systematic emulsion breaking there are several steps included. The first step is to characterize the nature of the emulsion to be either O/W or W/O. Then investigate the nature of the two phases, and the sensitivity of the emulsifiers. Based on such an evaluation, design a chemical addition to neutralize the effect of the emulsifier, followed by mechanical methods to complete the phase separation [4].

If an emulsion is stabilized by electrical repulsive forces, then demulsification could be induced by overcoming or reducing these forces. In this context, the addition of electrolyte to an emulsion could be used to achieve the critical aggregation concentration (CAC) [4].

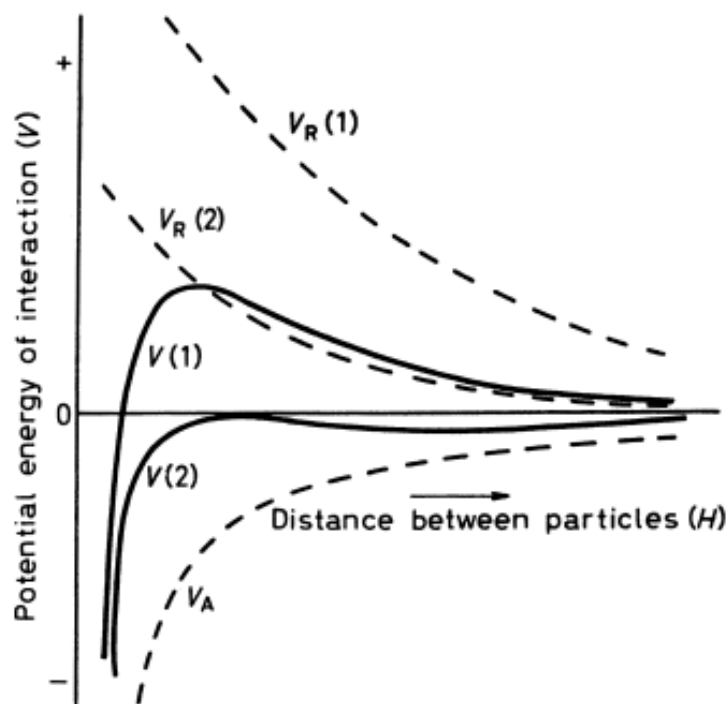


Figure 2.21: The effect of different repulsive and attractive forces (1 and 2) [4].

Derjaguin and Landau, and independently Verwey and Overbeck, developed a quantitative theory for the stability of lyophobic colloids, now known as the DLVO (Derjaguin, Landau, Verwey and Overbeck) theory. The theory was developed to account for the observation that colloids coagulate quickly at high electrolyte concentrations, slowly at low electrolyte concentrations, and with a very narrow electrolyte concentration range over which the transition from one to the other occurs. This narrow electrolyte concentration range defines the critical aggregation concentration (CAC). Illustrated in figure 2.21, the DLVO theory accounts for the energy changes that take place when two droplets approach each other, and involves estimating [4]:

- The energy of attraction vs. inter particle distance.
- The energy of repulsion vs. inter particle distance.

Illustrated in figure 2.21 and equation 2.4, the total interaction energy is the sum of the energy of attraction and the energy of repulsion:

(eq. 2.4)

$$V_A + V_R = V$$

V_A : Energy of attraction.

V_R : Energy of repulsion.

V : Total interaction energy.

In simplicity, a relative large positive value for the total interaction energy will result in an emulsion stable to aggregation, and the colloidal droplets should rebound without contact. If on the other hand, the total interaction energy is not so high, then slowly aggregation should occur.

3 Multiphase flow

3.1 Basics about multiphase flow

The production of crude oil is most often associated with several distinctive phases. Hence, the production flow is commonly named as a multiphase flow. Three-phase flow of gas and two immiscible liquids (oil and water) occurs frequently in production wellbores and transport pipelines. The complexity of multiphase pipe flow is mainly due to the co-existence and motion of multiple phases separated in different layers while simultaneously being dispersed with arbitrary complexity in these layers. In a multiphase flow where separated and dispersed fields coexist, each continuous fluid layer of one phase may contain dispersed fields of other phases. This is illustrated in figure 3.1, with a large-scale interface (LSI) between layers of continuous fluids (in this case gas, oil and water) [1][14].

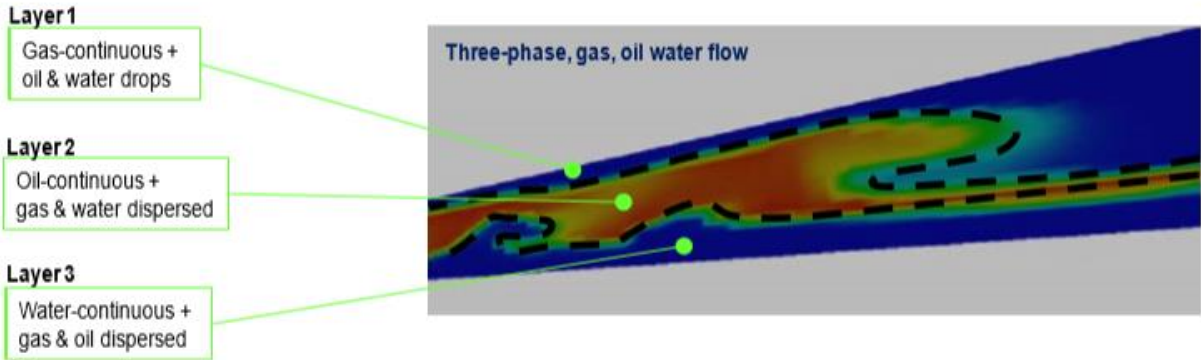


Figure 3.1: Large-scale interface between layers of continuous fluids [14].

3.2 Flow regimes

The multiphase flows can take any of an infinite number of forms. However, these forms can be classified into types of interfacial distributions, commonly called flow regimes or flow patterns [15].

The flow regimes of gas-liquid flows will typically be quite different than the flow regimes of liquid-liquid flows.

3.2.1 Flow regimes of liquid-liquid flows

According to a paper reported by Brauner [21], there are five basic prototypes of flow pattern generated during the simultaneous flow of liquid-liquid mixtures in horizontal pipes [2]:

1. Stratified/separated flow, with a layer with either smooth or wavy interface.
2. Dispersed flow, with a dispersion of relatively fine drops of one liquid in the other.
3. Annular flow, where one of the liquids forms the core and the other liquid flows in the annulus.
4. Slug/plug flow, with large slugs/plugs, elongated or spherical, of one liquid in the other.
5. A combination of the basic types of flow.

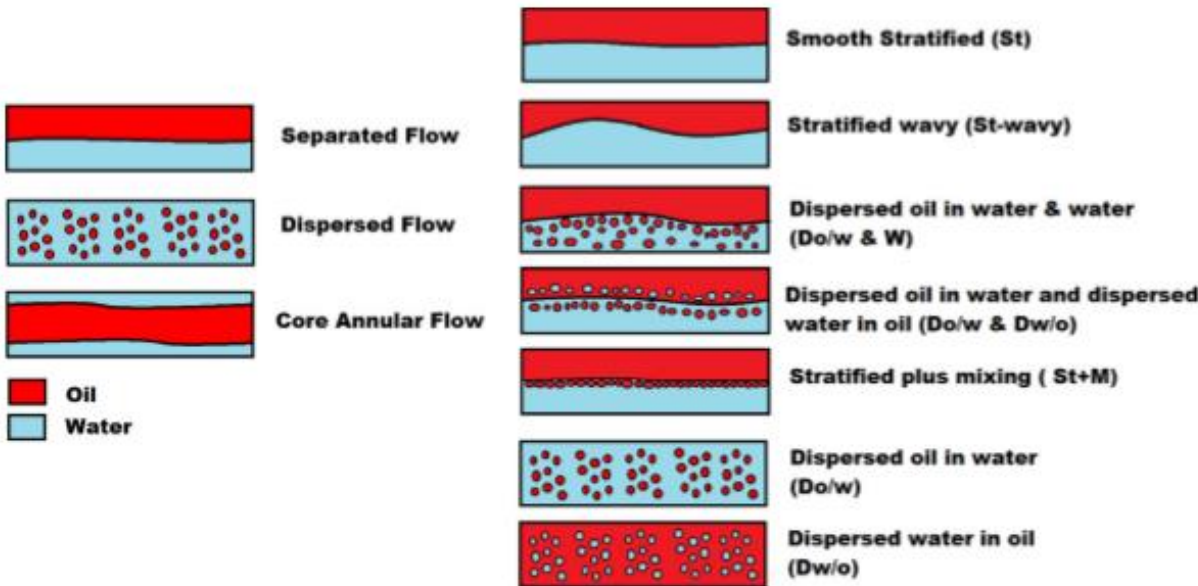


Figure 3.2: Liquid-liquid flow patterns [16].

Stratified/separated-, dispersed- and annular flow is illustrated in figure 3.2, and slug/plug flow is illustrated in figure 3.3.



Figure 3.3: Slug/plug flow [17].

Stratified/separated flows

Stratified/separated flows arise from density differences of the two phases, where the oil (lighter phase) flows over the water (heavier phase) at low superficial velocities. Different interfaces are found in separated flows such as smooth interface (stratified flow), wavy interface (stratified wavy) or an interface with mixing of oil droplets in water near the interface (stratified with mixing) [16].

Dispersed flows

At higher flow rates, the oil from the stratified layer is broken off as droplets into the water (or vice versa), hence forming a dispersion of oil and water, better described as dispersed flow regime. Dispersed flow can be broadly classified O/W and W/O dispersions, depending on the continuous phase [16].

Core annular flow

Core annular flow is the third configuration of the flow regimes possible with liquid-liquid flow in pipes. Termed as a “gift of nature” by many, core annular flows occur when the high viscous oil forms an inner core, and water flows around the core as an annular film, reducing the contact of oil with the pipe walls, and reducing occurring pressure drop massively. Core annular flows are achieved when the density of the oil is close to that of water, thus reducing the buoyancy forces acting on the oil core [16].

Annular flow typically occurs at higher flow rates of the less dense phase (oil), i.e. core annular flow are mostly obtained at the highest oil flow-rates within low water fraction [2].

Slug/plug flow

A typical definition of slug flow is “a multiphase-fluid flow regime characterized by a series of liquid slugs/plugs separated by relatively large gas pockets, or vice versa” [18]. Although, that definition is reserved for gas-liquid flow, the same principal is applicable for liquid-liquid flow, except in that case there are no gas pockets, but only two separated fluids with different densities. In liquid-liquid slug/plug flow, one of the fluids may travel inside the other fluid as the form of a large droplet (instead of a large bubble).

Combinations of several flow regimes

The nature is not always in perfect order, and different flow regimes can simultaneously coexist. This can be observed in figure 3.2, when some of the flow regimes are partly stratified- and partly dispersed flow. Figure 3.4 also illustrate an example of a combination of several flow regimes.

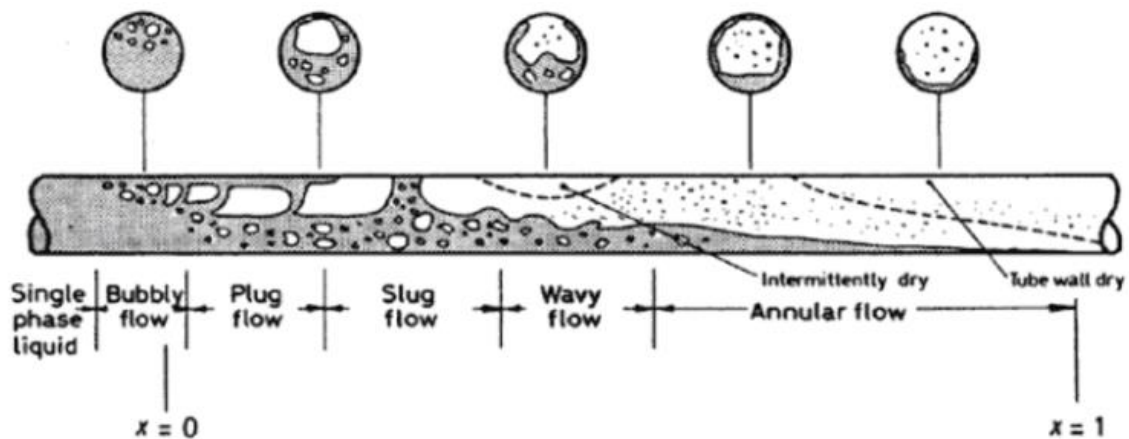


Figure 3.4: A combination of several flow regimes [19].

The definition of flow patterns has not been standardized and thus different researchers recognize diverse types of flow regimes. In experimental studies, there are many possible flow patterns that can be observed apart from those mentioned. Attention should be given to inclination, since it also marks a significant effect to flow patterns [2].

3.2.2 Flow regimes of gas-liquid flows

Similar as for liquid-liquid flows, the pipe inclination is an important parameter in determining flow regimes for gas-liquid flows, which is observed in figure 3.5 and figure 3.6 [15].

Some of the flow regimes for gas-liquid flows are similar as the flow regimes for liquid-liquid flows, but there will also be some flow regimes that are unique for this particular type of flow. The regimes encountered in vertical flows are illustrated in figure 3.5.

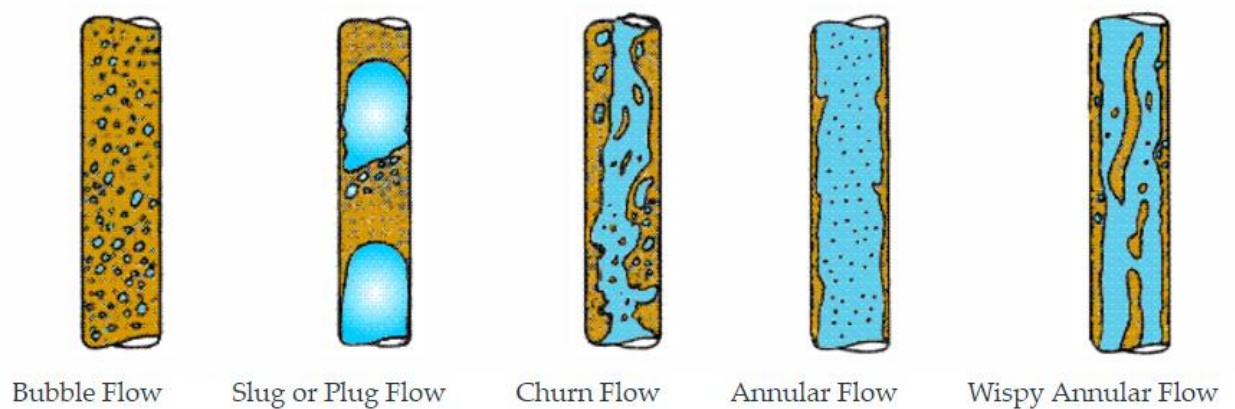


Figure 3.5: Gas-liquid flow pattern in vertical flow [15].

The regimes encountered in horizontal flows are illustrated in figure 3.6. Here, as gravity acts normally to flow direction, separation of the flow occurs [15].

Hence, the stratified flow regime observed for liquid-liquid flow will also occur for gas-liquid flow. Other flow regimes that occur for both gas-liquid flows and liquid-liquid flows is the annular flow.

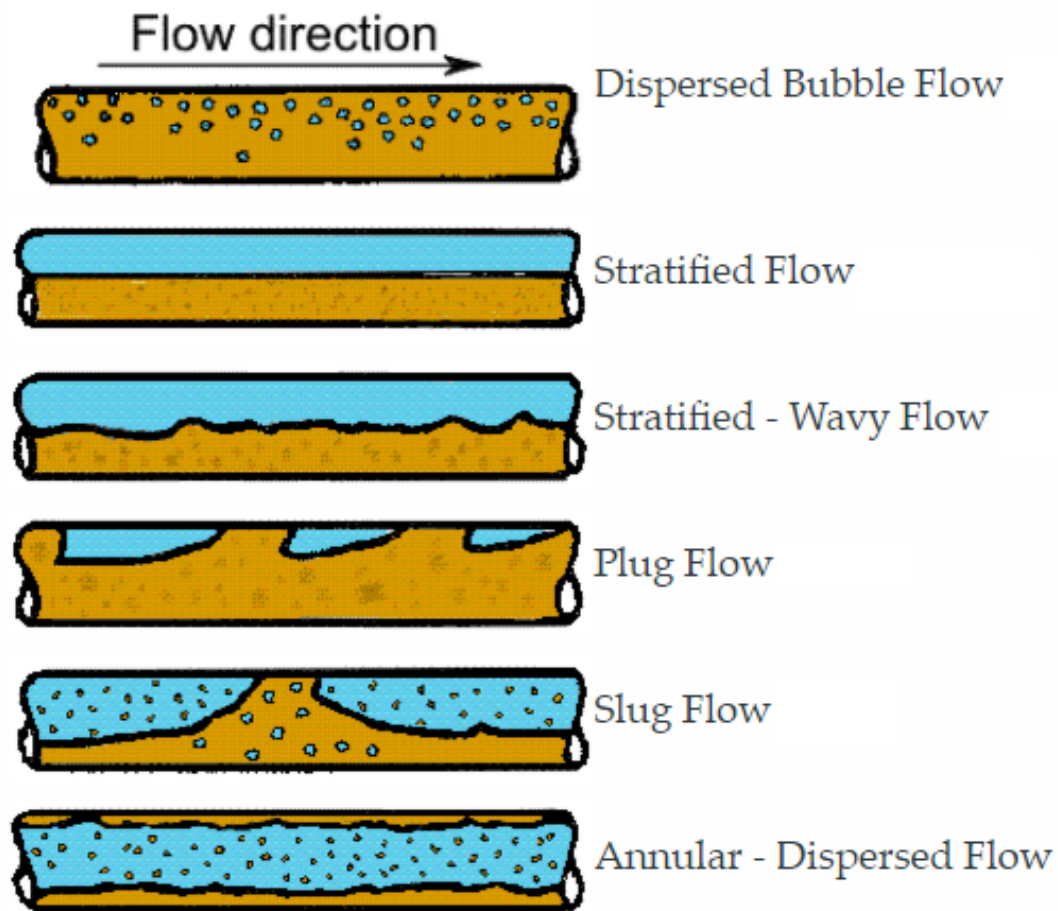


Figure 3.6: Gas-liquid flow pattern in horizontal flow [15].

3.3 Gas-liquid vs. liquid-liquid flows

The significant difference between gas-liquid and liquid-liquid flows is the physical properties that govern them, which refer to density and viscosity of both phases.

A gas-liquid system involves extremely high density and high viscosity differences.

Whereby, liquid-liquid systems might also be characterized by high viscosity differences, but always a low-density difference between the phases [2].

Another major difference between gas-liquid and liquid-liquid flows, is that the slug flow is frequently occurred in the gas-liquid systems, but is rarely observed in the liquid-liquid systems [2].

	Gas-liquid flows	Liquid-liquid flows
Density differences	Extremely high	Low
Viscosity differences	Extremely high	High
Slug flow occurrence	Frequently observed	Rarely observed

Table 3.1: Gas-liquid vs liquid-liquid flows [2].

The differences in characteristics in liquid-liquid flows are mainly caused by the larger momentum transfer capacity, small buoyancy effects, lower free energy at interface, and a smaller dispersed phase droplet size in liquid-liquid flows. The flow behaviour of oil and water in pipes heavily rely on the volume fraction and droplet size distribution of the dispersed phase, because of finite density differences between oil and water phase [2].

As earlier mentioned, the phenomena of the wettability of the pipe wall are known to greatly influence the pressure drop characteristics. During a liquid-liquid flow, both liquids are in favour to wet the wall of the pipe. The favourability depends on the wettability characteristics of the pipe material. This situation is different in the case of a gas-liquid flow where only liquid can wet the wall of the pipe [2].

3.4 Prediction of multiphase flow behaviour

Unlike single-phase flow, multiphase flow cause less predictable flow patterns, and the transition from one flow pattern to another is not always easy to determine.

Since the 1990s, with advanced instruments and techniques, different flow patterns parameters have been measured more accurately, and flow patterns of oil-water flow have been analysed objectively [1].

However, it seems to be lack of consensus about how many flow regimes that exist, and it probably depends on how broadly you define the distinctions from one flow regime to another.

Accurate knowledge of the behaviour of multiphase flow in a pipeline is crucial to design and optimize production, transportation, and processing facilities.

Many researchers have attempted to generalize the liquid-liquid or two-phase flow system through mechanical models and developed means for predicting the flow patterns, pressure drop and water holdups.

However, in general, it is difficult to determine oil-water flow patterns. Oil properties can be quite diverse, and the emulsion viscosity ratio can vary from approximately a million to less than one centipoise (figure 2.13), and its rheological behaviour can be Newtonian or non-Newtonian. To worsen the situation, most empirical correlations and mechanical models developed were designed for low viscosity oils (and gas-liquid flow), which is unpractical when oil viscosity varies widely. In addition, other factors, such as pipe geometry and surface tension play an important role in the flow pattern transition [1][2][14].

3.5 Prediction of oil-water flow characteristics

An accurate prediction of oil-water flow characteristics, such as flow pattern, water holdup, and pressure gradient, is important in many engineering applications. These including designing water-lubricated pipelines, production optimization, production logging interpretation, downhole metering and artificial lift design and modelling [2].

3.5.1 Pressure drop

Co-current flow of oil-water mixture is very common and can cause significant flow assurance problems during production. The formation of emulsions will in most cases result in higher viscosity of the fluid mixture, hence, leading to higher pressure drop e.g. Energy loss in the pipeline is due to friction between the pipe wall and oil, and pipe wall and water. With increasing pressure drop, the effect of natural drive (were crude oil is pushed from the reservoir towards the surface due to high underground pressure) will be reduced. To maintain effective and economical production of hydrocarbons, it is essential to try to reduce the pressure drop in the pipeline. In a fully developed steady flow, the change in pressure over length (dp/dx) is related to the systems effective

viscosity [16].

From figure 2.18 (subchapter 2.9), it can be observed that the PIP (phase inversion point) occurs at the maximum apparent viscosity. Therefore, it is natural to believe that the pressure drop will be at its maximum around the phase inversion point.

As depicted in figure 3.7, the pressure drop increases as oil fraction and flow rates increases. The dispersion of water in oil and loss of water continuity will lead to an increase in pressure drop. At low flow rates and high water fraction the pressure drop will be low, because the water phase will flow and continuously wet the pipe wall, thus reducing drag, while dominating over the lighter phase (i.e., oil). When the flow becomes dispersed and emulsions are made, crude oil (emulsions) flow together with the water, forming thin layers of oil on the pipe wall, thus increasing the shear stress and substantially cause an increase in pressure drop [20].

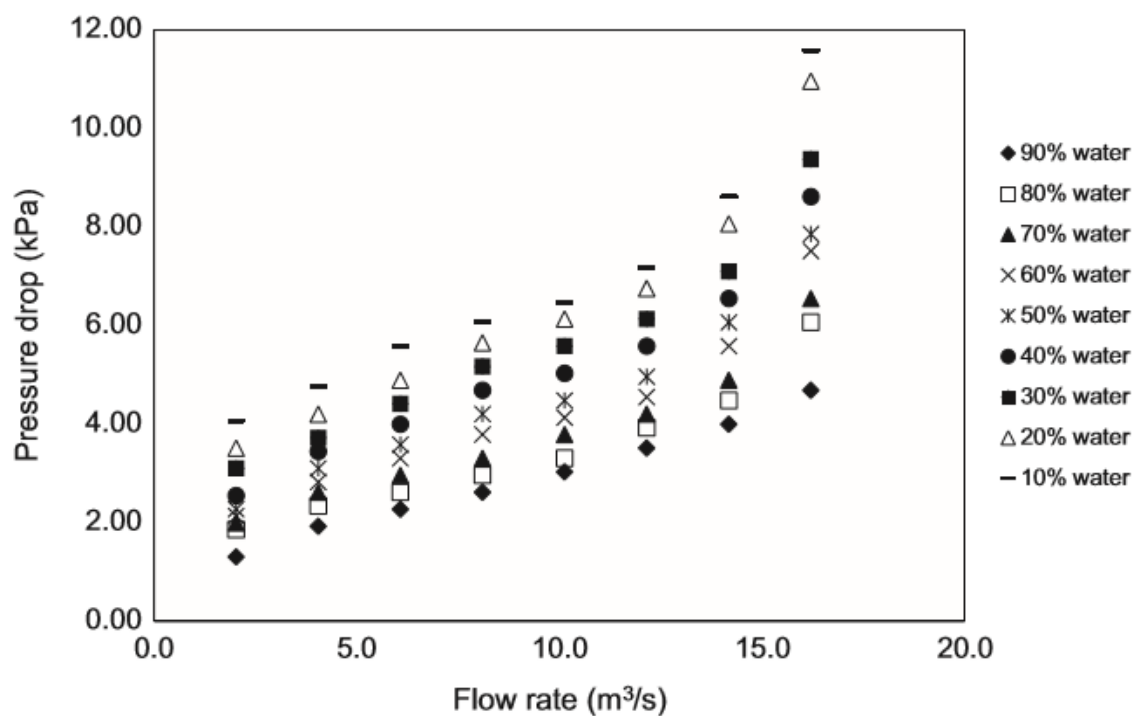


Figure 3.7: Pressure drop vs. flow rate at various water fractions [20].

3.5.2 Water holdup

Water holdup (H_w) is the in-situ volume fraction of water in a specific length of a test section. H_w is expected to increase with the increase of the superficial water velocity (V_{sw}) and decrease with the increasing superficial oil velocity (V_{so}) [2].

Figure 3.8 illustrates how increasing water fraction leads to increasing H_w . Studies show that holdup is influenced by the input volume fraction at the minimum flow rate as well as the increase in slip ratio. This trend is due to the contact between the liquid and the pipe, and the liquid is likely to be accumulated in the pipe at a slower velocity. When oil and water travels concurrently in a pipe, oil is found to travel faster than water, causing a slippage between the phases. For stratified flow, study shows that the slippage effect is significant since oil is lighter than water in terms of density thus it moves faster than water in a horizontal condition. However, in a dispersed flow, the same studies show that the slippage effect is insignificant [20].

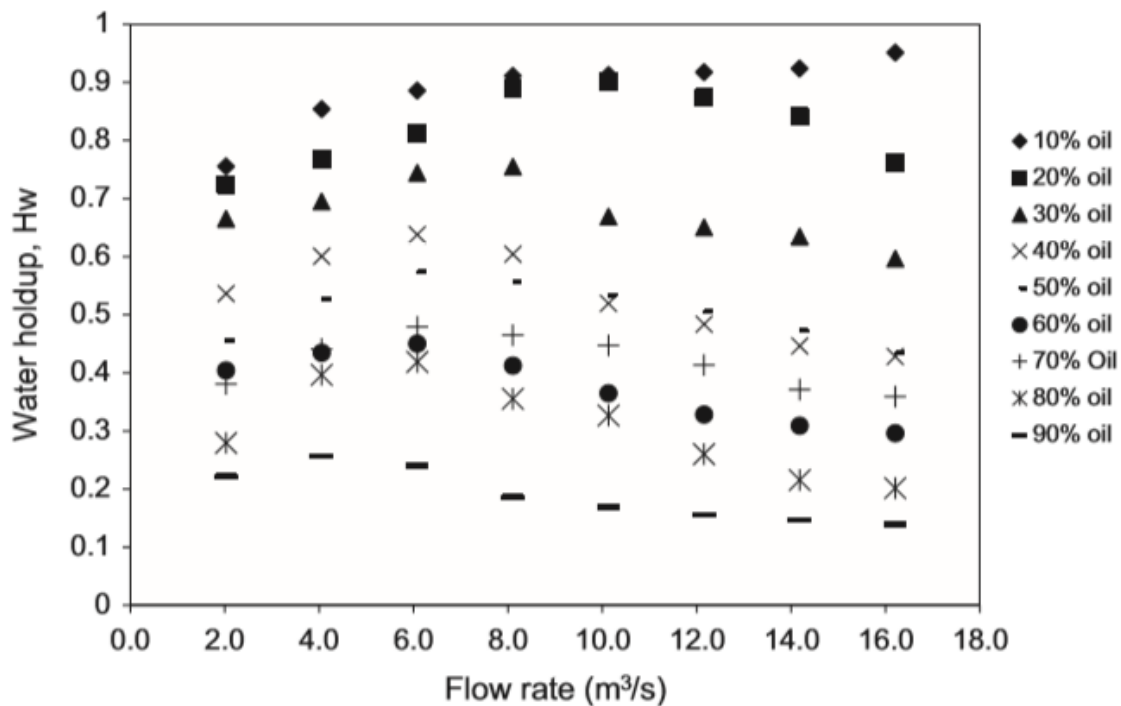


Figure 3.8: Water holdup vs. flow rate at various oil fractions [20].

Knowledge about water holdup is important, because it might help to understand how to decrease the pressure drop. Figure 3.9 and figure 3.10 illustrate how the pressure drop increases when oil holdup increases (water holdup decreases). The figures also illustrate how the pressure drop increases with increasing fluid mixture velocity, and that the pressure drop is at its maximum around the PIP [16].

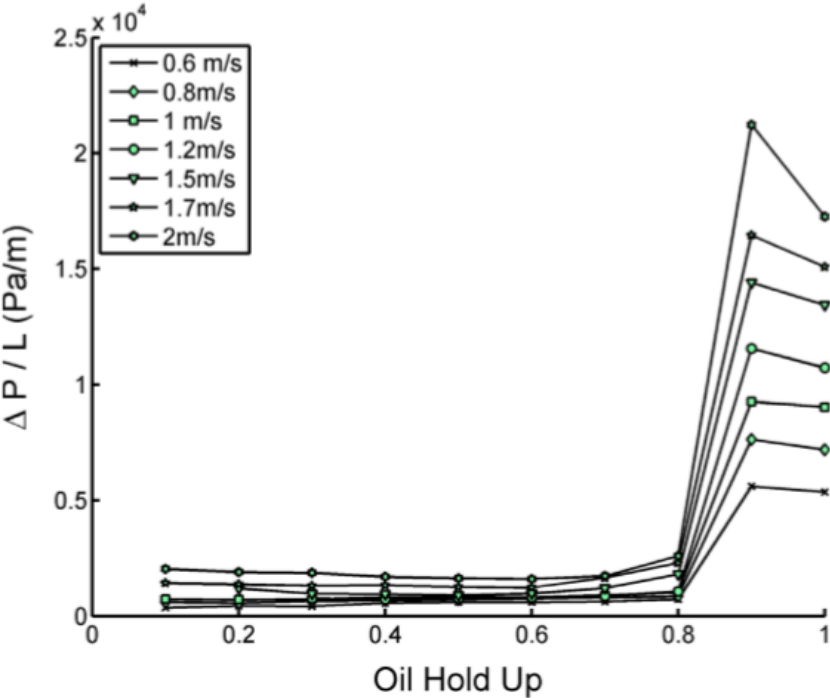


Figure 3.9: Pressure drop per unit length against oil hold up (heavy oil-water flow) [16].

From comparing figure 3.9 and 3.10 it can be seen that the pressure drop for the heavy oil-water flow is higher in magnitude when compared to light-oil water flow, which is related to the higher viscous resistance between viscous oil and pipe wall. Note that the y-axis for figure 3.9 is raised with “10 to the fourth power” [16].

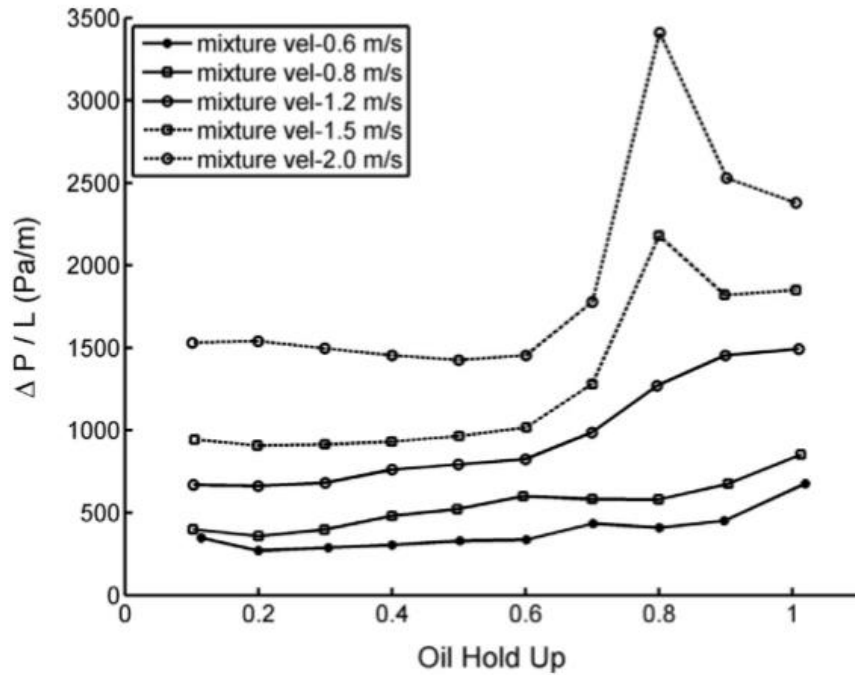


Figure 3.10: Pressure drop per unit length against oil hold up (light oil-water flow) [16].

3.5.3 Flow pattern

It is necessary to predict flow patterns as a basis for carrying out calculations on multiphase flow. The usual procedure is to plot the information in terms of a flow regime/pattern map. Many of these maps are plotted in terms of primary variables (for instance superficial velocity of the phases, or mass flux and quantity), but there has been a great deal of work aimed at generalising the plots, so that they can be applied to a wide range of channel geometries and physical properties of the fluids [15].

The prediction of flow pattern transition, in oil-water systems, is a complex hydrodynamic problem. The literature shows that there is no generalized flow pattern map for the flow of two immiscible liquids [1].

Figure 3.11 illustrates how the separated flow regimes of the heavy oil-water flow transition earlier, to become dispersed flow regimes, compared to the light oil-water flow regime. The dotted blue lines represent the transition boundaries of heavy oil-water flow regimes. The black solid lines represent the transition of light oil-water flow regimes [16].

Transition boundaries are becoming more complex with the presence of dispersed flow and inclination angle. To predict the transition character in dispersed flow, especially at a given inclination angle, understanding the mechanism of droplet breakup and coalescence is crucial. In the liquid-liquid dispersed flow, the transition character involves a complex hydrodynamic problem. Therefore, in order to predict the transition characters, careful analysis of flow stability, factors influencing the hydrodynamic conditions, fluid physical properties, droplet size distribution, and as well mean droplet size is required [2].

Different fluids for the two-phase flow, gives different flow patterns at different conditions. The boundaries of the flow patterns, are mainly affected by viscosity of the crude oil as well as the existence of surface active components such as asphaltenes, resin, etc., which can decrease significantly the surface energy between oil and water phases [20].

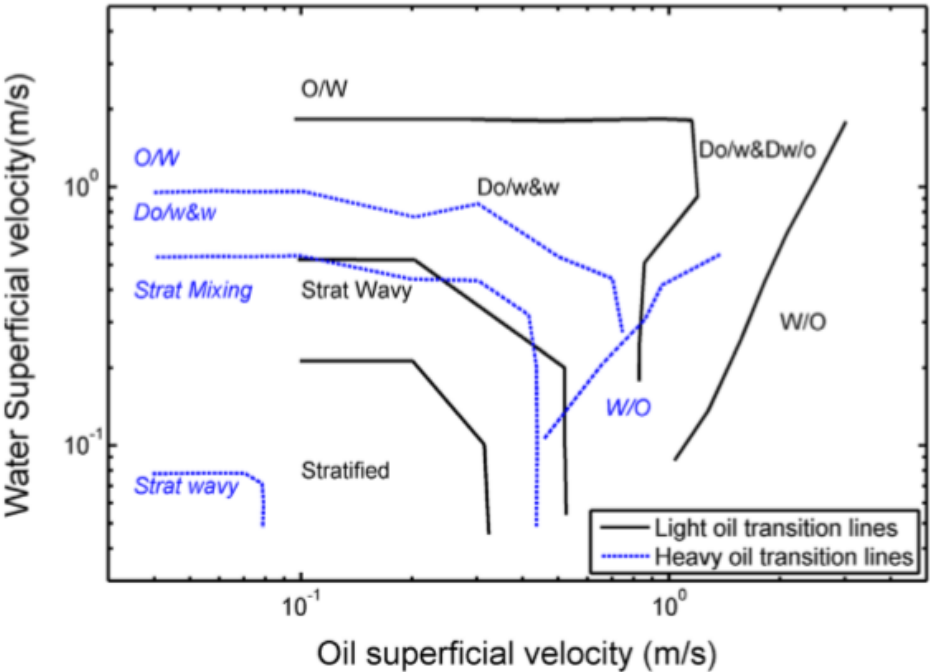


Figure 3.11: Flow pattern comparison of heavy and light oil-water flows [16].

3.5.4 Correlation with the experiment and analysis in this master thesis

As a summary, the most important keyword in this context is viscosity.

Increasing viscosity leads to increasing pressure drop, which results in production challenges. Decreasing water holdup leads to increasing probability that the oil is in contact with the pipeline wall, and oil has a higher viscosity than water. Thus, this leads to increasing pressure drop. Hence, it is important to understand these phenomena. Finally, it is important to know something about the transition between various flow regimes, since the various flow regimes highly effect the effective viscosity (laminar flow and turbulent flow will have different effective viscosity, due to the creation of emulsions in turbulent flow).

Later in this thesis it will be presented how we use a computer program to analyse how viscosity evolves in a fluid mixture, and further how this affects the torque in a flow wheel simulator. The measured torque can be compared with pressure drop, since they are both affected by the viscosity and the friction between the fluid and the pipe wall.

4 CFD modelling

4.1 Description of CFD modelling

Computational Fluid Dynamics (CFD), is defined as the set of methodologies that enable a computer to provide us with a numerical simulation of fluid flows. The word simulation is used to indicate that we use the computer to solve numerically the physical laws that govern the movement of fluids, in or around a material system, where its geometry is also modelled on the computer [22].

The fundamental basis of almost all CFD problems is the Navier-Stokes equations (which describes the motion of viscous fluid substances). These equations can be simplified by removing terms describing viscous actions to yield the Euler equations. The Euler equations represent Cauchy equations of conservation of mass (continuity), and balance of momentum and energy, and can be seen as particular Navier-Stokes equations with zero viscosity and zero thermal conductivity [23][24][25].

The Navier-Stokes equations for fluid flows describe the changes of momentum (mass*velocity) per time in a control volume, related to the inflow and outflow of fluids and the forces that work on the control volume (friction, pressure drop, gravitation etc.). In addition, the continuity equation is solved, which describes the transport of mass per time in the control volume as a function of inflow and outflow (equation 4.1). The momentum equation and the continuity equation are continuous equations. To solve these equations on a computer, it is necessary to discretize.

(eq. 4.1)

$$\frac{\partial \rho}{\partial t} + \nabla(\rho u) = 0$$

ρ : Fluid density [kg/m³].

t : Time [s].

u : Fluid velocity [m/s].

∇ : $\frac{d}{dx} + \frac{d}{dy} + \frac{d}{dz}$

In mathematics, discretization concerns the process of transferring continuous functions, models, and equations into discrete counterparts. This process is usually carried out as a first step toward making them suitable for numerical evaluation and implementation on digital computers [26].

To plot a continuous function on a computer, it is necessary to select which data points to plot, since the computer will not be able to plot an infinite number of points. For the same reason, to be able to solve a continuous equation, the simulation domain must be divided into a finite number of discrete grid cells. A pipe is a 3-dimensional object, and can be divided into grid cells which extends in height, width and length. The grid cells need to be approximately the same size as the smallest wave/structure that one may want to have a resolution for. If it is desirable to simulate waves with wavelength of 1 cm, then the grid cell size must be less than 1 cm in height, width, and length.

Simulations solved for a large 3-dimensional system (e.g. 30 miles long pipeline) will have a lot of grid cells, and it will naturally take a very long time to solve these equations for the entire system. To simulate an entire pipeline with 3-dimensional grids would take many years. It is therefore necessary to limit the equations to solve only small parts of the 3-dimensional system. To reduce the calculation time, a 3-dimensional problem can be transformed into a 2-dimensional problem, by solving the mean value in one of the dimensions. Consequently, some information is lost, which makes this solution less accurate, but still time-saving. One can also attempt to reintroduce some of the information lost in the averaging from empirical correlations.

In all CFD approaches the same basic procedure is followed. A pre-processor is used by the subsequent computer simulation. In computer aided engineering (CAE) a pre-processor is a program which provides a graphical user interface (GUI) to define physical properties [27].

During pre-processing these following steps are followed:

- 1) The geometry and physical bounds of the problem can be defined using computer aided design (CAD). From there, data can be suitably processed and the fluid volume (or fluid domain) is extracted.
- 2) The volume occupied by the fluids is divided into discrete cells (the mesh). The mesh may be uniform or non-uniform, structured or unstructured, consisting of a combination of hexahedral, tetrahedral, prismatic, pyramidal or polyhedral elements. (e.g., figure 4.2)
- 3) The physical modelling is defined. For example, the equations of fluid motion + enthalpy + species conservation.
- 4) Boundary conditions are defined. This involves specifying the fluid behaviour and properties at all bounding surfaces of the fluid domain. For transient problems, the initial conditions are also defined.
- 5) The simulation is started and the equations are solved iterative as a steady-state (an unvarying condition in a physical process, were the variables, which define the behaviour of the system or the process, are unchanging in time) or transient.
- 6) Finally, a postprocessor can be used for the analysis and visualization of the resulting solution [23].

4.2 The LedaFlow tool

4.2.1 Historical background

Research on the multiphase transport of oil, gas and water in pipelines was well documented by the mid-90s. At this point, the industry was ready to continue to the next stage of the development, namely, to design new transport systems completed with precipitation and possible deposition on the pipeline walls of wax, gas hydrates, scale, asphaltenes and even produced sand. Production has begun to mature, which means that water production begins to increase considerably. Due to the possibility of back-flow, with the water and the oil flowing downstream and the gas upstream, made it difficult to continue the development of design tools in only one dimension. SINTEF realized that they had to develop a software tool able to calculate in several dimensions for the purpose of capturing the effect of different complex multiphase phenomena on the design of a pipeline. ConocoPhillips funded the Leda R&D (research and development) project from 2001 and Total joined it in 2002. In addition to the funding, both companies have also contributed greatly by providing professional expertise in the development work and have thus been very active partners in the development of LedaFlow [28].

4.2.2 Modelling capabilities

At present, the models in LedaFlow include the 1D model and the LedaFlow-Q3D model. The LedaFlow field approach includes detailed modelling of water and oil dispersions, and gas bubbles in liquid phases. Separate fields are characterized with volume fractions, field velocities, enthalpy, particle size (bubbles and droplets), physical properties, temperature and composition. The models can be separated in 2-phase systems (with 4 fields) and 3-phase systems (with 9 fields). Figure 4.1 illustrates the 3-phase system with 9 associated fields. 3 continuous phases (water, oil, gas), and 6 dispersed phases (G/W, O/W, G/O, W/O, W/G, O/G) [28].

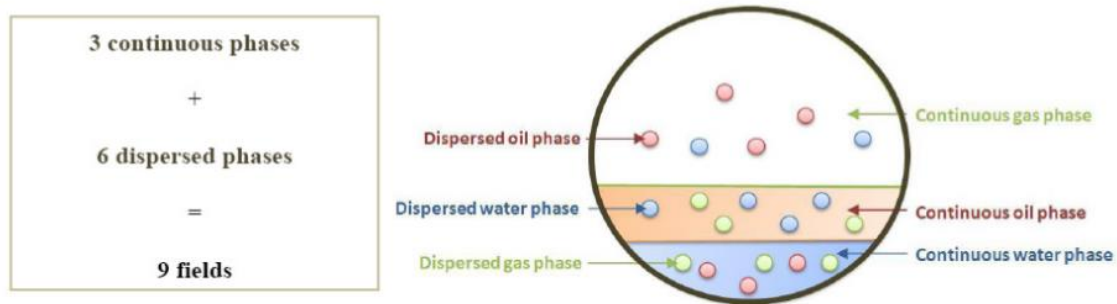


Figure 4.1: The 3-phase system, with 9 associated fields. [28]

Leda 1D

The 1D model is a fully transient code for two-phase (oil and gas) and three-phase (oil, gas, and water) cases. The 1D transient code models heat and mass transfer, complex network with junctions, composition tracking, inhibitor tracking, slug capturing, valve, PID-controllers, wells, mass source and pigging [28].

Leda 1D use a Navier-Stokes equation as a function of length, integrated over width and height. When discretizing this equation, there is only use of grid cells in the length-direction, as a one-dimensional grid system. With this method, there will be less grid cells involved in the calculations, and consequently it is possible to complete the simulation quicker than the Leda Q3D model.

Leda Q3D

The LedaFlow-Q3D model is based on a turbulent pipe flow of multiple types of fluids and multiple numbers of fields, with reconstruction and tracking of the large scale interfaces (LSIs, see figure 3.1) and modelling of the local transport phenomena at these interfaces. The LedaFlow-Q3D model is something in between a CFD code and the Leda 1D model. A 2D approximation of the 3D pipe flow is performed by averaging the flow over horizontal slices in the pipe cross section, while maintaining the important wall effects (e.g., wall shear stress and turbulence production) which play a crucial role in characterizing multiphase pipe flow [28].

Figure 4.2 illustrates a quasi-3D mesh for the pipe geometry. The cross section of the pipe (left) is sliced and analytically integrated to produce slice-averaged flow quantities on the mid plane, which is discretized from bottom wall to top wall and along the pipe (right). [14]

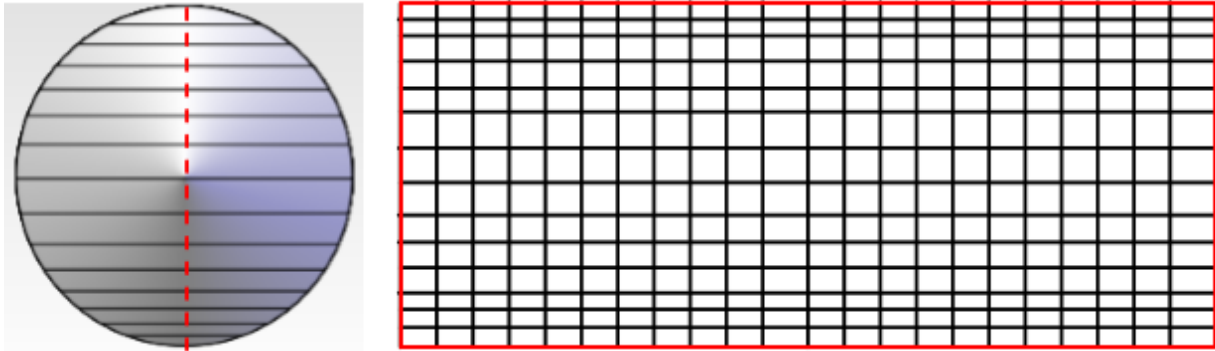


Figure 4.2: A quasi-3D mesh for the pipe geometry [6].

Moreover, dynamic modelling of the evolution of the cell averaged bubble and droplet size is accomplished by solving a transport equation for the mean particle diameter, which includes source and sink terms representing coalescence and break up of bubbles and droplets. Turbulence for all phases is modelled by a filter based one-equation turbulence model. Gas compressibility is taken into account by either assuming a constant value for $\frac{\partial \rho}{\partial P}$ or using PVT (pressure volume temperature) tables (similar to what it is in 1D modelling). Multiphase flow modelling in bends and curved pipes in vertical plane is achieved by adding Coriolis and Centrifugal forces in the momentum equations [28].

With the LedaFlow-Q3D modelling tool, complete transient quasi three-dimensional CFD modelling of complex multiphase pipe flows is made available for oil and gas pipe flow applications. This provides engineers and scientists with more detailed data for their analyses. In addition to the two- and three-phase pipe flows, the Q3D model can also compute single phase pipe flow as well as single phase and multiphase flow in two-dimensional channels [28].

5 Simulation of the wheel flow simulator in LedaFlow Q3D

5.1 Description of the rotating flow wheel simulator

The high-pressure Flow Wheel Simulators at the SINTEF Multiphase Flow laboratory are specially designed to study hydrocarbon fluid systems under realistic conditions.

They are compact flow loops without a pump or compressor. The wheels are installed vertically, and the fluids inside the wheels “see” an endless pipe through which they flow as a multiphase mixture. In general, the gravitational force keeps the liquid stationary, while the wheel itself is rotating. Figure 5.1 shows a schematic figure of the wheel flow simulator in a temperature regulated chamber [29].

Figure 5.4, in subchapter “5.2 Description of the simulation work in LedaFlow Q3D,” shows how this wheel flow simulator looks like in LedaFlow Q3D.

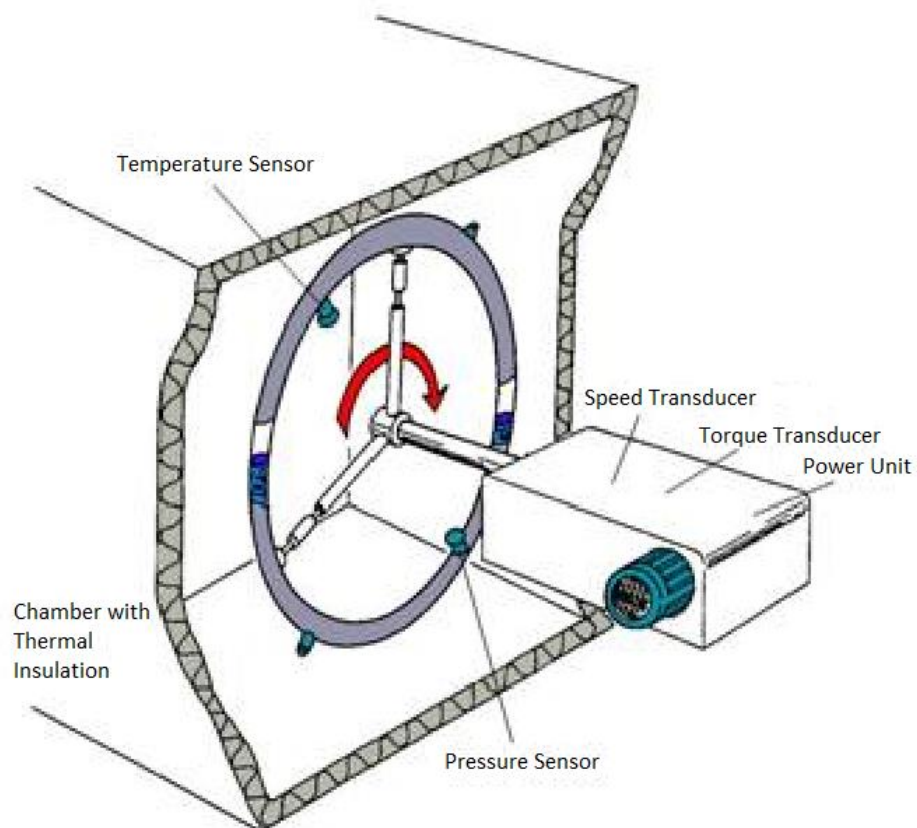


Figure 5.1: Schematic figure of the wheel flow simulator [29].

The SINTEF Multiphase Flow Laboratory possesses 3 different wheel flow simulators:

- 2" Ultra-high pressure wheel flow loop (actual ID: 57 mm).
- 2" High pressure wheel flow loop with observation window (actual ID: 52.5 mm).
- 5" Medium pressure wheel flow loop (actual ID: 121 mm) [29].

In this thesis, test results from the 2" high pressure wheel flow loop will be compared with simulation results using LedaFlow Q3D. Figure 5.2 is a picture of the three different SINTEF wheel flow simulators; the ultra-high pressure wheel (left), the high-pressure wheel with window and rotating camera (middle), and the medium pressure wheel (right).



Figure 5.2: SINTEF wheel flow simulators [29].

The main applications for the SINTEF wheel flow loops are:

- Realistic testing of fluid behaviour in general (no additives).
- Testing of low-dosage hydrate inhibitors (LDHIs) (kinetic and antiagglomerant inhibitors).
- Testing of thermodynamic hydrate inhibitors (alcohols, glycols, salts).
- Testing of drag reducers in high-viscosity fluids.
- Testing of viscosity modifiers in heavy fluids.
- Testing of oil-based and water-based mud properties [29].

In this thesis, the test results from realistic testing of fluid behaviour in general will be used to compare simulation results using LedaFlow Q3D. The aim is to investigate how various input parameters affects the simulation results, and see if we can tune the simulation results in LedaFlow to match with the test results from the wheel flow simulator. Description of the simulation work in general, will be given in the next subchapters. Detailed explanation regarding procedures as setup, running simulations and plot results, will be given in appendix.

The wheel experiment which will be compared with simulations in LedaFlow was conducted on a fluid system of 60 % nitrogen, 30 % water (tap water), and 10 % oil (Exxsol D80) by volumes. The initial temperature and pressure was 25 °C and 1 bar. The tested profile of the wheel experiment was a stepwise velocity scan from 0.1 m/s to 2 m/s. However, in this thesis when simulating in LedaFlow the focus will be on a wheel velocity of 2 m/s. The gradually change in velocity and the following change in torque from the wheel experiment is illustrated in figure 5.3. The fluid properties of the fluid system are given in table 5.1.

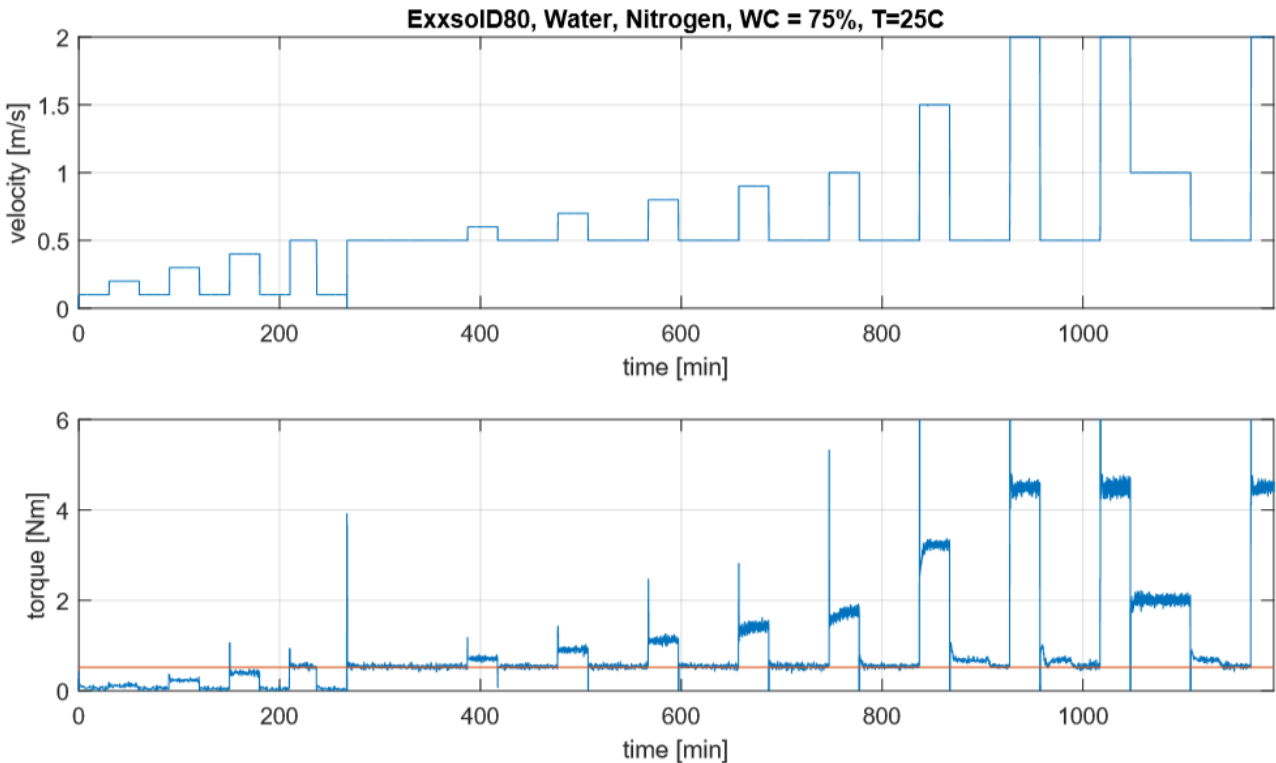


Figure 5.3: Velocity and torque versus time for the wheel experiment [30].

	Densities [Kg/m ³]	Viscosity [Pa*s]	Compressibility [kg/m ³ /bar]
Nitrogen	1.1347	1.7794*10 ⁻⁵	1.1303
Oil	790	0.0018	0
Water	997	0.00089	0

Table 5.1: Fluid properties of the wheel experiment.

5.2 Description of the simulation work in LedaFlow Q3D

The necessary steps to follow when creating a case, edit the initial case settings, update input parameters, choosing which formulas to use in the simulations, initializing the case, and finally running the case and plotting the results, will be explained in the appendix.

Figure 5.5 shows the initial state for gas, oil, and water, before starting the flow wheel simulator (for a fluid system with 60% gas, 10% oil and 30% water). This figure also illustrates how the fluids are mixed when the flow wheel is rotating. The red colour indicates pure phase of the specific fluid phase of interest (phase fraction is 1), and the blue colour indicate that the phase fraction is zero for the specific fluid phase of interest (the specific fluid phase of interest is the fluid phase that has been chosen by the user to be visualized in the drop-down menu, illustrated in figure B.4 in the appendix). For phase fractions between zero and one, the colour shifts between light blue, green and yellow (figure 5.4).

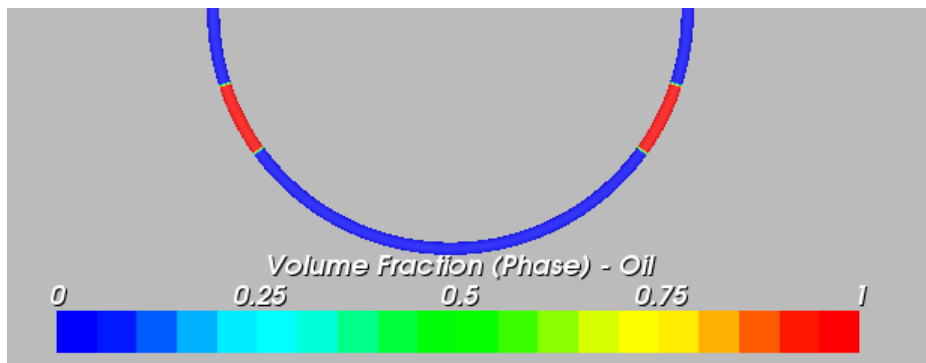


Figure 5.4: Colour codes for phase fractions between zero and one.

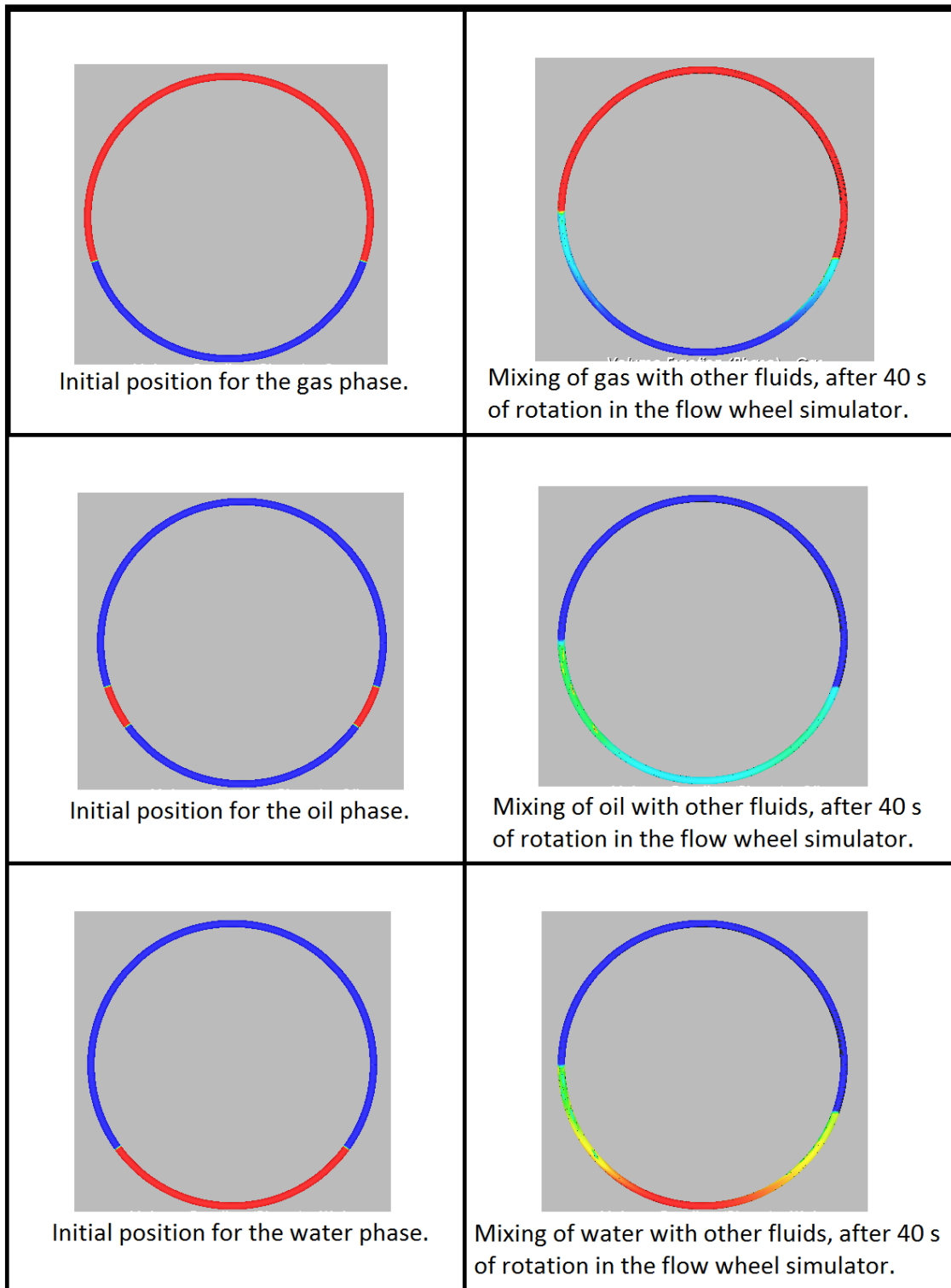


Figure 5.5: Initial boundary conditions, and fluid mixing.

Calculating the start coordinates for the fluid phases

The coordinates for the fluid phases are calculated in excel, and is a function of the phase fractions of the fluid phases.

Input phase fractions:

- Gas: 0.6
- Oil: 0.1
- Water: 0.3

Input pipe geometry parameters:

- Pipe diameter [m]: 0.0524
- Wheel radius [m]: 1
- Total pipe length [m]: $2 \cdot \pi \cdot \text{wheel radius} = 6.28$
- Bottom of wheel [m]: $2 \cdot \pi \cdot \text{wheel radius} \cdot 0.75 = 4.71$
- Top of wheel [m]: $2 \cdot \pi \cdot \text{wheel radius} \cdot 0.25 = 1.57$

When calculating coordinates, we calculate the start length and the stop length of the fluid phase (from left to right). Figure 5.6 illustrate a sketch of how we imagine the coordinate system of the flow wheel, with the left middle section of the pipe (nine O'clock) as the start (0 m) and the end (6.28 m) of the pipe.

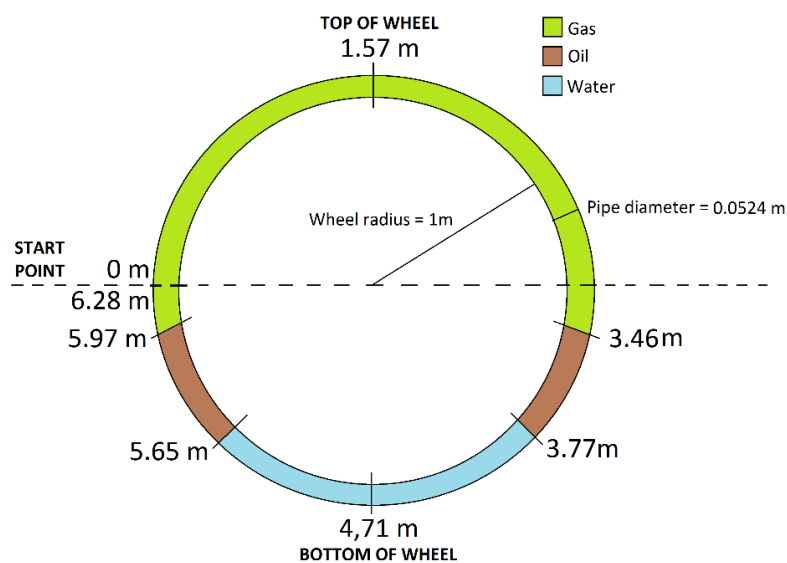


Figure 5.6: Coordinate system of the flow wheel.

Coordinates for the initial position for the gas phase:

Start length:

$$\begin{aligned} & (\text{Top of the wheel}) - (0.5 * (\text{total length of gas phase})) = \\ & (1.57 \text{ m}) - (0.5 * (6.28 * 0.6) \text{ m}) = -0.314 = \underline{5.97} \text{ m} \end{aligned}$$

Stop length:

$$\begin{aligned} & (\text{Top of the wheel}) + (0.5 * (\text{total length of gas phase})) = \\ & (1.57 \text{ m}) + (0.5 * (6.28 * 0.6) \text{ m}) = \underline{3.46} \text{ m} \end{aligned}$$

Coordinates for the initial position for the water phase:

Start length:

$$\begin{aligned} & (\text{Bottom of the wheel}) - (0.5 * (\text{total length of water phase})) = \\ & (4.71 \text{ m}) - (0.5 * (6.28 * 0.3) \text{ m}) = \underline{3.77} \text{ m} \end{aligned}$$

Stop length:

$$\begin{aligned} & (\text{Bottom of the wheel}) + (0.5 * (\text{total length of water phase})) = \\ & (4.71 \text{ m}) + (0.5 * (6.28 * 0.3) \text{ m}) = \underline{5.65} \text{ m} \end{aligned}$$

Coordinates for the initial position for the oil phase (left side):

Start length:

$$\begin{aligned} & = \text{The stop length of the initial position for the water phase.} \\ & = \underline{5.65} \text{ m} \end{aligned}$$

Stop length:

$$\begin{aligned} & = \text{The start length of the initial position for the gas phase.} \\ & = \underline{5.97} \text{ m} \end{aligned}$$

Coordinates for the initial position for the oil phase (right side):

Start length:

= *The stop length of the initial position for the gas phase.*

= 3.46 m

Stop length:

= *The start length of the initial position for the water phase.*

= 3.77 m

5.3 Settings in closures Q3D

When creating the simulation cases, there were some settings in the closures menu that were of special interest. These settings are listed in table 5.2, with the values used in the simulation cases. The values in these settings was systematically adjusted in the simulation work, except the option flag “Emulsion flag” (the original value was 0, which means false, and the viscosity calculations was turned “on” by changing its input parameter to 1, which means true).

In short, the aim of the testing was to make changes in the input settings in closures Q3D (see appendix A., and figure A.6), that resulted in changes in the evolved particle size of droplets. The idea was that these changes could have an impact on the volume concentration of dispersion droplets in the continuous phase, and consequently this would have an impact on the viscosity model (The Krieger-Dougherty equation, chapter 2.6). If the adjustments of the parameters affect the emulsion viscosity, it might be possible to learn how sensitive these adjustments are on the simulation results, and later to use this knowledge to tune specific simulations in LedaFlow Q3D to be more or less identical with the results produced from the wheel flow simulator (subchapter 5.1). The test results from this work will be presented in chapter 7.

Settings in closures Q3D	
Particle size: Variable particle size	[1=0], [2=0], [3=0], [4=1] , [5=0], [6=1]
Emulsion flag	[1=1], [2=1], [3=1]
Particle size: constant size	[1=0.1], [2=0.1], [3=0.1], [4=0.1], [5=0.1], [6=0.1]
Particle size break up time constant	[4 (O/W) = 0,1], [6 (W/O) = 0,1]
Particle size coalescence time constant	[4 (O/W) = 1], [6 (W/O) = 1]
Particle size constant C1	[4 (O/W) = 0.02], [6 (W/O) = 0.02]
Particle size constant C2	[4 (O/W) = 0.002], [6 (W/O) = 0.002]

Table 5.2: Constant settings in Closures Q3D.

Variable particle size

Model options for Q3D simulations include the dynamic particle size (DPS) calculations (explained in appendix “A. Set up guide”). As explained in the set-up guide, the user can choose “yes” or “no” from the drop-down menu in order to include or exclude these DPS calculations (figure A.4, lower left). The DPS model is a transport equation (equation 5.1) for the evolution of average bubble and droplet size in the Q3D domain. In equation 5.1, $d_{p,km}$ is the local (cell) particle size, $d_{p,km}^E$ is the equilibrium (Sauter mean) particle size (see equation 5.3), and $t_{rel,km}^i$ is the intrinsic coalescence or break up time defined by equation 5.2, where t_B and t_C are the break up- and coalescence time scales, respectively, and t_K is the Kolmogorov time scale [28].

When the DPS model is turned “off,” the constant particle sizes from the option flag “Particle size: Constant size” are used, which are defined in Closures Q3D (see figure A.6 in appendix “A.2 Edit case settings,” and figure 5.10). When it is turned “on,” the DPS model is applied to all dispersed fields (6 fields in 3-phase flow) and the following message appears: Particle size calculation enabled (figure 5.7) [28].

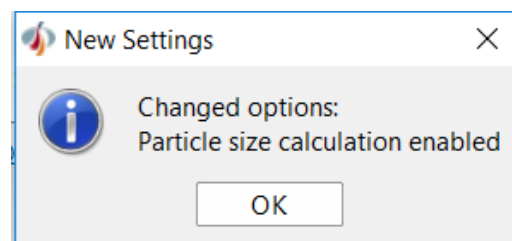


Figure 5.7: Particle size calculation enabled.

(eq. 5.1)

$$\frac{\partial}{\partial t} d_{p,km} + \nabla * (\bar{u}_{km}^i * d_{p,km}) = - \nabla * \left(\frac{\mu_K^T}{\rho_{km}} * \nabla d_{p,km} \right) + \frac{d_{p,km}^E - d_{p,km}}{t_{rel,km}^i}$$

$d_{p,km}$: The local (cell) particle size [m].

$d_{p,km}^E$: The equilibrium (Sauter mean) particle size, see equation 5.6 [m].

\bar{u}_{km}^i : The velocity of the droplet [m/s].

μ_K^T : The viscosity of the dispersed droplets [cP].

ρ_{km} : The fluid density of the dispersed droplets [kg/m³].

$t_{rel,km}^i$: The intrinsic coalescence or break up time, see equation 5.2 [s].

∇ : $\frac{d}{dx} + \frac{d}{dy} + \frac{d}{dz}$

(eq. 5.2)

$$t_{rel,km}^i = \begin{cases} \max(t_B, t_K; d_p \geq d_p^E \\ \max(t_C, t_K; d_p < d_p^E \end{cases}$$

t_B : Break up time scale [s].

t_C : Coalescence time scale [s].

t_K : Kolmogorov time scale [s].

The user also has the possibility of manually selecting the dispersed fields for which the DPS calculations are desired. The editing is done in the closures menu, by changing the input parameters in the flag option “Particle size: Variable particle size,” illustrated in figure 5.8 (false = 0, true = 1). Note that in the model option (lower left, figure A.4), the “Particle size calculation” must be set to “yes,” or else the DPS model will be turned “off” for all the fields (which is equivalent with manually writing 0 in all the fields in the flag option “Particle size: Variable particle size”) [28].

The fields are categorized from 1 to 6:

- Field number 1: Gas dispersed in oil (G/O).
- Field number 2: Gas dispersed in water (G/W).
- Field number 3: Oil dispersed in gas (O/G).
- Field number 4: Oil dispersed in water (O/W).
- Field number 5: Water dispersed in gas (W/G).
- Field number 6: Water dispersed in oil (W/O).

In this thesis, only the liquid-liquid dispersions are of interest. Therefore, for simplicity of the simulation, the field number 1, 2, 3, and 5 was set to false (0), and field number 4 and 6 was set to true (1), just like in figure 5.8 and table 5.2.

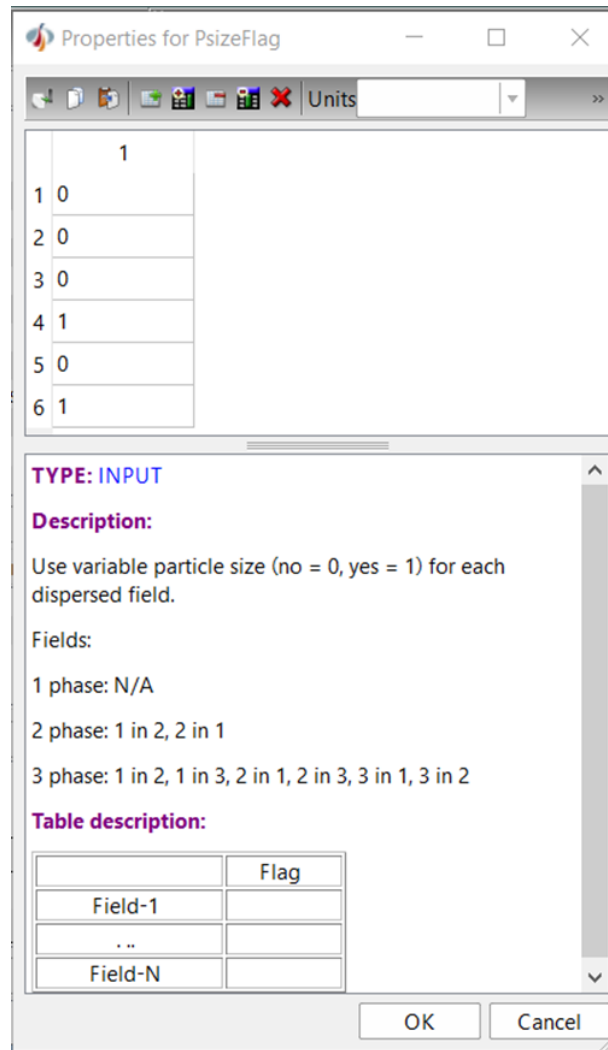


Figure 5.8: Particle size: Variable particle size flag

Emulsion: flag

To calculate the viscosity of the emulsion, LedaFlow uses the Krieger-Dougherty equation, which was explained in chapter 2.6. In the property editor in the closers menu (figure A.5), the user must click on the flag option **Emulsion: flag** and make sure that the viscosity calculations are turned “on,” by changing each of the three flag posts to true (1). The three flag posts represent the gas, oil and water phase, which all can have dispersed fields (figure 5.9).

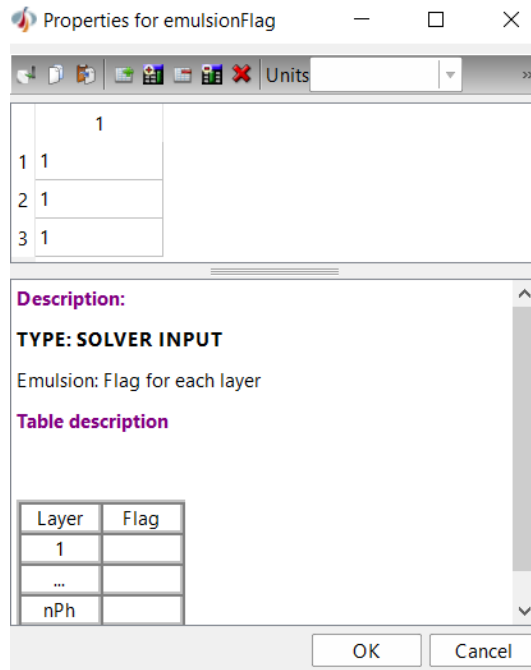


Figure 5.9: Emulsion: flag.

Particle size: Constant size

In the model option menu (in the case settings menu, figure A.4 in appendix), when “Particle size calculation” is turned “off,” the value of the particle diameter for dispersed fields is taken from this table (figure 5.10). The user can change the values manually. The default setting is 1 mm for bubbles and 0.5 mm for droplets. The simulation program has been very unstable during the work on this thesis. By changing the particle diameter to 0.1 mm, for all dispersed fields, the simulations became more stable. More information about this will be provided in chapter 6.

After looking at figure 2.10, and comparing the default settings with the droplet size distribution graph for emulsions, it probably makes sense that the simulation was unstable. 1 mm and 0.5 mm are enormous droplets compared to normal droplet sizes in typical emulsions. Even 0.1 mm is very large, and the largest droplets for typical emulsions are around this size. By changing the values in the option flag “Particle size: Constant size” to 0.01 mm, possibly an even more stable solution to the simulations could be accomplished, because this particle size diameter is in the middle of the normal distribution area for emulsion droplets (according to figure 2.10).

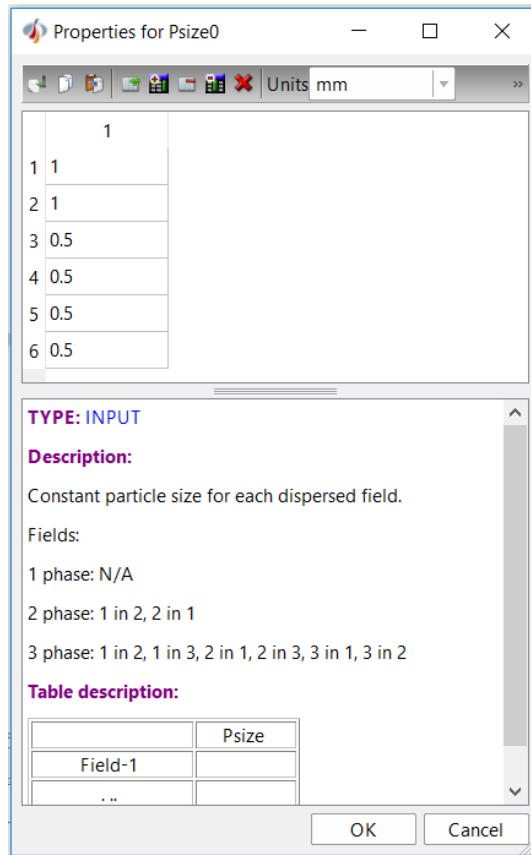


Figure 5.10: Particle size: Constant size

Particle break up- and coalescence time constants

“Particle break up time constant ($C_{breakup}$)” and “particle coalescence time constant ($C_{coalescenc}$)” are dimensionless time constants used in the equation for “break up time scale (t_B)” and “coalescence time scale (t_C)” for droplets and bubbles. This is illustrated in equation 5.3 and 5.4.

The calculated “break up time scale (t_B)” and “coalescence time scale (t_C)” are both presented in equation 5.2. When “the local particle size ($d_{p,km}$)” is equal to, or larger than, “the equilibrium (Sauter mean) particle size ($d_{p,km}^E$)”, than the greatest value of the “break up time (t_B),” and the “Kolmogorov time scale (t_K),” will be used as the value of $t_{rel,km}^i$, in equation 5.1. When “the local particle size ($d_{p,km}$)” is less than “the equilibrium (Sauter mean) particle size ($d_{p,km}^E$)”, than the greatest value of “the coalescence time scale (t_C)” and the “Kolmogorov time scale (t_K),” will be used as the value of $t_{rel,km}^i$, in equation 5.1.

(eq. 5.3)

$$t_B = C_{breakup} * \left(\frac{D^2}{\varepsilon} \right)^{\frac{1}{3}}$$

(eq. 5.4)

$$t_C = C_{coalescence} * \frac{D}{(0.2 * 6.9282 * \alpha * \sqrt{t_{ke}})}$$

- t_B : Break up time scale [s].
- t_C : Coalescence time scale [s].
- $C_{breakup}$: Break up time constant [dimensionless].
- $C_{coalescence}$: Coalescence time constant [dimensionless].
- D : Diameter of particle [m].
- ε : Turbulent dissipation (the rate at which turbulent kinetic energy is converted into thermal internal energy) [m^2/s^3].
- α : The volume fraction [dimensionless].
- t_{ke} : Turbulent kinetic energy (the mean kinetic energy per unit mass associated with eddies in turbulent flow) [Jm^2/s^2].

Kolmogorov microscales are the smallest scales in turbulent flow. The Kolmogorov microscales consist of the Kolmogorov length scale, Kolmogorov velocity scale and Kolmogorov time scale (equation 5.5). They are all universal and similar for every turbulent flow, and functions of the average of energy dissipation per unit mass ($\varepsilon, m^2/s^3$) and kinematic viscosity of the fluid ($\nu, m^2/s$) [31].

(eq. 5.5)

$$\tau_{\eta} = 6 * \left(\frac{\nu}{\varepsilon}\right)^{\frac{1}{2}}$$

- τ_{η} : The Kolmogorov time scale [s].
- ν : Kinematic viscosity of the fluid [m²/s].
- ε : Turbulent dissipation (the rate at which turbulent kinetic energy is converted into thermal internal energy) [m²/s³].

Note that the equation 5.5 is not the normal definition of Kolmogorov time scale. Going through the codes behind the LedaFlow Q3D simulation program, we discovered that the equation is multiplied by a factor of 6. There is no explanation available for this in the LedaFlow user manual.

By adjusting “the break up time constant ($C_{breakup}$)” and “the coalescence time constant ($C_{coalescence}$),” this should according to equation 5.3 and 5.4 affect “the break up time scale (t_B)” and “the coalescence time scale (t_C)”, which further will have an impact on the time value of $t_{rel,km}^i$.

Further, $t_{rel,km}^i$ has an impact on the DPS calculation (equation 5.1) for the evolution of average particle size. The viscosity model (Krieger-Dougherty equation, subchapter 2.6) is a function of the volume fraction of dispersion droplets in the continuous phase, and the maximum packing of dispersion droplets. If $t_{rel,km}^i$ has a significant effect on the evolution of average particle size, it would possibly result in an impact on the viscosity model as well. If the viscosity model is affected, this will show in the simulation results when calculating the torque.

Figure 5.11 illustrates the default values for the “particle break up time constant ($C_{breakup}$)” and “particle coalescence time constant ($C_{coalescence}$).”

As already mentioned, the fields are categorized from 1 to 6: [21]

- Field number 1: Gas dispersed in oil (G/O).
- Field number 2: Gas dispersed in water (G/W).
- Field number 3: Oil dispersed in gas (O/G).
- Field number 4: Oil dispersed in water (O/W).
- Field number 5: Water dispersed in gas (W/G).
- Field number 6: Water dispersed in oil (W/O).

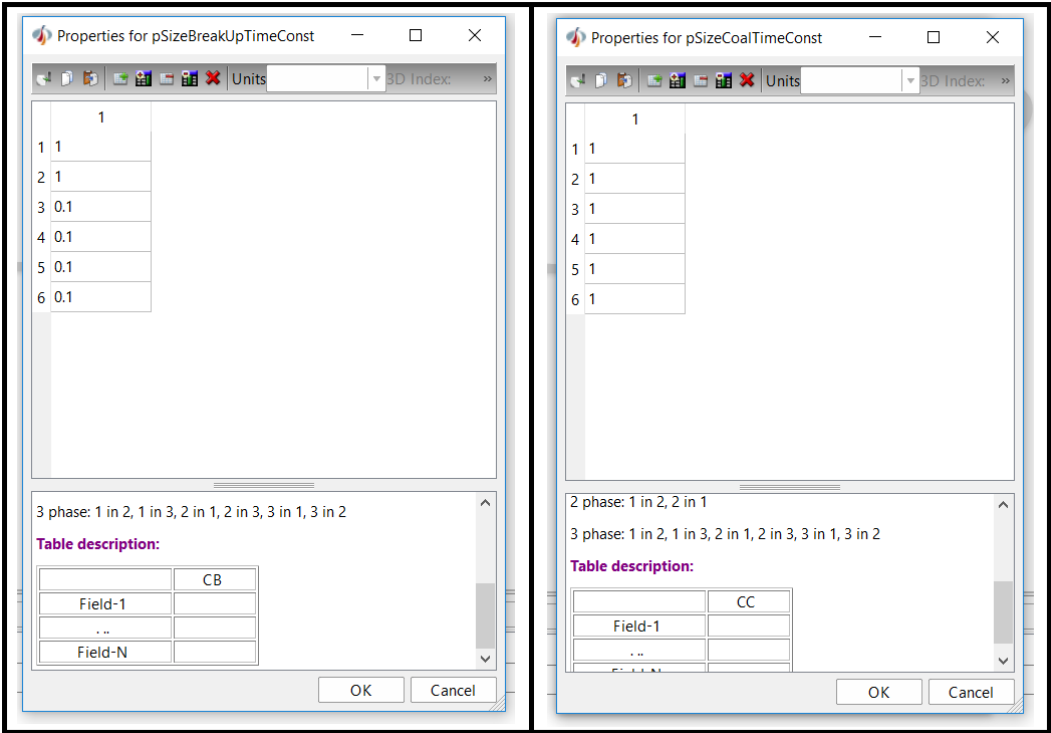


Figure 5.11: Particle break up- and coalescence time constants.

Particle size constant C_1 , C_2 , C_3

C_1 , C_2 and C_3 are model constants used in the Sauter mean diameter model (in fluid dynamics Sauter mean diameter is an average of particle size) for dispersed field (km), surrounded by continuous field (mm), illustrated in equation 5.6.

C_1 and C_2 are dimensionless constants used to tune the particle size calculation in equation 5.6. The default setting for C_1 is 1 for bubbles (field 1 and 2) and 0.02 for droplets (field 3, 4, 5 and 6), while C_2 is chosen to be $\frac{1}{10}$ of C_1 , illustrated in figure 5.12 (C_1 on the left, and C_2 on the right). C_3 represent the minimum particle sizes, with default values equal to 10 μm for bubbles and 1 μm for droplets [28].

(eq. 5.6)

$$d_{p,km}^E = \left(C_{1,km} \sqrt{\alpha_{km}^F} + C_{2,km} \right) \frac{\left(\frac{\sigma_{km}}{\rho_{mm}} \right)^{0.6}}{\varepsilon_{mm}^{0.4}} \left(\frac{\mu_{km}}{\mu_{mm}} \right)^{0.25} + C_{3,km}$$

$C_{1,km}$: Particle size constant, C_1 , of the dispersed phase [dimensionless].

$C_{2,km}$: Particle size constant, C_2 , of the dispersed phase [dimensionless].

$C_{3,km}$: Minimum particle size, of the dispersed phase [m].

$d_{p,km}^E$: The equilibrium (Sauter mean) particle size, of the dispersed phase [m]

α_{km}^F : The volume fraction, of the dispersed phase [dimensionless].

σ_{km} : Interfacial tension [mN/m].

ρ_{mm} : Fluid density, of the continuous phase [kg/m^3].

ε_{mm} : Turbulent dissipation, of the continuous phase [m^2/s^3].

μ_{km} : Fluid viscosity, of the dispersed phase [Pa-s].

μ_{mm} : Fluid viscosity, of the continuous phase [Pa-s].

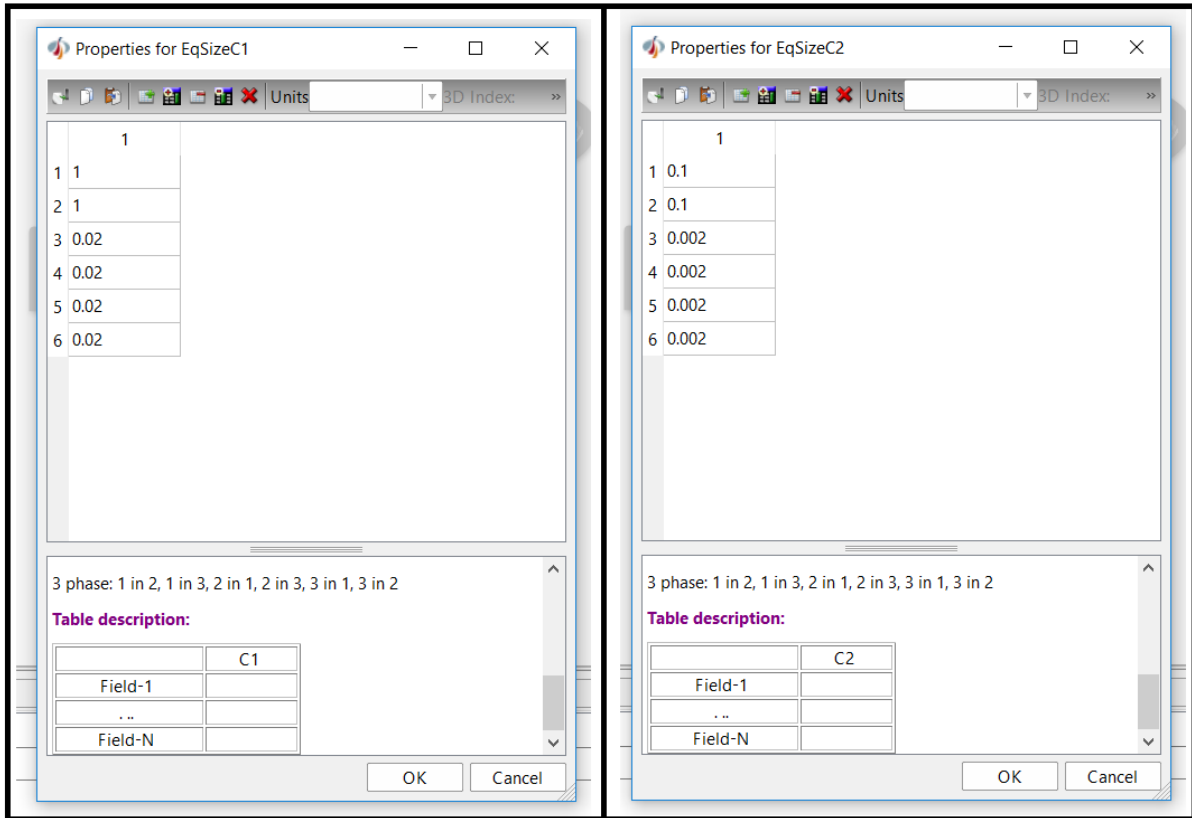


Figure 5.12: Default values for the C_1 (left) and C_2 (right) constants.

From the droplet size distribution graph in figure 2.10, it can be observed that the default bubble size ($10\ \mu\text{m}$) defined for C_3 are in between the normal distribution area for typical sizes for emulsion droplets, while the droplet size ($1\ \mu\text{m}$) is just outside the distribution area, on the lower side.

In this thesis, we focus on adjusting the dimensionless constants C_1 and C_2 , since they directly affect equation 5.6 when calculating the average particle sizes. We do not perform any adjustments on the C_3 constant. Simulation results from this work are given in chapter 7.

The main part of the performed simulation work in thesis, was to simulations with different values for the various input parameters (explained previously in this chapter), in order to determine their effect on the predicted emulsion viscosity and thus the torque values for the wheel. The results will be presented in chapter 7

6 Improvement of the LedaFlow Q3D model

Though the LedaFlow Q3D model has been developed over many years, this tool is still not a commercial tool, and has consequently not been tested and verified to the same extent as the LedaFlow 1D model. During the work of this thesis, the Q3D program has been improved along the way by SINTEF employees, as issues were identified in the testing. Several issues and improvements have been addressed.

6.1 Solving the stability problem

During the beginning of this thesis there were serious problems regarding the LedaFlow Q3D program. The simulation cases never managed to simulate more than a couple of seconds before error messages started to show up, and the simulations crashed. The program needed improvement, and have been updated several times during this period, before it finally worked as it should, in the beginning of May. In the meanwhile, numerous tests were conducted, to see if some of the input parameters could be adjusted to help stabilising the simulations.

Test no.1: To adjust the Courant number/CFL-number

In the beginning, it was attempted to use the DPS model (explained in section 5.3, and in the appendix) for all dispersed fields. There were problems getting a stable simulation, and the simulations often crashed after only a few seconds. First it was tested to reduce the Courant-Friedrichs-Lewy number (CFL-number, also referred to as the Courant number), which is a user-specified number that is multiplied by the automatically calculated time step based on the CFL-criterion.

To solve the physical models (transport equations for mass, momentum, energy and composition), LedaFlow solves a set of discretized equations. It integrates these equations between time points. The time interval used to integrate the equations between two time points is the size of the time step. The size of the time step is dynamic, and calculated at each new time step as a function of the results of the last time step (equation 6.1) [28][32].

The Courant number and Δt_{max} are specified by the user as the maximum allowed Courant number and maximum allowed time step-size respectively. These parameters can be adjusted in the numerical menu in the case settings, explained in appendix (lower right, figure A.4) [28].

The default value of the Courant number in LedaFlow Q3D is 0.3. It is well known that lowering the Courant number typically improves stability, and makes it easier for the solver to converge to a solution. The Courant number referred to as 0.8 in the appendix, and among the results and analysis in chapter 7, was decided as a standard value for the simulations, to speed up the process, after the stability problem was solved. In theory however, the simulation should be stable for any Courant number since the LedaFlow Q3D code is discretized fully implicit. Reducing the Courant number as low as 0.05 did however not lead to any significant improvement in the stability.

(eq. 6.1)

$$\Delta t = \min \left(\Delta t_{max}, CFL * \min_{k,i} \frac{\Delta x_i^u}{u_{k,i}} + \min_{k,i} \frac{\Delta y_i^u}{u_{k,i}} \right)$$

Δt : Calculated time step, calculated at the beginning of each new time step [s].

Δt_{max} : The maximum allowed time step-size [s].

CFL : The Courant number/CFL-number [dimensionless].

Δx : The axial grid size [m].

Δy : The radial grid size [m].

$u_{k,i}$: The velocity of field k in cell i [m/s].

Test no.2: To switch to first-order upwind scheme

It was then tested to switch from the default convection scheme to the more diffusive and stable first-order upwind (FOU) scheme to see if this could improve the results (see appendix, and figure A.5). The FOU scheme is known to be very stable, but also less accurate. This however did not lead to any significant improvement in the stability for the simulations in this thesis.

The convection schemes are used to calculate the values of e.g. velocity of the fluid, when this information is needed in parts of the discretized model where it is not defined. This is only done for the convection parts of the equations, since this is the only place we, of numerical stability causes, would need calculations like this.

The velocity is stored on the cell surfaces between the cells, while mass and energy (enthalpy) are stored in the middle of the cells. FOU scheme (named Interpol_US1 in LedaFlow Q3D) is a simplification method which take the values stored in the cells to the left or right, from the direction from which the velocity field comes from. From left for positive speed and right at negative speed.

For many other convection schemes, there is a more advanced interpolation function that involves the closest cells around the area of interest. The equation named Interpol_ACUTER in LedaFlow Q3D is one of these advanced interpolation functions. Many methods provide fairly similar and accurate answers, but the FOU stands out by being quite simple and robust (thus, also very stable because it smears out waves), but also less accurate than the other schemes.

Test no.3: To reduce the number of grid cells

Tests with a reduced number of grid cells were also performed, which lead to improved stability. This was however not desirable, as this also leads to more numerical diffusion and a less accurate results.

Test no.4: To turn “off” the dynamic particle size model

After further testing it was discovered that the stability issues were improved by turning “off” the DPS model. This was however not desirable, as we wanted to use the DPS model in our testing.

Test no.5: To turn “off” the dynamic particle size modelling for the dispersed fields of no interest (G/O, G/W, O/G, W/G)

More testing revealed that the stability issues were improved by turning “off” the DPS modelling for the dispersed fields that were not of interest in this study (gas in oil, gas in water, oil in gas, and water in gas). See section 5.3, and figure 5.8. Most likely, the default values for the particle size model for these fields are not good, and can lead to too large bubble/droplet sizes that seemed to cause the stability problems. It is possible that we could have obtained stable simulations with the DPS model turned “on,” by finding better input parameters for these fields for the DPS model. In this study however, we focused mainly on the O/W and W/O dispersions, and the experiments on the flow wheel simulator showed little or none entrained gas in the liquid, or entrained liquid in the gas. Turning “off” the DPS model for these fields led to more stable simulations, although simulations still stopped from time to time. It should also be mentioned that a small bug in the program was discovered (not explained in this thesis), and solving this bug also improved the stability of the simulations.

Test no.6: to adjust the user-specified constant particle sizes

Finally, it was discovered that also the user-specified constant particle sizes (see section 5.3, and figure 5.10, about input parameters in the option flag “Particle size: Constant size”) were important for the fields where the DPS model was used. This is because the DPS model is only used for turbulent flow, while for laminar flow the constant particle sizes are used. Since the simulations starts from zero velocity the flow will be laminar at the start of the simulation, and the constant sizes are used.

By reducing the input parameters to 0.1 mm for all the phases in the option flag “Particle size: Constant size,” the simulations became much more stable. Later it was discovered that the default settings for constant particle sizes were larger than the normal droplet size distribution for typical emulsions (figure 2.10). However, the adjustment of input

parameters in the option flag “Particle size: Constant size” was done before checking with the droplet size distribution graph. It turns out that 0.1 mm is among the largest droplets in the droplet size distribution area for emulsion.

6.2 Additional problems that was solved

Other improvements than stability issues, were also addressed during this study. During the initial testing, it was discovered that the emulsion-viscosity model in LedaFlow Q3D was only implemented for oil-gas mixtures. In this study, oil-water emulsions were the topic, and SINTEF had to implement a viscosity model for oil-water emulsions.

Some other details in the program were also improved, like the possibility to specify the initial pressure in the wheel (which was hardcoded before). The LedaFlow Q3D wheel simulator is a special version of the LedaFlow Q3D code, specifically altered to be able to simulate wheel-experiments. The two major differences from the regular Q3D code are periodic boundary conditions and a moving wall. The velocity of the wall was not taken into account everywhere for the wall friction, so this was also improved by SINTEF during the initial testing.

Additionally, some new data export functionality was added by SINTEF to the code towards the end of this study.

In summary, there has been significant improvements to the LedaFlow Q3D wheel code. The improvements are both in terms of the input values to the simulations, but also to the code itself from bug fixing and added functionality and physics.

7 Results and analysis of simulations

Multiple simulations have been completed, by systematically adjusting several input parameters like; break up time constant ($C_{breakup}$), coalescence time constant ($C_{coalescence}$), particle size constant (C_1 and C_2), constant particle sizes (with “Particle size calculations” ON or OFF), water cut/phase fractions, and wheel velocity.

“Break up time constant ($C_{breakup}$),” “coalescence time constant ($C_{coalescence}$)” and “particle size constant (C_1 and C_2),” were all tested to investigate how sensitive the simulation results are to these inputs, and to try to use these parameters to tune the simulations to match the output of torque in the wheel flow experiment (for the wheel velocity: 2 m/s, and output of torque: 4.5 Nm). The testing of various “constant particle sizes” (with or without the DPS model) and water cuts, was only performed to make sure that the LedaFlow Q3D program was working as it should do, and to illustrate the effect of these parameters on the simulations. Finally, in the end, the knowledge that was acquired from these simulation-tests were put to a final test. Some of the simulations was successfully tuned to match with the results from the wheel flow experiment (4.5 Nm), for a wheel velocity of 2 m/s. The final test was an attempt to check if the same input parameters that successfully tuned these simulations, would work when tuning simulations with a wheel velocity of 1 m/s (output torque: 1.7 Nm). An overview of the various tests is given in the flowcharts in figure 7.1 and figure 7.2.

While the settings in table 7.1 has been systematically changed throughout the testing, each simulation has been conducted with the standard input parameters in table 7.2.

Settings in closures Q3D	
Particle size: Variable particle size	[1=0], [2=0], [3=0], [4=1], [5=0], [6=1]
Particle size: constant size	[1=0.1], [2=0.1], [3=0.1], [4=0.1], [5=0.1], [6=0.1]
Particle size break up time constant	[4 (O/W) = 0.1], [6 (W/O) = 0.1]
Particle size coalescence time constant	[4 (O/W) = 1], [6 (W/O) = 1]
Particle size constant C1	[4 (O/W) = 0.02], [6 (W/O) = 0.02]
Particle size constant C2	[4 (O/W) = 0.002], [6 (W/O) = 0.002]
Phase fractions	[Gas = 0.6], [Oil = 0.1], [Water = 0.3]

Table 7.1: Settings in closures Q3D.

PVT object	
Gas density [kg/m ³]	1,1347
Gas viscosity [Pa-s]	1,7794*10 ⁻⁵
Gas compressibility [kg/m ³ /bar]	1,1303
Oil density [kg/m ³]	790
Oil viscosity [Pa-s]	0,0018
Oil compressibility [kg/m ³ /bar]	0
Water density [kg/m ³]	997
Water viscosity [Pa-s]	0,00089
Water compressibility [kg/m ³ /bar]	0
Pressure, Pref [bar]	1
Temperature, Tref [C°]	25
Interfacial tension between O&W [N/m]	0,025
Interfacial tension between G/W [N/m]	0,072
Interfacial tension between G/O [N/m]	0,0207
Numerical	
Time to advance to solution [s]	40
CFL	0,8
Solver settings optimized for:	Robustness
Number of processors:	1
Initialize	
Friction pressure grad., bar/m	0
Temperature, Kelvin	298,15
Pressure, bar	1
Patches - initialization	
Gas (input fraction: 0,6)	Start length: 5,97, stop length: 3,45
Oil left side (input fraction: 0,1)	Start length: 5,65, stop length: 5,97
Oil right side (input fraction: 0,1)	Start length: 3,45, stop length: 3,77
Water (input fraction 0,3)	Start length: 3,77, stop length: 5,65
Settings in closures Q3D	
Emulsion flag	[1=1], [2=1], [3=1]

Table 7.2: Standard input parameters for all simulations.

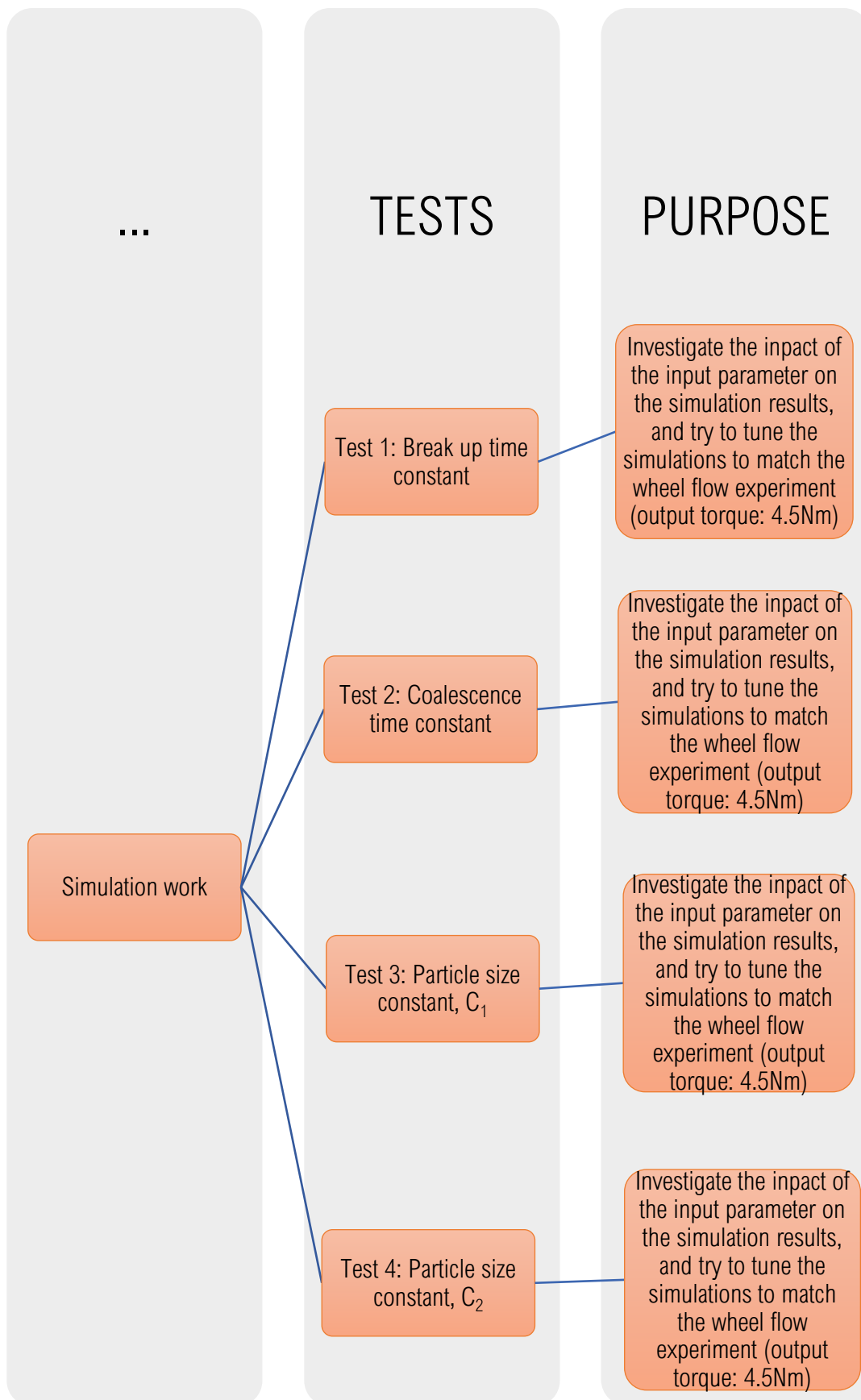


Figure 7.1: Flowchart of test 1 – 4.

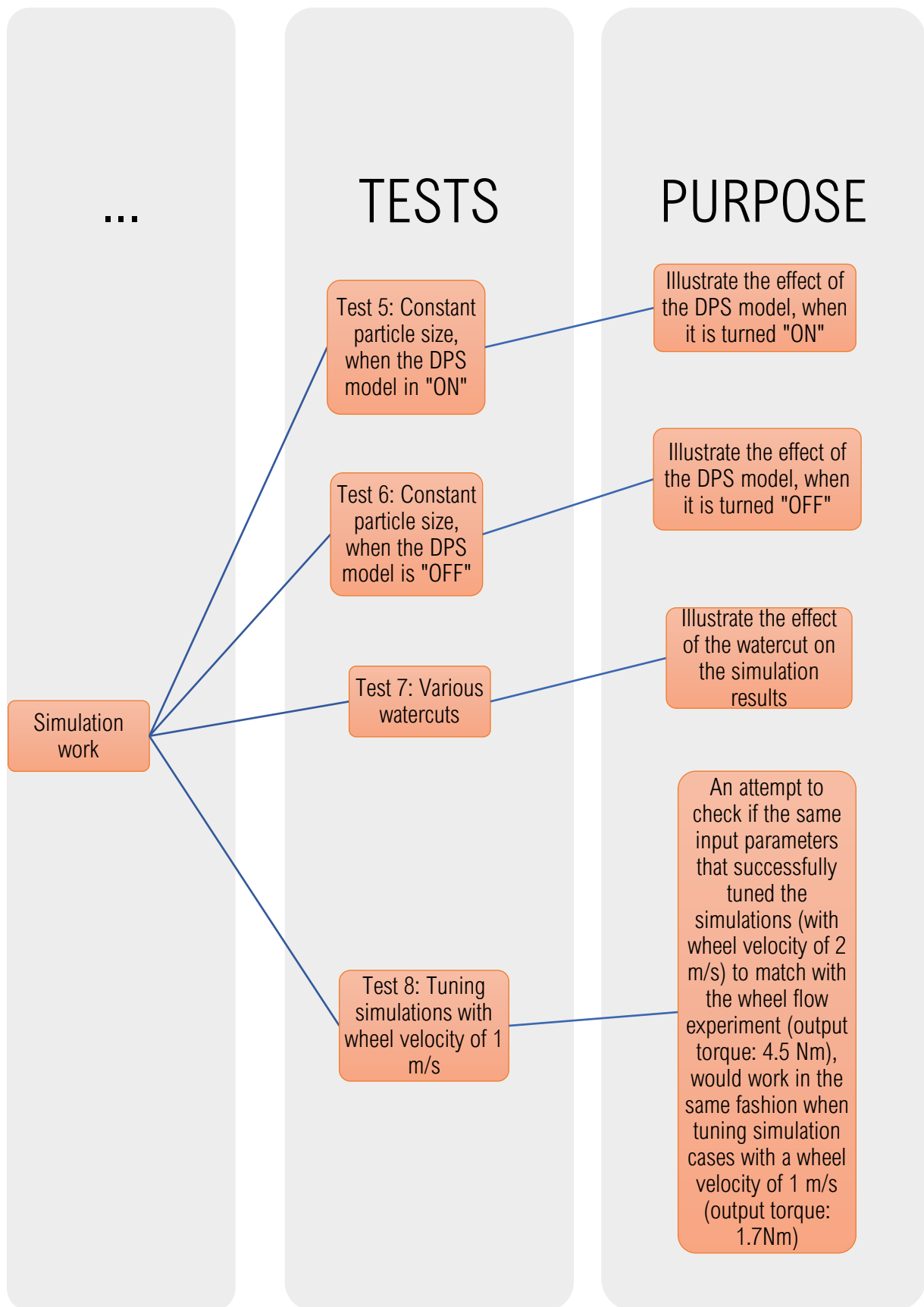


Figure 7.2: Flowchart of test 5 - 8.

7.1 Break Up Time Constant and Coalescence Time Constant

The purpose of test 1 and test 2

The reason why we wanted to perform tests on adjusting “the break up time constant ($C_{breakup}$)” and “the coalescence time constant ($C_{Coalescence}$)” was because of their role in equation 5.2, and indirectly in equation 5.1. Equation 5.2 illustrates how the value of $t_{rel,km}^i$ in equation 5.1 is decided, and equation 5.1 calculates the average particle size. When “the local particle size ($d_{p,km}$)” is equal to, or larger than “the equilibrium (Sauter mean) particle size ($d_{p,km}^E$)”, then the greatest value of “the break up time scale (t_B),” and “the Kolmogorov time scale (t_K),” will be used as the value of $t_{rel,km}^i$. When “the local (cell) particle size ($d_{p,km}$)” is lower than “the equilibrium (Sauter mean) particle size ($d_{p,km}^E$)”, then the highest value of “the coalescence time scale (t_C)” and “the Kolmogorov time scale (t_K),” will be used as the value of $t_{rel,km}^i$, in equation 5.1.

By adjusting “the break up time constant ($C_{breakup}$),” we can adjust the value of “the break up time scale (t_B),” according to equation 5.3. Thus, it is possible to influence which of “the break up time scale (t_B),” and “the Kolmogorov time scale (t_K)” that has the highest value. In the same way, by adjusting the value of “the coalescence time constant ($C_{Coalescence}$),” we can adjust the value of “the coalescence time scale (t_C),” according to equation 5.4. Thus, it is also possible to influence which of “the coalescence time scale (t_C)” and “the Kolmogorov time scale (t_K)” that has the highest value.

To calculate the ratio between the various time scales, equation 5.3 and 5.5 were combined into equation 7.1, and equation 5.4 and 5.5 into equation 7.2. By calculating these equations, we could investigate which of the time scales that would be represented by $t_{rel,km}^i$ in equation 5.1, and possibly get the understanding of whether we should increase or decrease “the break up time constant ($C_{breakup}$)” and “the coalescence time constant ($C_{Coalescence}$),” to be able to influence the value of $t_{rel,km}^i$.

If the results from the calculations was larger than 1, then “the Kolmogorov time scale (t_k)” would be the largest value, and hence represent $t_{rel,km}^i$ in equation 5.1, and vice versa. A summary of this process is given in the flowchart in figure 7.3.

(eq. 7.1)

$$\frac{t_k}{t_B} = \frac{6 * \left(\frac{\nu}{\varepsilon}\right)^{\frac{1}{2}}}{C_{breakup} * \left(\frac{D^2}{\varepsilon}\right)^{\frac{1}{3}}}$$

(eq. 7.2)

$$\frac{t_k}{t_c} = \frac{6 * \left(\frac{\nu}{\varepsilon}\right)^{\frac{1}{2}}}{C_{coalescence} * \frac{D}{(6.9282 * \alpha * \sqrt{t_{ke}})}}$$

- t_B : Break up time scale [s].
- t_k : The Kolmogorov time scale [s].
- t_c : Coalescence time scale [s].
- $C_{breakup}$: Break up time constant [dimensionless].
- $C_{coalescence}$: Coalescence time constant [dimensionless].
- D : Diameter of particle [m].
- ε : Turbulent dissipation (the rate at which turbulent kinetic energy is converted into thermal internal energy) [m^2/s^3].
- ν : Kinematic viscosity of the fluid [m^2/s].
- α : The volume fraction [dimensionless].
- t_{ke} : Turbulent kinetic energy (the mean kinetic energy per unit mass associated with eddies in turbulent flow) [m^2/s^2].

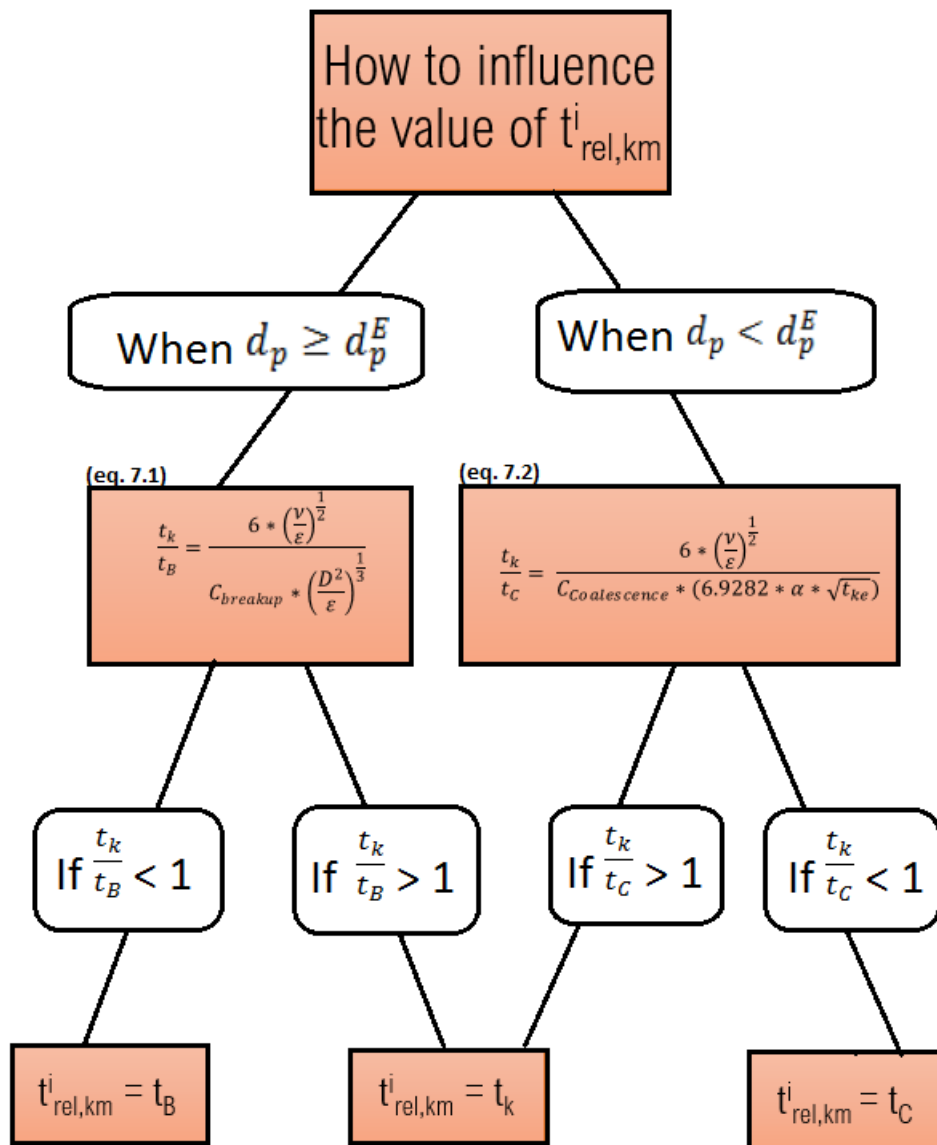


Figure 7.3: Flowchart of how to influence the value of $t^i_{rel,km}$.

Equation 5.1 is very complex, and it is difficult to put the “local (cell) particle size ($d_{p,km}$)” alone on one side of the equation. Thus, it is also difficult to know exactly how much $t^i_{rel,km}$ will affect the evolution of “the local particle size ($d_{p,km}$).” The aim is to try to adjust “the break up time constant ($C_{breakup}$)” and the “the coalescence time constant ($C_{Coalescence}$)” enough, so we can simulate cases with various values for $t^i_{rel,km}$ and further see how sensitive these parameters are regarding the simulation results.

By adjusting the value of “the break up time constant ($C_{breakup}$)” and “the coalescence time constant ($C_{Coalescence}$),” we should in theory be able to make an effect on the value of $t_{rel,km}^i$, which influence the calculation of the evolution of average particle size. As already mentioned, the viscosity model (Krieger-Dougherty equation, subchapter 2.6) is a function of the volume concentration of dispersion droplets in the continuous phase, and the maximum packing of dispersion droplets. If $t_{rel,km}^i$ has a significant effect on the evolution of average particle size, it would possibly result in an impact on the viscosity model as well. If the viscosity model is affected, this will show in the simulation work when calculating the torque. Thus, it might be possible to use this knowledge to tune specific simulations in LedaFlow Q3D to be more identical with the results produced from the wheel flow simulator (output of torque: 4.5 Nm, see figure 5.3).

Execution method and input parameters, for test 1 and test 2

The default value of “the break up time constant ($C_{breakup}$)” was 0.1. Table 7.3 illustrates the various values of “the break up time constant ($C_{breakup}$)” for the simulation cases 1.1 – 1.13 (simulation 1.4 and 1.5 has been left out since they had a different velocity than the rest). In advance, we did not know which was the greatest value of “the break up time scale (t_B),” and “the Kolmogorov time scale (t_K),” for the default values of input parameters. In our first attempts (simulation 1.1 – 1.10) we tried to simulate several cases when the value of “the break up time constant ($C_{breakup}$)” was both systematically increased and decreased, to investigate if this made any effect on the simulation results.

	Break up time constant
Simulation 1.1/ Default value	0.1
Simulation 1.2	0.05
Simulation 1.3	0.2
Simulation 1.6	0.005
Simulation 1.7	0.001
Simulation 1.8	20
Simulation 1.9	0.0005
Simulation 1.10	100
Simulation 1.11	500
Simulation 1.12	5000
Simulation 1.13	10 000

Table 7.3: Input values for “break up time constant.”

The default value of “the coalescence time constant ($C_{Coalescence}$)” was 1. Table 7.4 illustrates the values of “the coalescence time constant ($C_{Coalescence}$)” for the various simulation cases. In advance, we did not know which was the highest value of “the coalescence time scale (t_c)” and “the Kolmogorov time scale (t_K),” for the default values of the input parameters. In our first attempts (simulation 2.1 – 2.4) we tried to simulate several cases when the value of “the coalescence time constant ($C_{Coalescence}$)” was both systematically increased and decreased, to investigate if this made any effect on the simulation results.

	Coalescence time constant
Simulation 1.1/Default value	1
Simulation 2.1	0.5
Simulation 2.2	2
Simulation 2.3	0.005
Simulation 2.4	200
Simulation 2.5	0.000001
Simulation 2.6	1000'000

Table 7.4: Input values for “coalescence time constant”.

After completing the first simulations (simulation 1.1 – 1.10, and simulation 2.1 – 2.4), we wanted to try to calculate the ratio between the various time scales (t_B , t_c , t_K), to investigate which of these time scales that had the largest value, for a given time step at a given position, in the various simulations. If the Kolmogorov time scale is always larger than the other time scales, then the adjustment of the coalescence- or break up time constants will have no effect on the simulation results.

Matlab codes, written by Ivar Eskerud Smith at SINTEF, made it easier to extract the necessary data from the simulations in LedaFlow Q3D, introduce them to equation 7.1 and 7.2, and calculate the results for user defined time steps (e.g between two specific time steps, or information from the entire simulation). When “the local particle size ($d_{p,km}$)” was equal to, or larger than, “the equilibrium (Sauter mean) particle size ($d_{p,km}^E$)”, then equation 7.1 was calculated. When “the local particle size ($d_{p,km}$)” was lower than “the equilibrium (Sauter mean) particle size ($d_{p,km}^E$)”, then equation 7.2 was calculated (see figure 7.3).

The output of the Matlab calculations was a plot of $\frac{t_{kol}}{t_{rel}}$ versus position (t_{kol} is “the Kolmogorov time scale (t_K),” and t_{rel} is either “the break up time scale (t_B)” or the “the coalescence time scale (t_C),” depending on the particle sizes). It is important to understand that the Matlab codes cannot calculate the ratio of $\frac{t_{kol}}{t_{rel}}$ (equation 7.1 or 7.2) without the output data from a previous completed simulation. It is also important to understand that the ratio of $\frac{t_{kol}}{t_{rel}}$ versus position will most likely vary for different time steps in the simulation period, because the average particle size vary a lot during the simulation. In other words, the ratio of $\frac{t_{kol}}{t_{rel}}$ versus position will possibly have various solutions whether the calculated time steps are in the beginning of the simulation period (when the fluids start to mix) or in the end of the simulation period (when the simulation has reached a steady state, with an equilibrium between break up and coalescence). Due to this it was decided to calculate the ratio of $\frac{t_{kol}}{t_{rel}}$ for the entire simulation period.

The valuable information to look for in these graphs ($\frac{t_{kol}}{t_{rel}}$ versus position) are the values on the y-axis. The reason for calculating the ratio of $\frac{t_{kol}}{t_{rel}}$ is simply to know which one of the various time scales (t_B, t_C, t_K) that represent $t_{rel,km}^i$ in equation 5.1. If the ratio of $\frac{t_{kol}}{t_{rel}}$ is lower than 1, it means that $t_{rel,km}^i$ is represented by either “the break up time scale (t_B)” or “the coalescence time scale (t_C).” If the ratio of $\frac{t_{kol}}{t_{rel}}$ is higher than 1, then “the Kolmogorov time scale (t_K)” has the highest value, and hence represent $t_{rel,km}^i$ in equation 5.1 (look at figure 7.3).

The Matlab calculations was calculated for the following simulations:

- Simulation 1.1 (with the default values).
- Simulation 1.9 (with the lowest value of $C_{breakup}$, of the simulations 1.1 – 1.10).
- Simulation 1.10 (with the highest value of $C_{breakup}$, of the simulations 1.1 – 1.10).
- Simulation 2.3 (with the lowest value of $C_{Coalescence}$ of the simulation 2.1 – 2.4)
- Simulation 2.4. (with the highest value of $C_{Coalescence}$ of the simulation 2.1 – 2.4)

The results from these Matlab calculations gave an insight, that led to the choice of values for the input parameters in the last simulations for test 1 and test 2.

In the last simulations for test 1 (simulation 1.11, 1.12 and 1.13) the values for “the break up time constant ($C_{breakup}$)” was increased significantly to see how this affected the output of torque, viscosity distribution and particle size distribution. This decision was based on the output from the Matlab calculations, which revealed that the ratio of $\frac{t_{kol}}{t_{rel}}$ versus position was:

- Around 1 for simulation 1.1 (maximum ratio of 3.8, minimum ratio of approximately 0, and average ratio around 1).
- Very high values for simulation 1.9 (ratio from almost 0 to 1000, with average of approximately 200).
- Very low values for simulation 1.10 (ratio always less than 0.005).

These Matlab results are illustrated in figure 7.4. From examining these results, it is understood that it is necessary to increase the value of “the break up time constant ($C_{breakup}$)” to make sure that the ratio of $\frac{t_{kol}}{t_{rel}}$ is less than 1. By decreasing the value of $C_{breakup}$ in simulation 1.9, the ratio of $\frac{t_{kol}}{t_{rel}}$ became very large. Vice versa, by increasing the value of $C_{breakup}$ in simulation 1.10, the ratio of $\frac{t_{kol}}{t_{rel}}$ became very small.

Since simulation 1.10 showed a calculated ratio of $\frac{t_{kol}}{t_{rel}}$ less than 1, this means that $t_{rel,km}^i$ was represented by “the break up time scale (t_B)” in this simulation. By increasing the value of “the break up time constant ($C_{breakup}$),” it would therefore be possible to simulate several cases with varying values of $t_{rel,km}^i$, and investigate how this would impact on the output of torque.

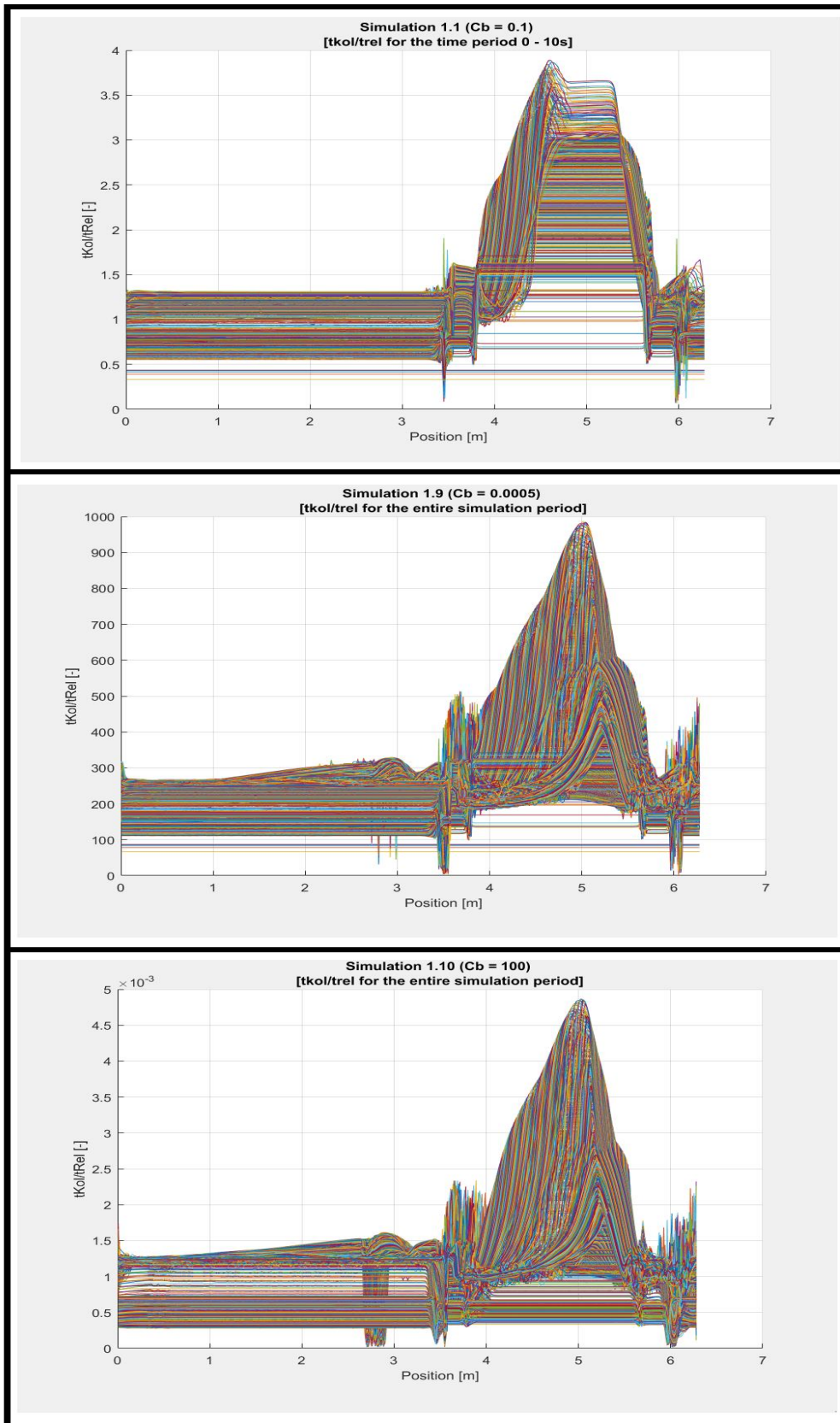


Figure 7.4: “ t_{kol}/t_{rel} vs. position” for simulation 1.1, 1.9 and 1.10.

In the last simulations for test 2 (simulation 2.5 and 2.6), the values for “the coalescence time constant ($C_{Coalescence}$)” was increased and decreased by a factor for 10^6 to investigate how this affected the output of torque, viscosity distribution and particle size distribution. This decision was also based on the Matlab calculations of the ratio of $\frac{t_{kol}}{t_{rel}}$ versus position (figure 7.5). In this case, the matlab calculations revealed that changing the $C_{Coalescence}$ had no influence on ratio of $\frac{t_{kol}}{t_{rel}}$ versus position for the simulations 2.3 and 2.4. In a final attempt to influence the ratio of $\frac{t_{kol}}{t_{rel}}$, and hence the output of torque, it was decided to increase and decrease the values for “the coalescence time constant ($C_{Coalescence}$)” significantly.

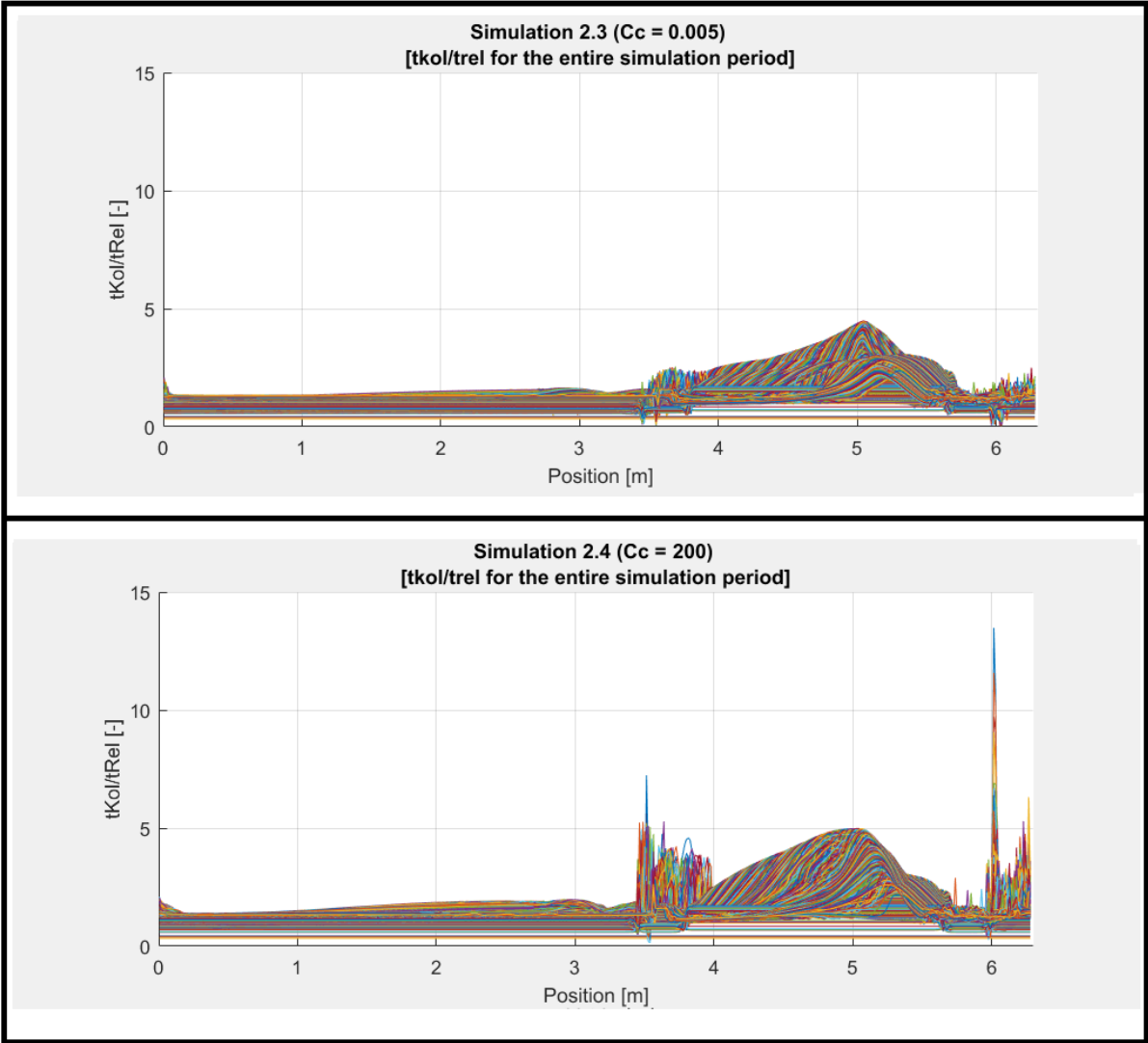


Figure 7.5: “ t_{kol}/t_{rel} vs. position” for simulation 2.3 and 2.4.

Presentation of the simulation results for test 1 (break up time constant)

Figure 7.6 illustrates the simulation cases 1.1 – 1.10 (simulation 1.4 and 1.5 has been left out in figure 7.1, on purpose). In these cases, the adjustments of “the break up time constant ($C_{breakup}$)” was not large enough to affect the output of torque. Note that the ratio of $\frac{t_{kol}}{t_{rel}}$ was less than 1 in simulation 1.10 (figure 7.4). This illustrates that, although $t_{rel,km}^i$ was represented by the value of “the break up time scale (t_B)” in simulation 1.10, the value of t_B (represented as $t_{rel,km}^i$ in equation 5.1) was still not large enough to have a visible impact on the output of torque.

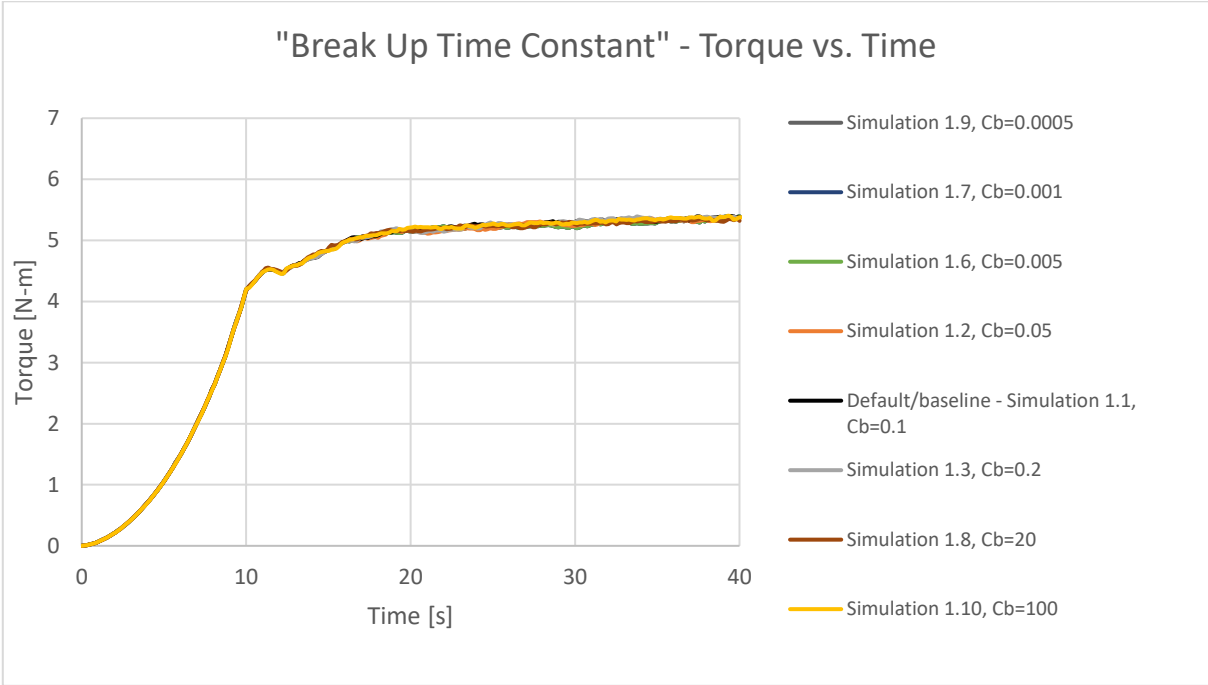


Figure 7.6: Break up time constant - Torque vs. Time, simulation 1.1 – 1.10.

After realizing that “the break up time constant ($C_{breakup}$)” had to be increased by a significant factor, to make sure to make an impact on the calculation of torque, the simulation cases 1.11 – 1.13 was conducted (figure 7.7).

Figure 7.7 illustrates that “the break up time constant ($C_{breakup}$)” of 500 (simulation 1.11) was still not high enough to make a visible impact on the simulation results of torque. In simulation 1.12 and 1.13, “the break up time constant ($C_{breakup}$)” was

increased to 5000 and 10 000, respectively. In these cases, eventually “the break up time scale (t_B)” (represented as $t_{rel,km}^i$) was large enough to make a visible impact on the output of torque. Compared to the factors that “the break up time constant ($C_{breakup}$)” had been increased, the impact on the simulation results of torque was low, but visible.

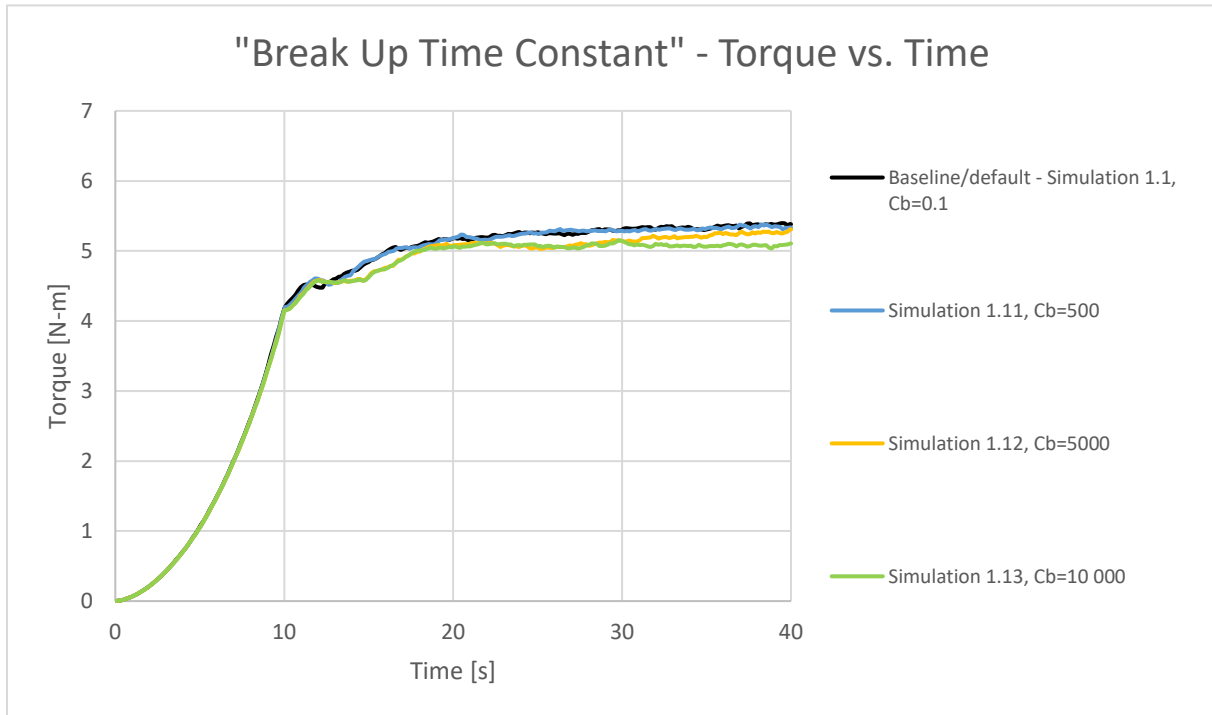


Figure 7.7: Break up time constant – Torque vs. Time, simulation 1.11 – 1.13.

Figure 7.8 illustrates the particle size distribution inside the wheel, for the specific time of 38 s after the simulation process has started. Position 0 m and 6.28 m, illustrates the middle left part of the wheel (“nine O’clock,” see figure 5.6). The y-values (represented as various coloured lines in the graphs) represent ten different heights in the cross section of the wheel pipe (see figure 4.2).

As one can see, the particle size distribution is almost identical for simulation 1.1, 1.9, 1.10 and 1.11. However, for the last two simulations (simulation 1.12 with $C_{breakup}=5000$, and simulation 1.13 with $C_{breakup}=10\ 000$), the particle sizes has started to increase. The reason for the peaks observed around the positions 3.5 m and 6.2 m, is because these areas represent the transition areas between the oil and water phases during the rotation of the wheel. The area between these peaks will eventually

experience a steady state, but the transition areas will stay more turbulent and still experience mixing of the fluid phases. The various coloured lines in the graphs, represent the various positions in the lateral direction of the cross section of the pipe. From these lines, it is understood that there will be some differences between the particle sizes depending on the lateral position in the pipe.

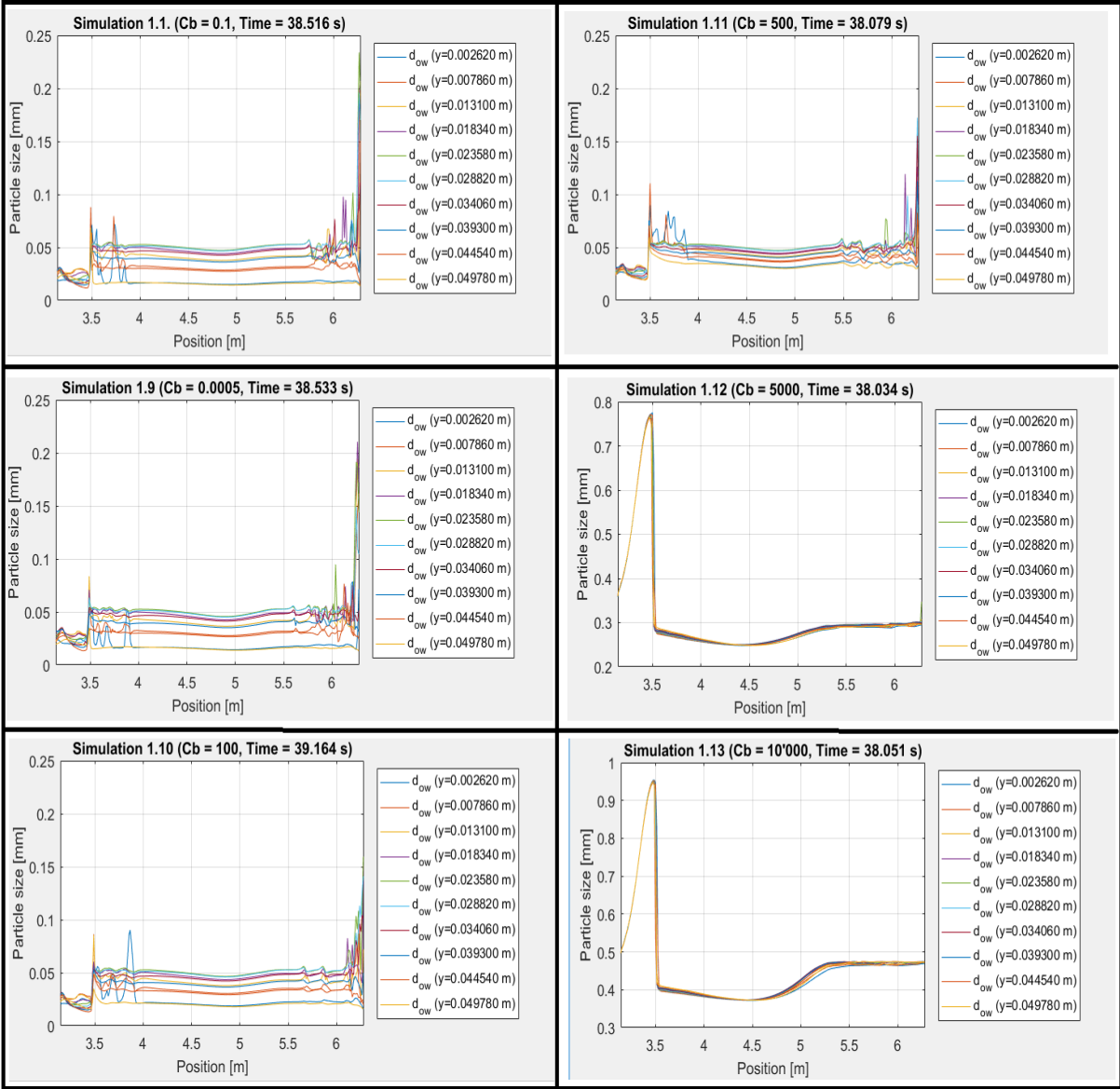


Figure 7.8: Break up time constant – Particle size vs. Position

Figure 7.9 illustrates the viscosity of the fluid inside the wheel, at various positions on the lower half of the wheel, for the specific time of 38 s after the simulation process has started. Position 3.14 m is at the middle right of the wheel (“three o’clock”), and the

position 6.28 m is at the middle left of the wheel (“nine o’clock,” see figure 5.6). The y-values, represented as coloured lines in the graphs, represent ten different heights in the cross section of the wheel pipe (see figure 4.2).

As one can see, the mix. field viscosity distribution stays almost identical for simulation 1.1, simulation 1.9, simulation 1.10 and simulation 1.11. However, for the last two simulations (simulation 1.12 with $C_{breakup}=5000$, and simulation 1.13 with $C_{breakup}=10\ 000$), the mix. field viscosity distribution has started to change. The reason for the peaks observed around the positions 3.5 m and 6.2 m, is the same explained for the particle size distribution graph. These areas represent the transition areas between the oil and water phases during the rotation process of the wheel. The area between these peaks will eventually experience a steadier state, but the transition areas will be more turbulent and still experience mixing of the fluid phases.

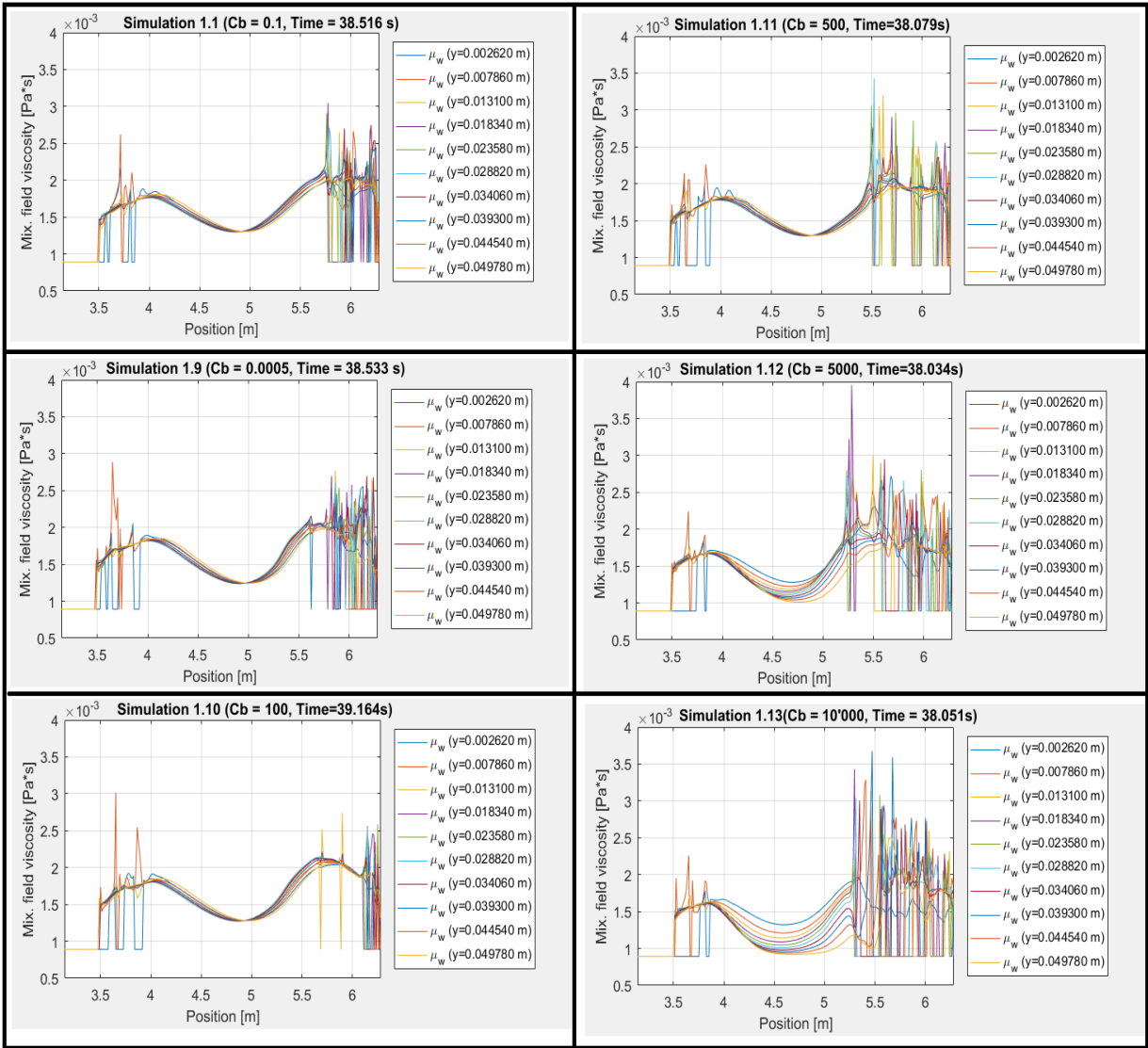


Figure 7.9: Break up time constant – Viscosity vs. Position.

Presentation of the simulation results for test 2 (coalescence time constant)

Figure 7.10 illustrates how changing “the coalescence time constant ($C_{Coalescence}$)” affected the torque, for the simulation cases 2.1 – 2.6. It is obvious that changing “the coalescence time constant ($C_{Coalescence}$)” did not affect the output of torque in this system. Before investigating the simulation cases in Matlab, we could not know for sure the reason for these results. Figure 7.5 (simulation 2.3 and 2.4) and 7.11 (simulation 2.5 and 2.6) illustrates that $\frac{t_{kol}}{t_{rel}}$ ratio does not really change by adjusting “the coalescence time constant ($C_{Coalescence}$).”

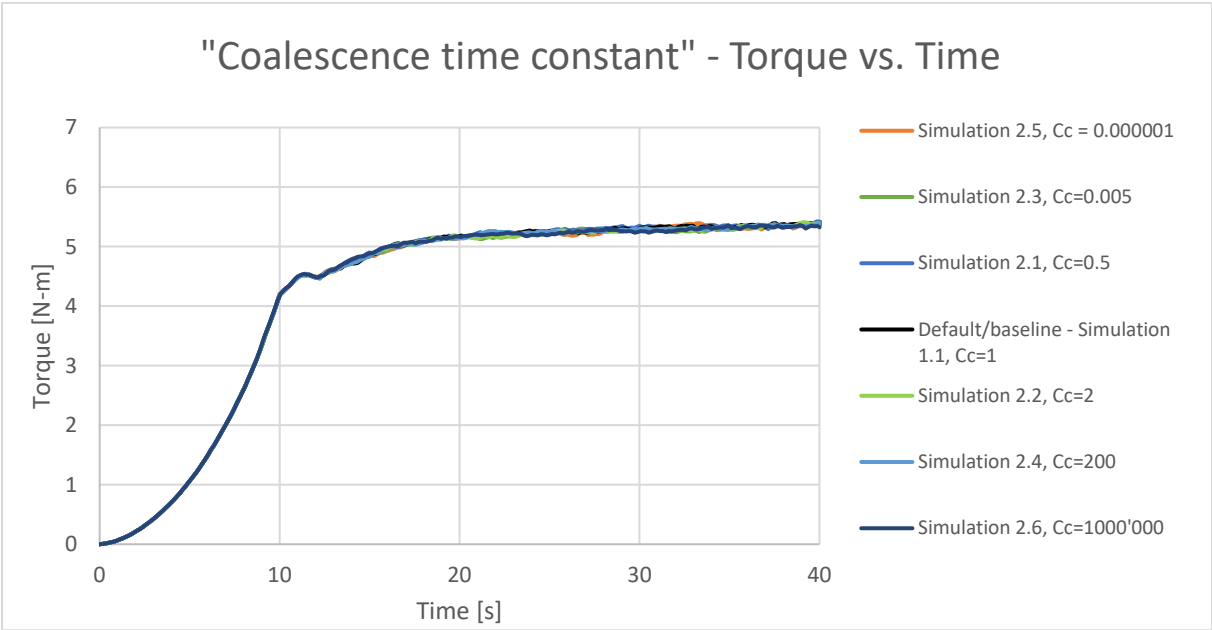


Figure 7.10: Coalescence time constant – Torque vs. Time.

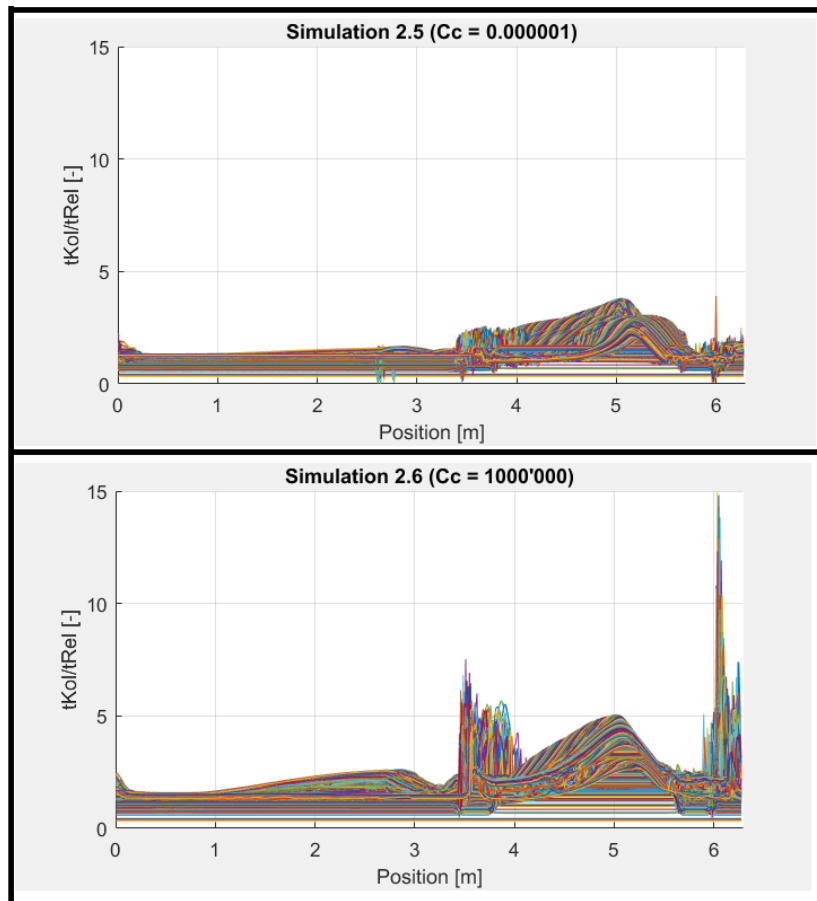


Figure 7.11: “ t_{kol}/t_{rel} vs. position” for simulation 2.5 and 2.6.

Figure 7.12 illustrates the particle size distribution inside the wheel, at a specific time step in the end of the simulation period. Position 0 m and position 6.28 m, illustrates the middle left part of the wheel (“nine o’clock,” see figure 5.6). The y-values in the figure (represented as coloured lines in the graphs) represent ten different heights in the cross section of the wheel pipe (see figure 4.2). Note the values of the y-axis on the graphs for simulation 2.4 and 2.6.

Figure 7.12 illustrates that, decreasing the value of “the coalescence time constants ($C_{Coalescence}$)” did not influence the particle size distribution (simulation 2.1, 2.3 and 2.5). However, by increasing the value of “coalescence time constants ($C_{Coalescence}$),” the particle sizes were gradually decreasing (simulation 2.2, 2.4 and 2.6). This is the opposite effect of the phenomenon observed when increasing “the break up time constant ($C_{breakup}$),” illustrated in figure 7.8.

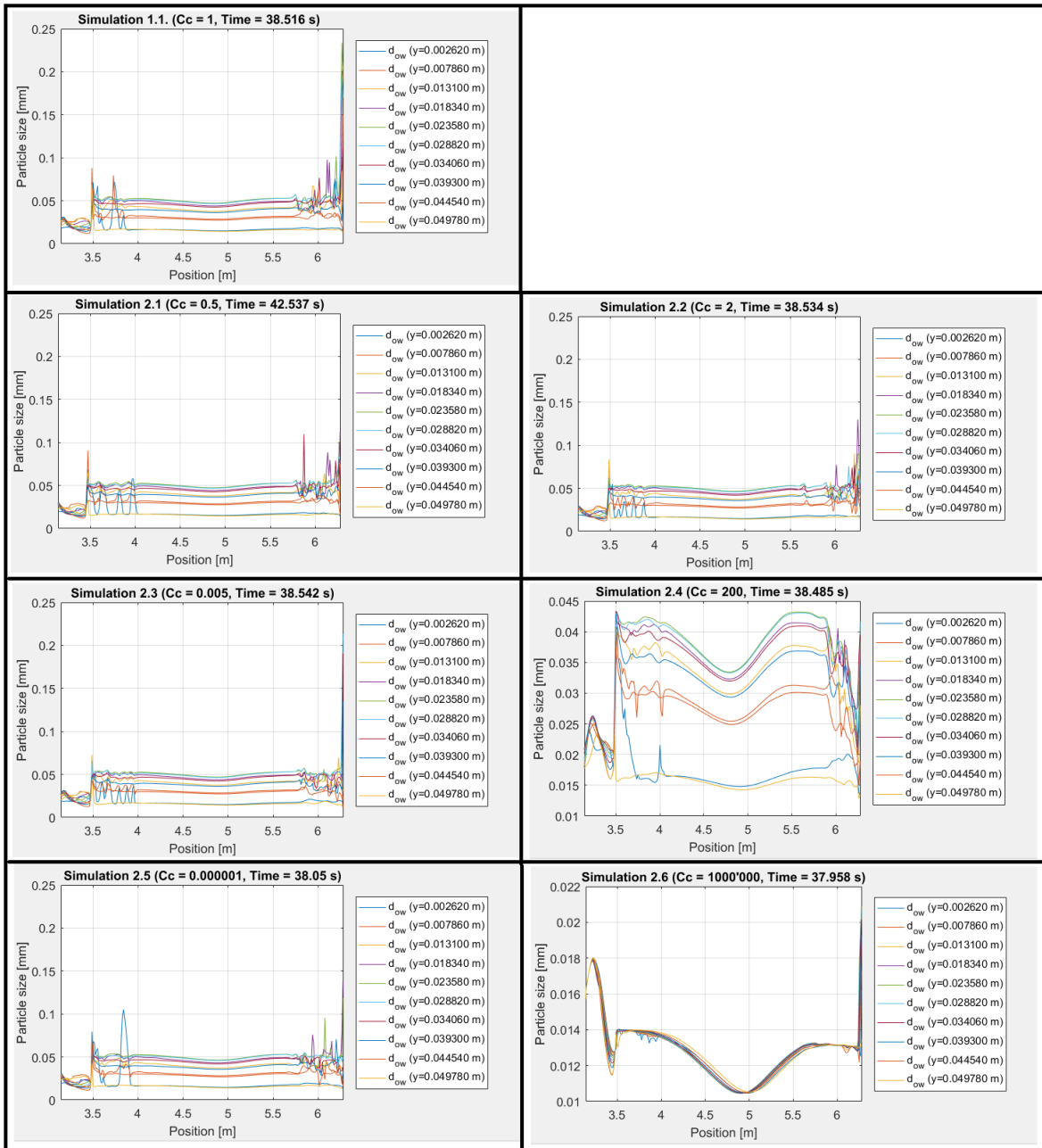
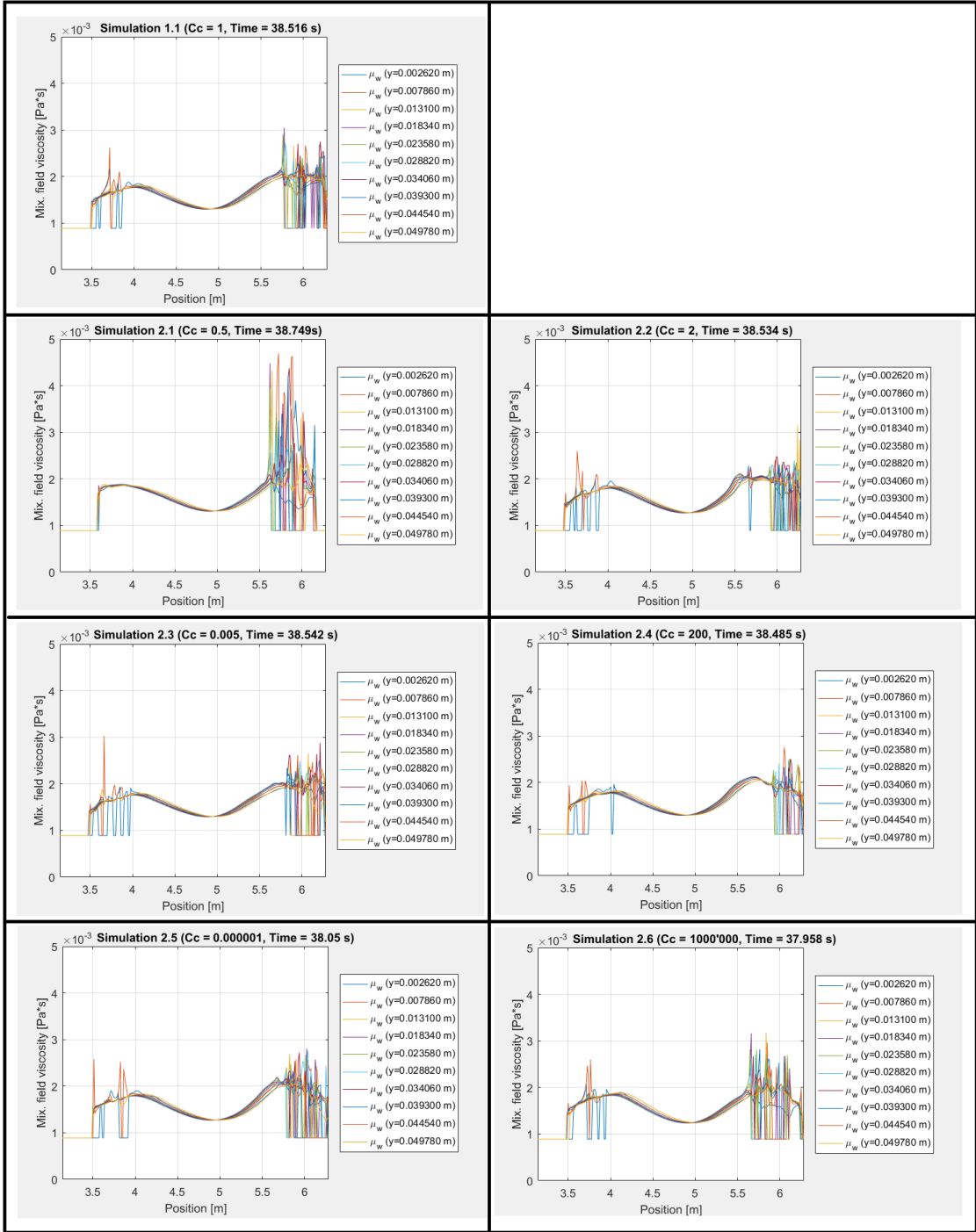


Figure 7.12: Coalescence time constant – Particle size vs. Position.

Figure 7.13 illustrates the viscosity distribution of the fluid inside the wheel, at various positions of the lower part of the wheel, for the specific time of 38 s after the simulation process has started. Position 3.14 m illustrates the middle right position of the wheel (“three o’clock”), and the position 6.28 m illustrates the middle left position of the wheel (“nine o’clock,” see figure 5.6). The y-values in the figure represent ten different heights in the cross section of the wheel pipe (see figure 4.2).

Figure 7.13 illustrates that there is some activity in the positions 3.5 m and 6 m. The viscosity for the various simulations, in these areas, is slightly different for each time “the coalescence time constants ($C_{Coalescence}$)” is adjusted. This is probably because of the transition between oil and water phases in these areas. Nevertheless, the average value of the viscosity stays constant for all simulations.



Particle 7.13: Coalescence time constant – Viscosity vs. Position.

Explanation of the simulation results, for test 1 (break up time constant)

It was expected that sufficient adjustment of “the break up time constant ($C_{breakup}$)” would adjust the “break up time scale (t_B)” to be either smaller or larger than “the Kolmogorov time scale (t_K),” and consequently influence the value of $t_{rel,km}^i$ (eq. 5.1). From the work in Matlab, and the results in figure 7.4, it was experienced that “the break up time constant ($C_{breakup}$)” needed to be increased, compared to the default value, in order to make the value of “the break up time scale (t_B)” become larger than the value of the “the Kolmogorov time scale (t_K),” and hence affect the calculation of equation 5.1. The evolution of torque, in figure 7.6, made it obvious that “the break up time constant ($C_{breakup}$)” needed to be increased a lot, if it was going to make any effect on the calculation of torque.

Increasing particle sizes (figure 7.8), due to the increasing “break up time constant ($C_{breakup}$),” and following “break up time scale (t_B),” makes sense when you consider that the longer it takes to break up the emulsion droplets, the larger they will be after a given time.

The changes in particle sizes, observed in figure 7.8, for the simulations 1.12 and 1.13, led to changes in the mix. field viscosity distribution as well (figure 7.9). This change in viscosity is probably the reason for the change that was observed for the torque in figure 7.7, and confirms the theory explained previously: Affecting $t_{rel,km}^i$ will impact the calculation of the evolution of average particle size, which will play a role in the calculation of viscosity, which finally has a relation with the calculation of torque.

As a summary, “the break up time constant ($C_{breakup}$)” can be used as a tool to tune the calculation of torque for specific simulations in LedaFlow Q3D. However, in this system (phase fraction and wheel velocity) “the break up time constant ($C_{breakup}$)” showed little significance on the simulation results and output of torque. Note that this may be different for other systems.

Explanation of the simulation results, for test 2 (coalescence time constant)

In the same way as with the “the break up time constant ($C_{breakup}$),” it was expected that sufficient adjustment of “the coalescence time constants ($C_{Coalescence}$)” would adjust the “the coalescence time scale (t_C)” to be either smaller or larger than “the Kolmogorov time scale (t_K),” and consequently influence the value of $t_{rel,km}^i$ (eq. 5.1).

The Matlab calculations (figure 7.5 and 7.11) illustrated that the adjustment of “the coalescence time constants ($C_{Coalescence}$)” did not affect the average value of the $\frac{t_{kol}}{t_{rel}}$ ratio, and “the Kolmogorov time scale (t_K)” was larger than the “the coalescence time scale (t_C)” for all of the simulations. There might be plenty of reasons for this. The most likely reason is that “the local particle size ($d_{p,km}$)” was equal to, or larger than, “the equilibrium (Sauter mean) particle size ($d_{p,km}^E$)” for all positions in the flow wheel during the entire simulation period (see equation 5.2, and figure 7.3). If that is true, then the $\frac{t_{kol}}{t_{rel}}$ ratio would always be a calculation of equation 7.1, and adjusting “the coalescence time constants ($C_{Coalescence}$)” would not make any effect on the $\frac{t_{kol}}{t_{rel}}$ ratio. In other words, “the coalescence time scale (t_C)” would never represent $t_{rel,km}^i$, in equation 5.1, no matter how much “the coalescence time constants ($C_{Coalescence}$)” was adjusted.

Nevertheless, there were some increasing peaks were the ratio between “the Kolmogorov time scale (t_K)” and “the coalescence time scale (t_C)” became even larger. These peaks were located at the bottom of the flow wheel, approximately around the position 5 m from the start point (see figure 5.6). In this area, the fluid phases of oil and water are mixed, and this might explain the peaks in figure 7.5 and 7.11.

On the other hand, figure 7.12 illustrates that increasing “the coalescence time constants ($C_{Coalescence}$)” results in a gradually decrease in particle size. In emulsion theory, this makes sense. If it takes longer time to coalesce the emulsion droplets, the emulsion droplets should consequently be smaller in size after a given time. However, it is surprising that the simulation program can calculate changes in the particle size distribution, if $t_{rel,km}^i$, in equation 5.1 was never influenced by the changes in “the coalescence time constants ($C_{Coalescence}$).” Due to this observation, it probably means

that for some few positions, or time periods, $t_{rel,km}^i$, had to be represented by “the coalescence time scale (t_c).”

Figure 7.13 illustrates that the mix. field viscosity distribution stayed approximately constant for all the simulations. The changes in particle sizes observed in figure 7.10 was obviously not large enough to make an impact on the viscosity model. This is probably the reason why the adjustments of “the coalescence time constants ($C_{Coalescence}$).” did not have any effect on the calculation of torque.

As a summary, “the coalescence time constants ($C_{Coalescence}$)” was not able to tune the calculation of torque in this fluid system. However, it might possibly work in other situations (with different water cut, wheel velocity etc.), if the conditions for equation 5.2 is different.

7.2 Particle Size Constants, C_1 and C_2

The purpose of test 3 and test 4

The reason why we wanted to perform tests on adjusting the “particle size constants, C_1 and C_2 ,” was because of their role in equation 5.6, which calculates “the equilibrium (Sauter mean) particle size ($d_{p,km}^E$).” Since C_1 and C_2 affects the calculation of $d_{p,km}^E$ this will in turn have an effect on “the local particle size, $d_{p,km}$,” in equation 5.1.

Since the viscosity model (Krieger-Dougherty equation, subchapter 2.6) is a function of the volume concentration of dispersion droplets in the continuous phase, and adjusting the “particle size constants, C_1 and C_2 ,” influence the evolution of particle sizes in the dispersion, this will probably affect the viscosity of the fluid mixture as well. By plotting torque, mix. field viscosity distribution and particle size distribution for the various simulations, the effect of these input parameters was examined. The aim of the testing was to investigate how effectively these input parameters could tune specific simulations in LedaFlow Q3D, and if it was possible to tune the output of torque to match with the results produced from the wheel flow experiment (figure 5.3)

Execution method and input parameters, for test 3 and test 4

The default value for “particle size constant, C_1 ,” was 0.02. Table 7.5 illustrates the value for “particle size constant, C_1 ” for each simulation case. As before, in our first attempts (simulation 3.1 – 3.4), we tried to investigate the effect of the input parameter by systematically increasing and decreasing the input value of “the particle size constant, C_1 .” The fourth attempt (simulation 3.4) gave us satisfactory results on affecting the torque. Due to the examination of this result the simulations 3.5 – 3.8 was made. These simulations were performed to investigate if we could use this input parameter, to tune the simulation results to become more identical with the results produced from the wheel flow experiment (subchapter 5.1). Our attempt was to tune the simulation results to converge around the same value for torque as for the wheel flow experiment with rotational speed of 2 m/s (approximately 4.5 Nm, figure 5.3).

	Particle size constant, C_1
Simulation 1.1/Default value	0.02
Simulation 3.1	0.01
Simulation 3.2	0.04
Simulation 3.3	20
Simulation 3.4	0.00002
Simulation 3.5	1
Simulation 3.6	5
Simulation 3.7	0.5
Simulation 3.8	0.75

Table 7.5: Input values for “particle size constant, C_1 .”

The default value for “particle size constant, C_2 ” was 0.002. Table 7.6 illustrates the value for “particle size constant, C_2 ,” for each simulation case. As always, in our first attempts (simulation 4.1 – 4.4), the input parameter was systematically increased and decreased to investigate how this influenced the simulation results. The third attempt (simulation 4.3) gave satisfactory results on affecting the output of torque. In the next simulations (4.5 – 4.8) the aim was to tune the output of torque to converge around 4.5 Nm (which was identical with the wheel flow experiment, with rotational speed of 2 m/s).

	Particle size constant, C_2
Simulation 1.1/Default value	0.002
Simulation 4.1	0.001
Simulation 4.2	0.004
Simulation 4.3	2
Simulation 4.4	0.000002
Simulation 4.5	1
Simulation 4.6	0.75
Simulation 4.7	0.5
Simulation 4.8	0.25

Table 7.6: Input values for “particle size constant, C_2 .”

Presentation of the simulation results for test 3 (Particle size constant, C_1)

Figure 7.14 illustrates how changing this input parameter affected the torque. When the value of C_1 became large enough, the adjustment of this input parameter resulted in a change of torque. Nevertheless, if the adjustment of C_1 was insufficient, there would not be any changes in the output of torque (as for the values of C_1 between 0.00002 - 0.04). There was a good comparison between simulation 3.8 ($C_1 = 0.75$) and the results from the wheel flow experiment.

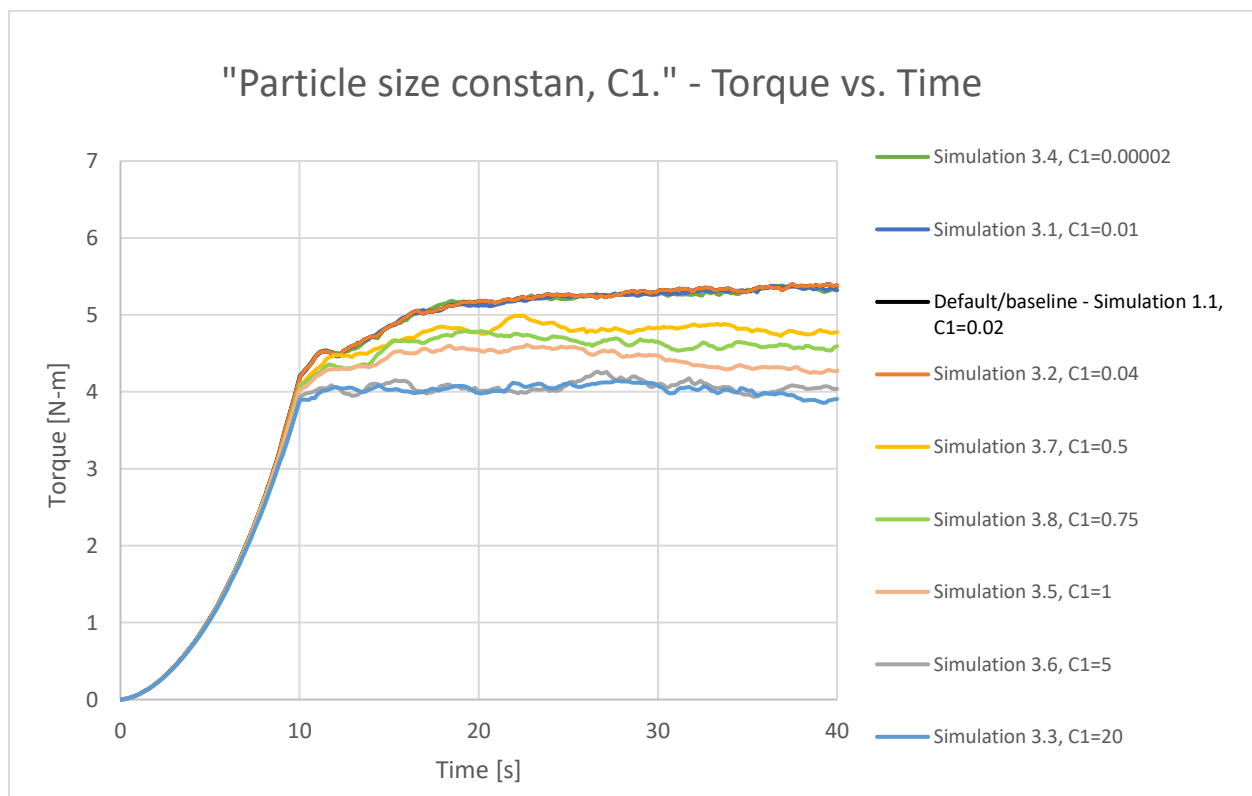


Figure 7.14: Particle size constant, C_1 – Torque vs. Time.

Figure 7.15 and 7.16 illustrates the particle size distribution inside the wheel for various values of “particle size constant, C_1 ,” in the end of the simulation period (around 38 s after the simulation had started). Position 0 m and position 6.28 m, illustrates the middle left part of the wheel (“nine o’clock,” see figure 5.6). The y-values (represented by coloured lines) in the figure represent ten different heights in the cross section of the wheel pipe (see figure 4.2).

Figure 7.15 illustrates how the particle sizes decreased when the “particle size constant, C_1 ,” was gradually decreased. In figure 7.16, the opposite phenomenon can be observed. When the “particle size constant, C_1 ,” was gradually increased, the particle sizes would gradually increase as well. The first visual effect on the particle size distribution was observed for simulation 3.7, with C_1 equal to 0.5. Note that the values on the y-axis for the graphs in figure 7.16 vary a lot.

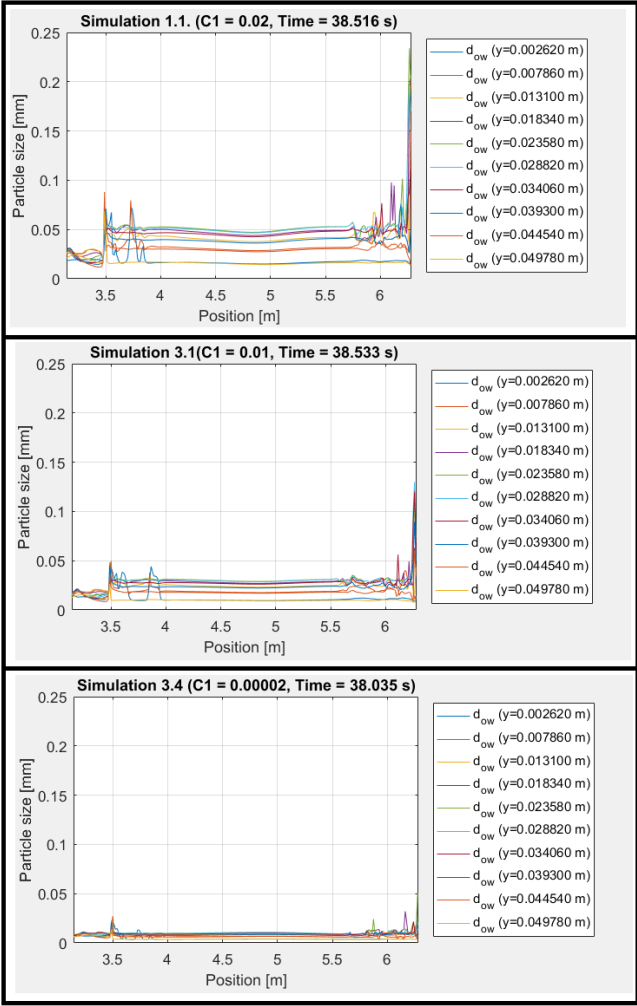


Figure 7.15: Particle size constant, C_1 – Particle size vs. Position (decreasing C_1)

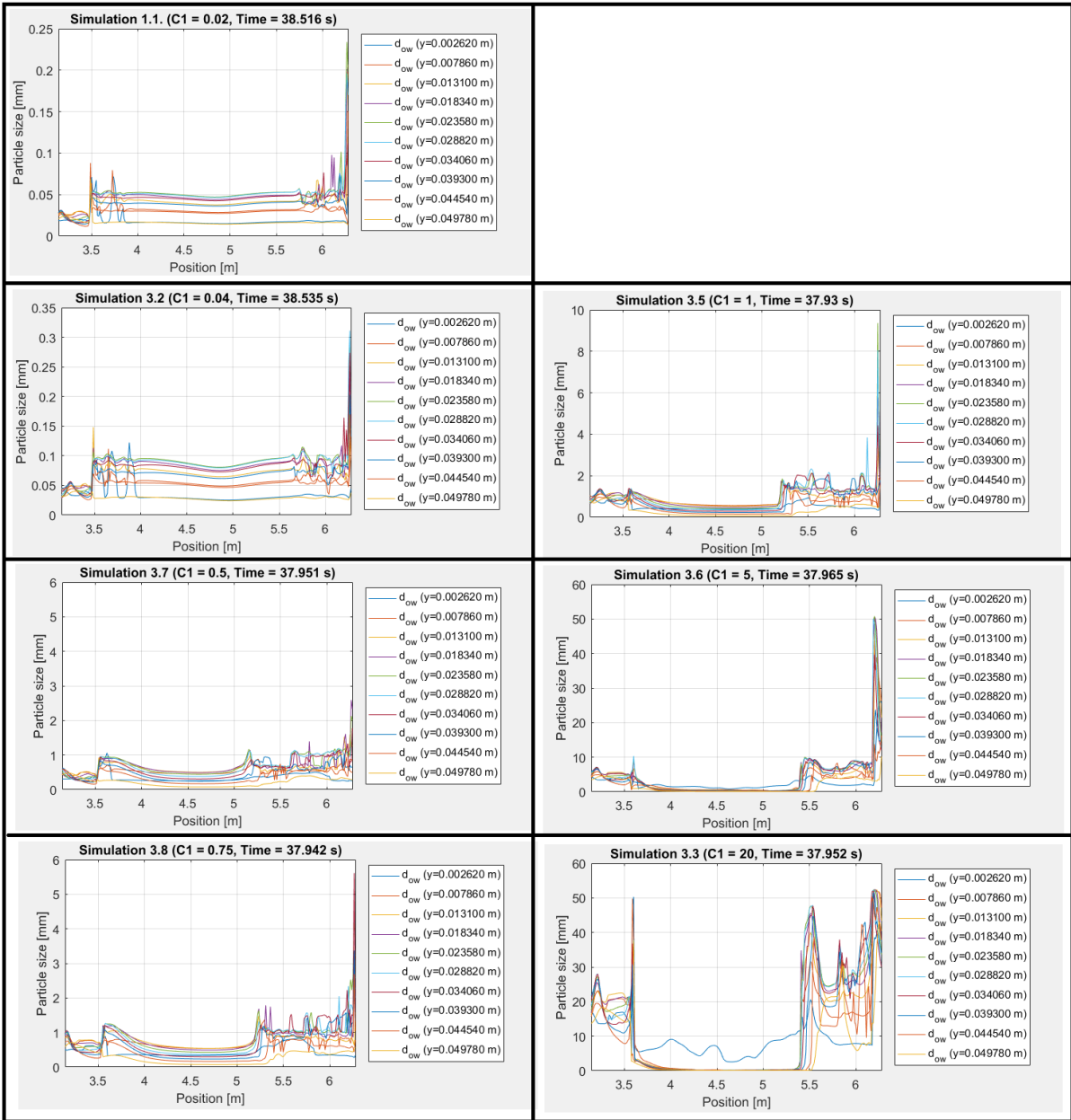


Figure 7.16: Particle size constant, C_1 – Particle size vs. Position (increasing C_1).

Figure 7.17 and 7.18 illustrates the mix. field viscosity distribution, on the lower part of the wheel, in the end of the simulation period (around 38 s after the simulation had started). Position 3.14 m illustrates the middle right of the wheel (“three O’clock”), and the position 6.28 m illustrates the middle left of the wheel (“nine O’clock,” see figure 5.6). The y-values in the figure represent ten different heights in the cross section of the wheel pipe (see figure 4.2).

Figure 7.17 illustrates that gradually decreasing the value of the “particle size constant, C_1 ,” does not influence the mix. field viscosity distribution. In figure 7.18 it is observed that gradually increasing the “particle size constant, C_1 ,” results in a gradually change in the mix. field viscosity distribution. The first visual effect on the mix. field viscosity distribution was for simulation 3.7, with C_1 equal to 0.5.

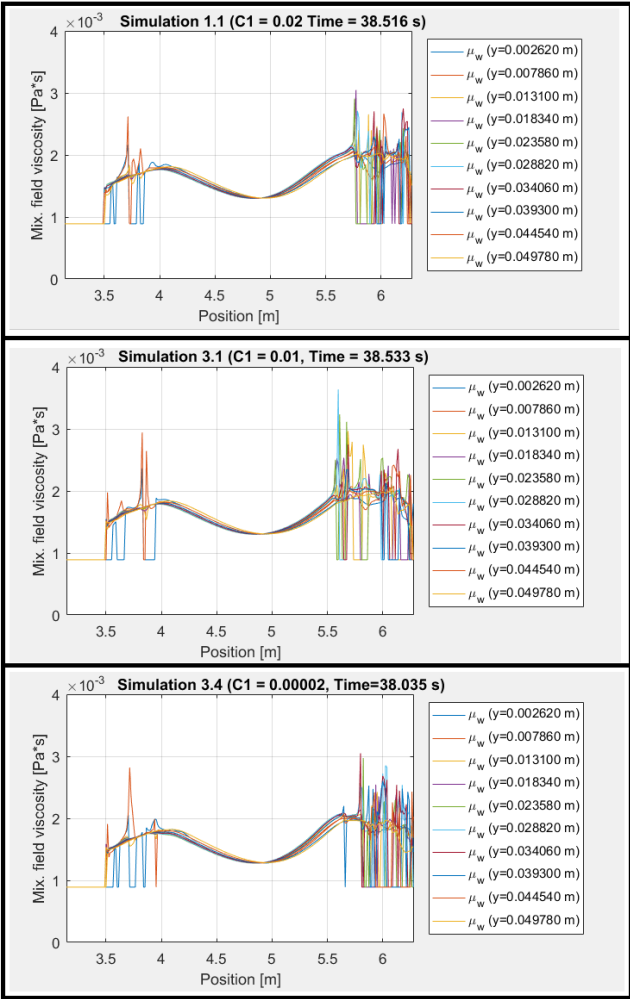


Figure 7.17: Particle size constant, C_1 – Viscosity vs. Position (decreasing C_1).

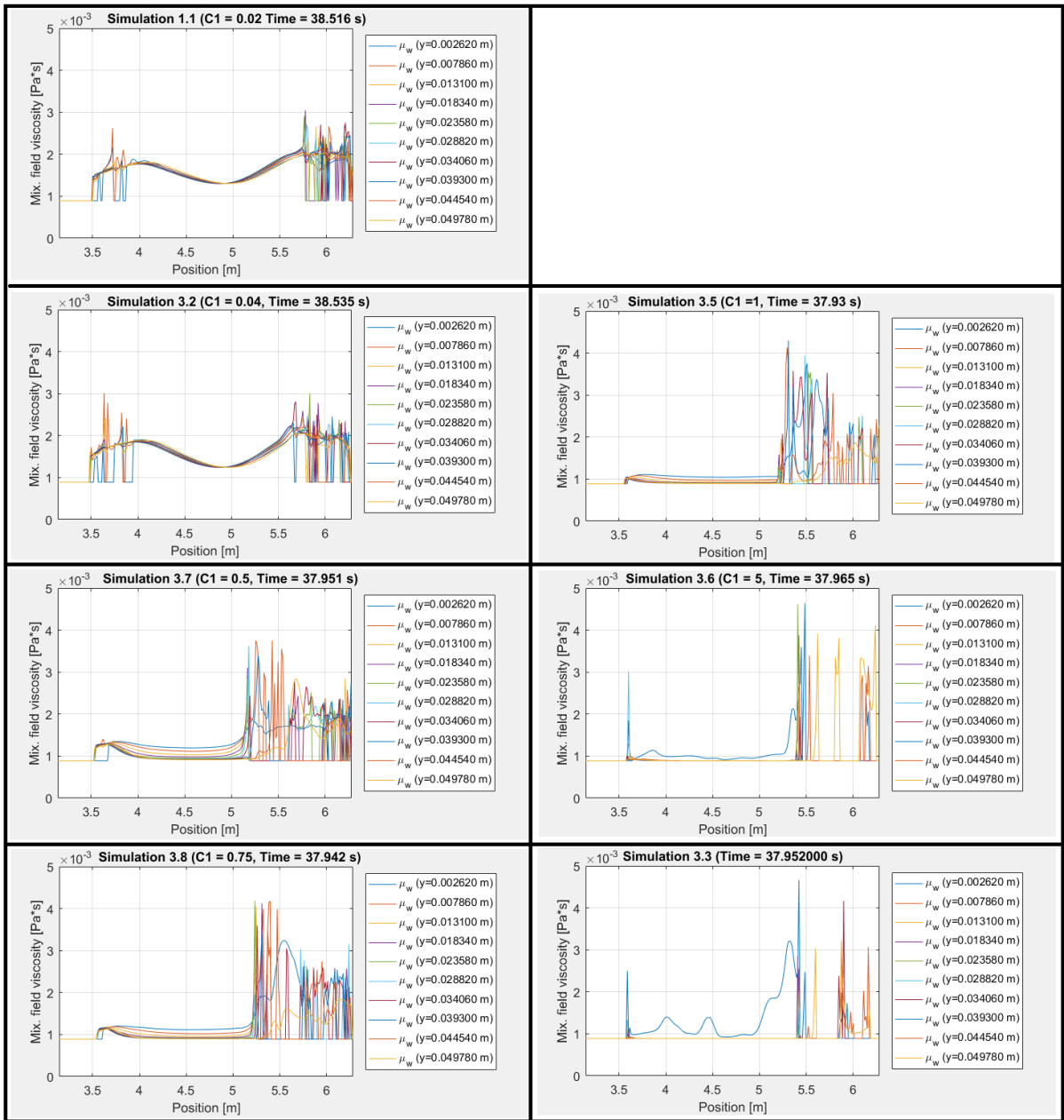


Figure 7.18: Particle size constant, C_1 – Viscosity vs. Position (increasing C_1).

Presentation of the simulation results for test 4 (Particle size constant, C₂)

Figure 7.19 illustrates how adjusting C₂ affected the torque. When the value of C₂ became large enough, this resulted in a change in the output of torque. Nevertheless, if the adjustment of C₂ was insufficient, there would not be any changes in the output of torque (as for the values of C₂ between 0.000002 - 0.004). It was a large step between C₂ equal to 0.004 and 2. In simulations 4.5 – 4.8, the attempt was to gradually tune the output of torque in between the input values in simulation 4.3 (C₂ = 2) and 4.4 (C₂ = 0.000002). Simulation 4.5, 4.6 and 4.7 all converged at approximately the same values of torque as for simulation 4.3. However, simulation 4.8 converged around 4.7 Nm, which is close to the results from the wheel flow experiment (subchapter 5.1). By continuing adjusting the input parameter, it would probably be possible to find a value for C₂ that would be able to tune the simulation to have exactly 4.5 Nm as the output of torque.

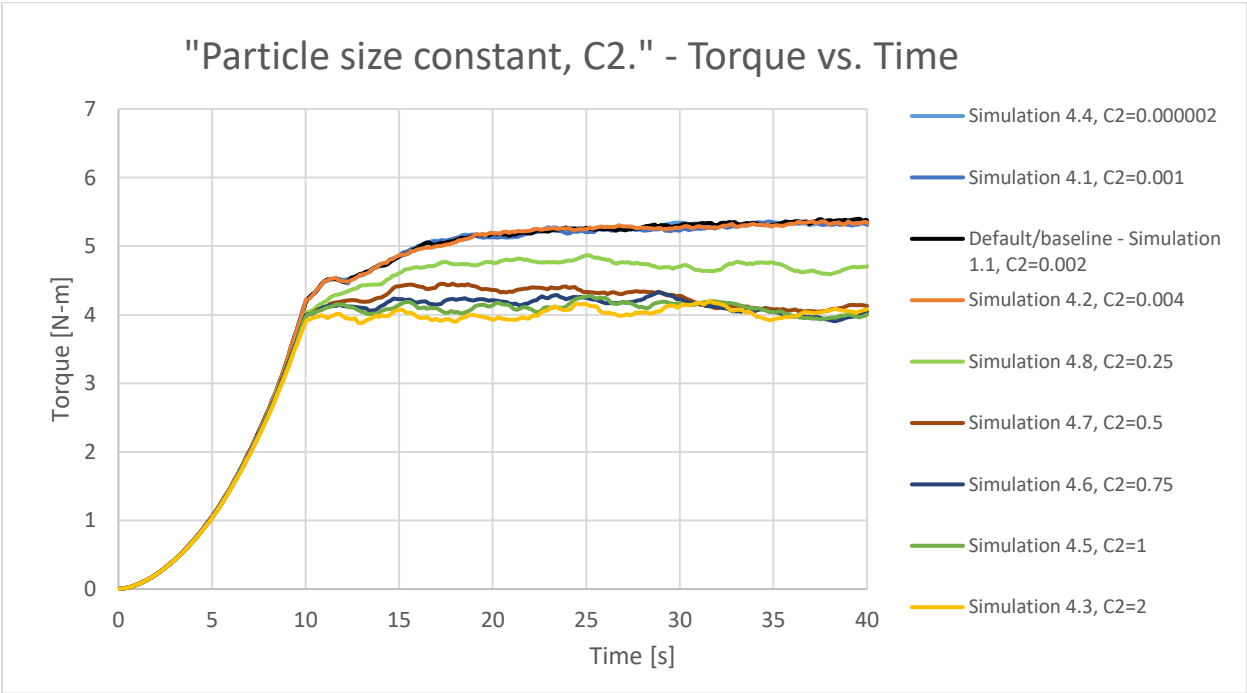


Figure 7.19: Particle size constant, C₂ – Torque vs. Time.

Figure 7.20 and 7.21 illustrates the particle size distribution inside the wheel for various values of “particle size constant, C2,” in the end of the simulation period (around 38 s after the simulation had started). Position 0 m and position 6.28 m, illustrates the middle left part of the wheel (“nine o’clock,” see figure 5.6). The y-values (represented as coloured lines) in the figure represent ten different heights in the cross section of the wheel pipe (see figure 4.2).

Figure 7.20 illustrates that the average particle sizes stays approximately constant when the “particle size constant, C2,” is gradually decreased. However, in figure 7.21 it is observed that the particle sizes gradually increase when the “particle size constant, C2,” is gradually increased. Note that the values on the y-axis vary a lot for the graphs in figure 7.21.

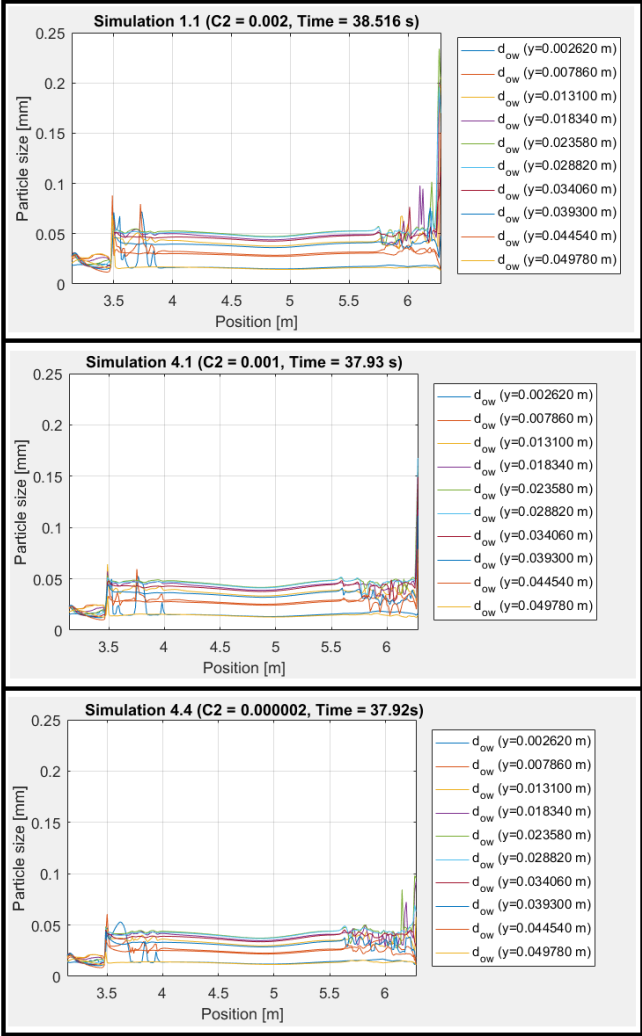


Figure 7.20: Particle size constant, C2 – Particle size vs Position (decreasing C2).

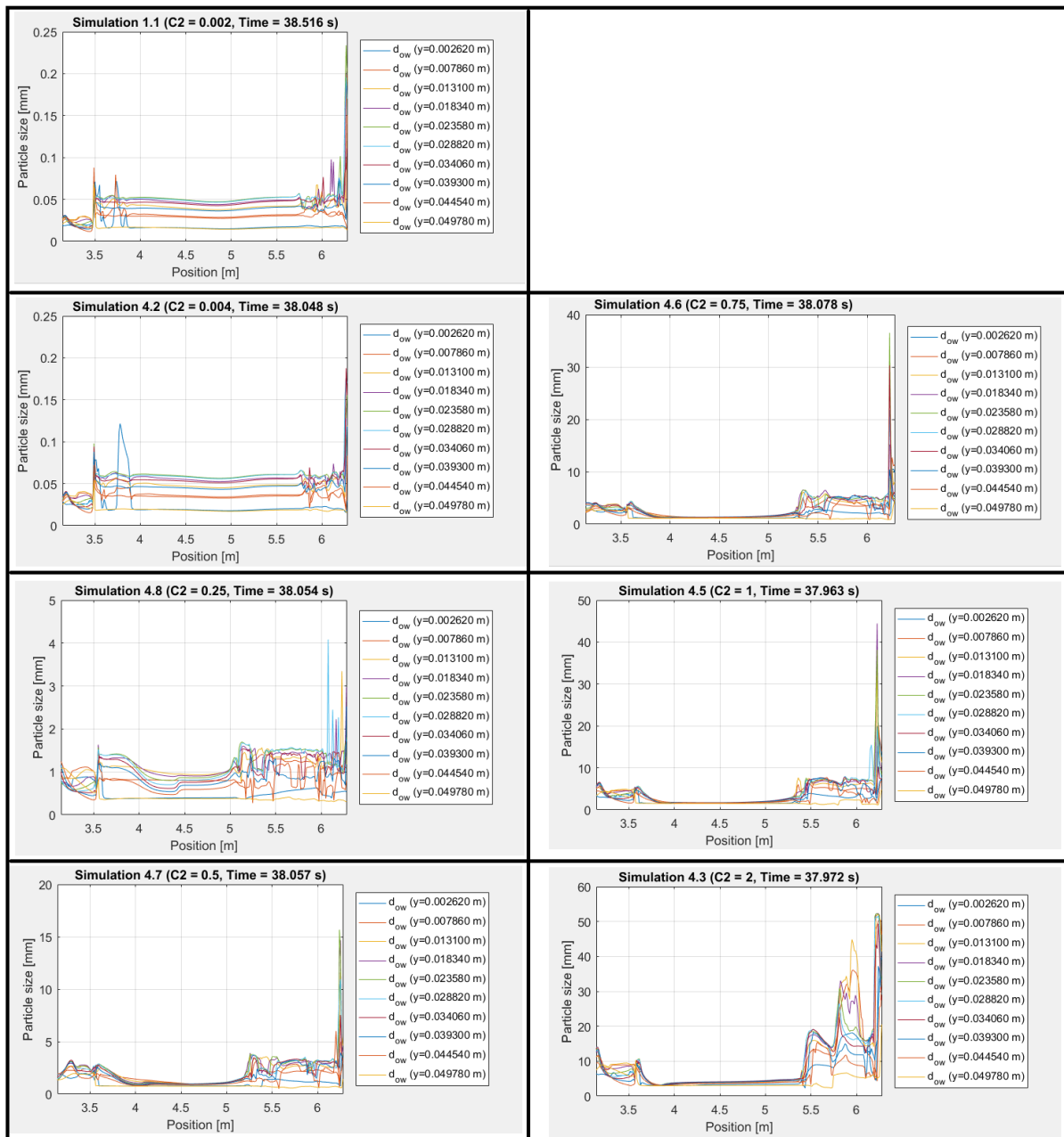


Figure 7.21: Particle size constant, C_2 – Particle size vs Position (increasing C_2).

Figure 7.22 and 7.3 illustrates the viscosity of the fluid inside the wheel, at various positions on the lower part of the wheel, in the end of the simulation period (around 38 s after the simulation had started). Position 3.14 m illustrates the middle right of the wheel (“three o’clock”), and the position 6.28 m illustrates the middle left of the wheel (“nine o’clock,” see figure 5.6). The y-values (represented as the coloured lines) in the figure represent ten different heights in the cross section of the wheel pipe (figure 4.2).

The figures illustrate the same trends as for “particle size constant, C_1 .” Figure 7.22 illustrates that gradually decreasing the value of the “particle size constant, C_2 ,” does not influence the mix. field viscosity distribution. In figure 7.23 it is observed that gradually increasing the “particle size constant, C_2 ,” results in a gradually change in the mix. field viscosity distribution. The first visual effect on the mix. field viscosity distribution was for simulation 4.8, with C_2 equal to 0.25.

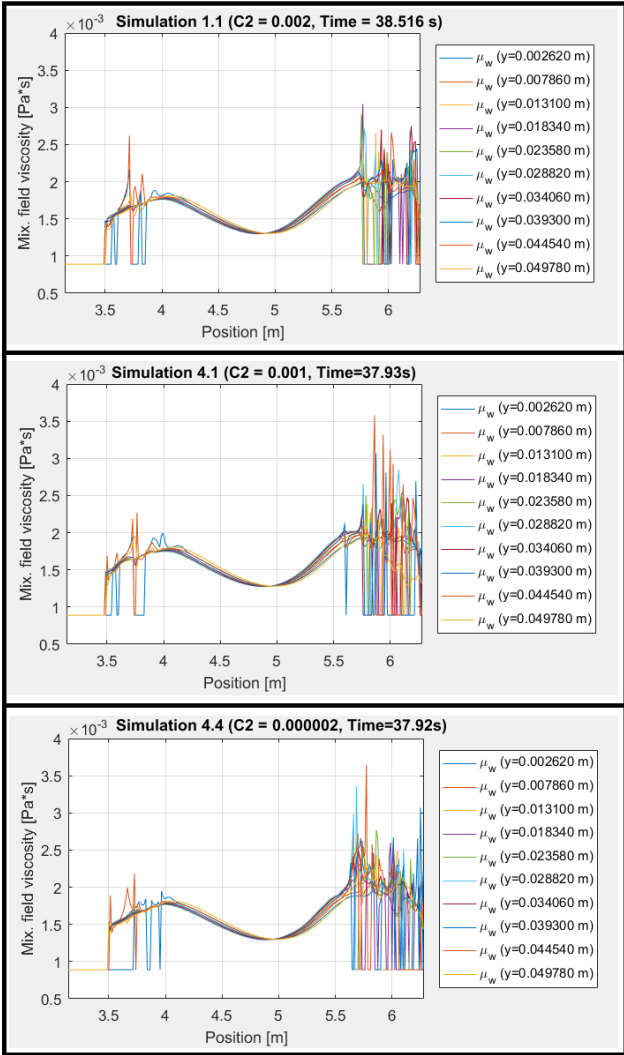


Figure 7.22: Particle size constant, C_2 – Viscosity vs. Position (decreasing C_2).

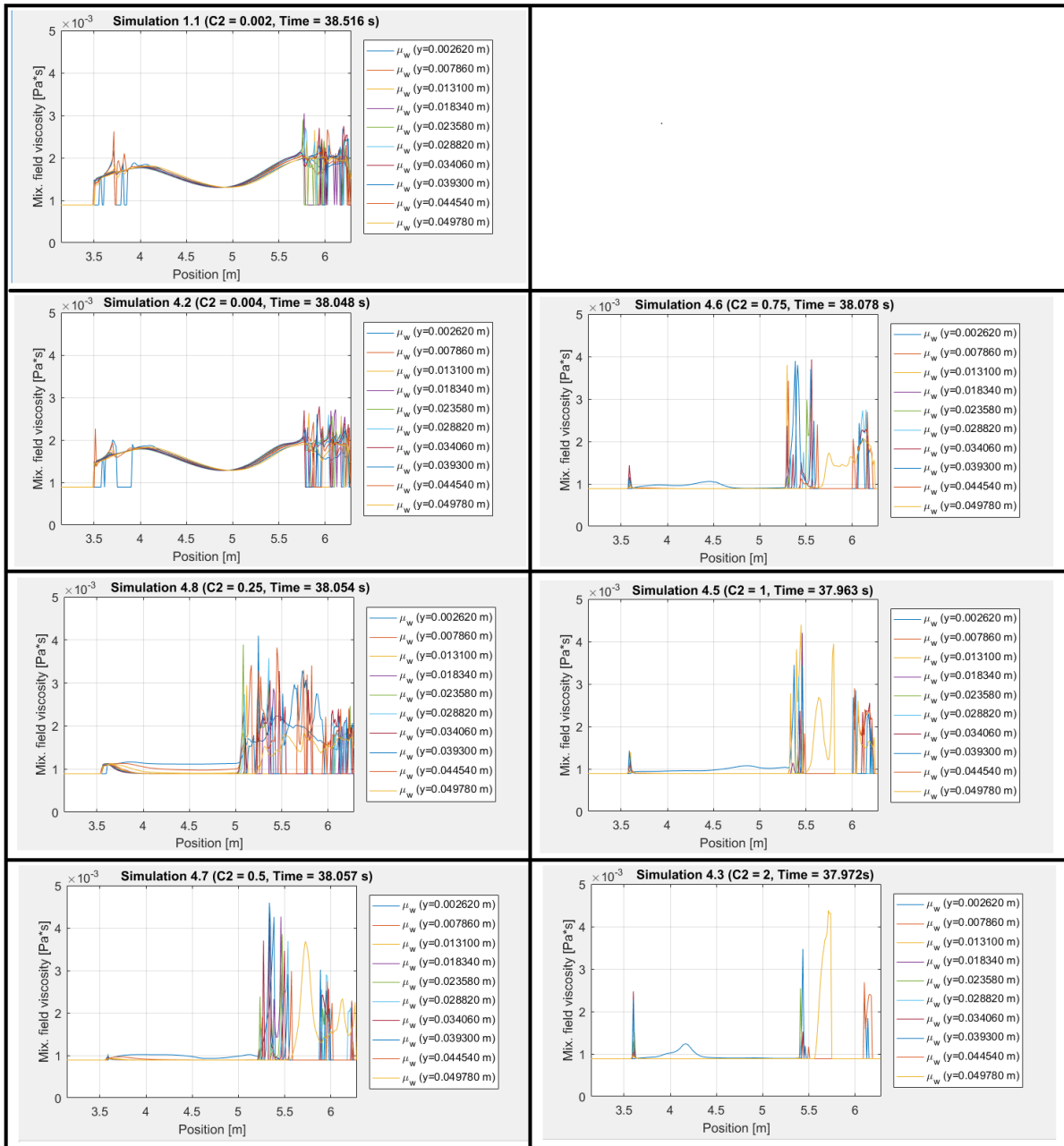


Figure 7.23: Particle size constant, C_2 – Viscosity vs. Position (increasing C_2).

Explanation of the simulation results, for test 3 (particle size constant, C_1)

From examination of equation 5.6, it makes sense that the particle sizes will increase when the “particle size constant, C_1 ,” is increased, and vice versa. This explains the results in figure 7.15 and 7.16.

The observation of changes in the mix. field viscosity distribution due to increasing “particle size constant, C_1 ,” explains the following changes in the output of torque in figure 7.14.

The results illustrated in figure 7.14 proves that the “particle size constant, C_1 ,” can be adjusted to effectively tune specific simulations in LedaFlow Q3D, to be more identical with the results produced from the wheel flow simulator (subchapter 5.1). Simulation 3.8 successfully managed to tune the torque to converge around approximately 4.5 Nm, which is identical with the wheel flow experiment (figure 5.3). However, the particle size distribution that resulted from the adjustment of this input parameter should be taken in consideration. Some of the particle sizes that were plotted for the various values of C_1 are not representative for emulsions (figure 2.10).

Explanation of the simulation results, for test 4 (particle size constant, C_2)

From examination of equation 5.6, it makes sense that the particle sizes will increase when the “particle size constant, C_2 ,” is increased. This explains the results in figure 7.20 and 7.21. However, keep in mind to consider that some of the particle sizes might not be representative for emulsions (figure 2.10).

The observation of changes in the mix. field viscosity distribution due to increasing “particle size constant, C_1 ,” explains the following changes in the output of torque in figure 7.19.

The results illustrated in figure 7.19 proves that tuning specific simulations in LedaFlow Q3D can be accomplished by adjusting the “particle size constant, C_2 .” Simulation 4.8 managed to tune the torque to converge around approximately 4.7 Nm, which is close to the results of the wheel flow experiment (figure 5.3).

7.3 Constant Particle Size, with DPS model turned ON

The purpose of test 5

In test 5 (simulation 5.1 – 5.4) we tried to investigate what happened if we adjusted the input parameters in the option flag “Particle size: Constant size” for field 4 (O/W) and field 6 (W/O), when the DPS model was turned “on” for these fields.

In theory, when the DPS model is in use, the input parameters for the option flag “Particle size: Constant size” in closures (see section 5.3.1) should be untouched by the equations producing the simulation results. In other words, the input values that are listed in “Particle size: Constant size” flag in closures are only used if the DPS model is turned “off” for all, or some, of the fields 1-6 (except when it is laminar and not turbulent flow in the wheel. Then the values in the “Particle size: Constant size” flag is used, although the DPS model is turned “on”).

In simulation 5.1 – 5.4 we had turned “off” the DPS model for field 1, 2, 3 and 5 (because we are not interested in the fields containing gas), but the DPS model was still “on” for field 4 (O/W) and field 6 (W/O). Thus, by adjusting the input parameters for “Particle size: Constant size” flag in closures for field 4 and 6, this change should in theory not make any effect on the simulation results.

Execution method and input parameters, for test 5

Table 7.7 illustrate the input values in the option flag “Particle size: Constant size” in closures (field 4 and 6) for simulation 1.1 (default values), and 5.1 - 5.4. To manage to turn the various fields “on” or “off,” we were using the input parameters in table 7.1, for the option flag “Particle size: Variable particle size” in the closures menu (0=false, 1=true). The particle sizes chosen may not be natural sizes for dispersion droplets, or bubbles, and are only chosen to prove a point.

	Constant Particle Size (field 4 and 6) [mm], with DPS model: ON
Simulation 1.1/Default value	0.1
Simulation 5.1	0.01
Simulation 5.2	1
Simulation 5.3	0.001
Simulation 5.4	10

Table 7.7: Input values for “Constant particle size” – DPS model “on.”

Presentation of the simulation results for test 5

Figure 7.24 illustrate the results from the simulation cases 1.1, and 5.1 – 5.4. The figure illustrates that adjusting the input values in the option flag “Particle size: Constant size” in closures (field 4 and 6) did not make any effect on the simulation results.

Figure 7.25 illustrate how the particle size distribution, and the mix. field viscosity distribution, remains the same while decreasing or increasing the “constant particle size,” when the DPS model is turned “on.”

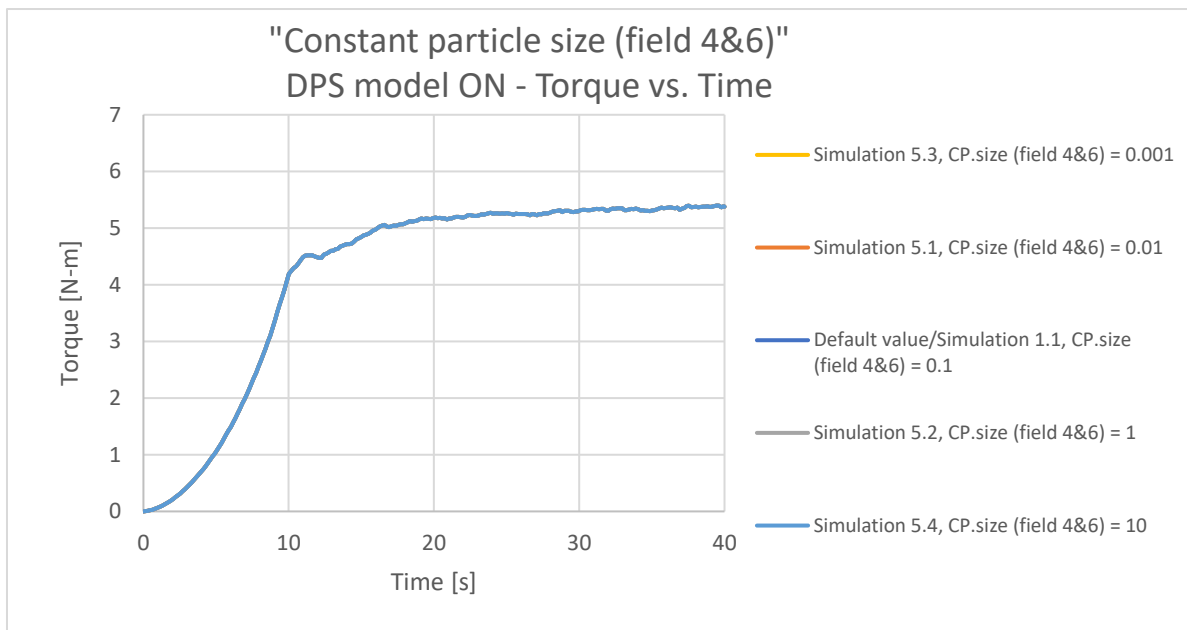


Figure 7.24: Constant particle size (field 4 and 6), DPS model turned ON – Torque vs. Time.

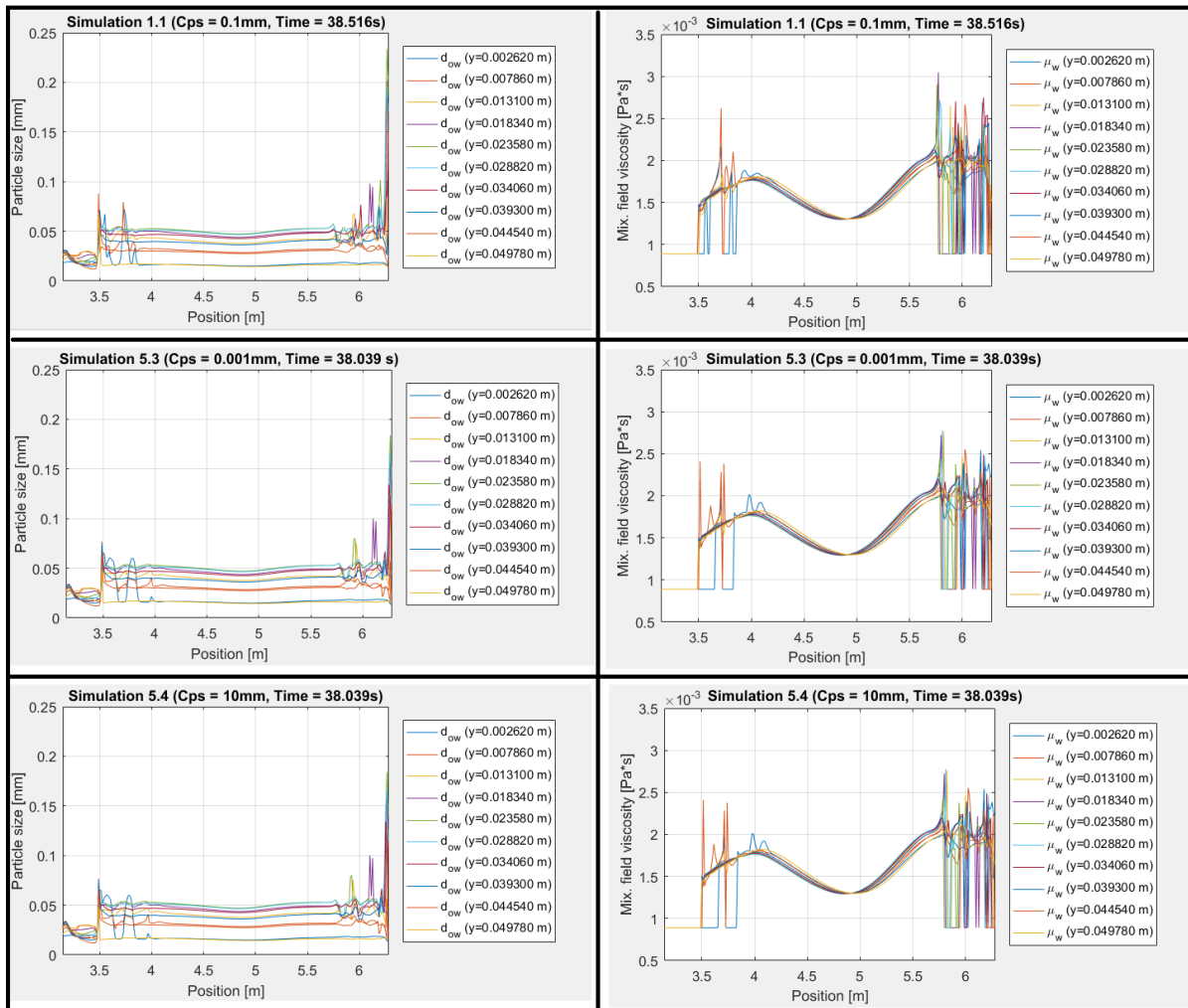


Figure 7.25: “Particle size vs. Position” & “Viscosity vs. Position,” DPS model ON.

Explanation of the simulation results, for test 5

These observations make sense, because when the DPS model is in use, the input parameters for the option flag “Particle size: Constant size” in closures (see section 5.3) will be untouched by the equations producing the simulation results. In other words, the input values that are listed in “Particle size: Constant size” flag in closures are only used if the DPS model is turned “off” for all, or some, of the fields 1-6. However, there were some fields where the DPS model was turned off (field 1, 2, 3, 5), but we did not change the input values for these fields. The only exception to this conclusion is when it is laminar and not turbulent flow in the wheel. Then the values in the “Particle size: Constant size” flag is used, although the DPS model is turned “on.” Nevertheless, the results illustrated in figure 7.24 show that the input values in the “Particle size: Constant size” flag had no effect on the simulation results in this system.

7.4 Constant Particle Size, with DPS model turned OFF

The purpose of test 6

In simulation 6.1 – 6.3 we try to investigate what happens if we adjust the input parameters for the option flag “Particle size: Constant size” for field 4 (O/W) and field 6 (W/O), when the DPS model is turned “off” for all fields.

In theory, when the DPS model is not in use, the equations producing the simulation results will use the constant particle sizes for each field listed in the option flag “particle size: Constant size” in the closures menu (see section 5.3). Thus, adjusting these input parameters should affect the simulation results.

Execution method and input parameters, for test 6

Table 7.8 illustrate the input values for the option flag “particle size: constant size” in closures (field 4 and 6) for simulation 1.1 (DPS model turned “on”), 6.1, 6.2 and 6.3. The particle sizes chosen, may not be natural sizes for dispersion droplets, or bubbles, and are only chosen to prove a point.

To manage to turn “off” the DPS model for the various fields, we were using the option flag “Particle size: Variable particle size” in the closures menu. By writing 0 (false) in all the fields, the DPS model was turned “off” (see subchapter “5.3 Settings in closures Q3D”). Another option could be to use the “option menu” in the “case settings” (lower left, figure A.4 in appendix), and from this location turn “off” the DPS model for all the fields.

	Constant Particle Size (field 4 and 6) [mm], with DPS model: OFF
Simulation 1.1/Default value	0.1 (DPS model turned «on»)
Simulation 6.1	0.1
Simulation 6.2	0.01
Simulation 6.3	1

Table 7.8: Input values for “Constant particle size” – DPS model “off.”

Presentation of the simulation results for test 6

Figure 7.26 illustrate how adjusting this input parameter affected the calculation of torque, when the DPS model was turned “off”. As expected, adjusting this parameter, when the DPS model was turned “off”, resulted in a change in the calculation of torque.

By decreasing the constant particle size to 0.01, there were no effect on the calculation results. Nevertheless, by increasing the constant particle size to 1, the enlargement of the constant particle size resulted in a lowering of the calculation results of torque. This is equivalent with the results from section 7.2 when a larger input parameter for the “particle size constants, C₁ and C₂, gave the same reaction on torque.

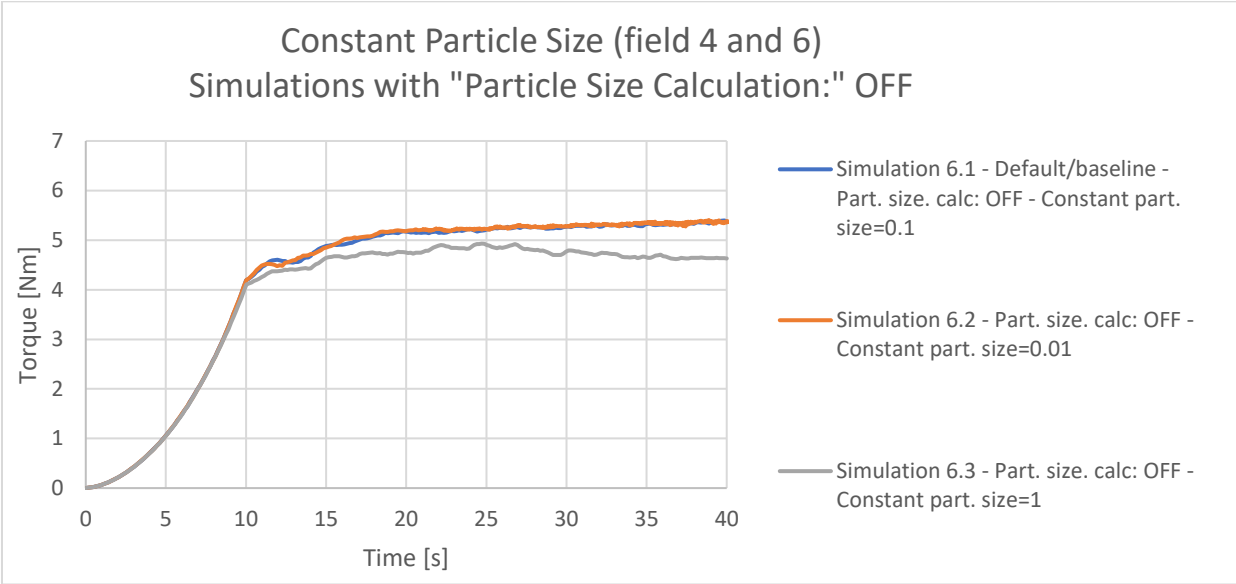


Figure 7.26: Constant particle size (field 4 and 6), DPS model turned OFF – Torque vs. Time.

Figure 7.27 illustrate the particle size distribution for simulation 1.1 (with default values, and DPS model turned “on”), and the particle size distribution for the simulations 6.1 - 6.3, where the DPS model is turned “off.” The graphs make it obvious that the DPS model is turned “off” for simulation 6.1, 6.2 and 6.3, since the particle size distribution shows a constant size for all positions in the wheel. The same figure illustrates that decreasing the “constant particle size,” from 0.1 mm to 0.01 mm, did not affect the mix. field viscosity distribution. However, increasing the “constant particle size,” from 0.1 mm to 1 mm, changed the viscosity distribution. These results explain the change in torque in figure 7.26.

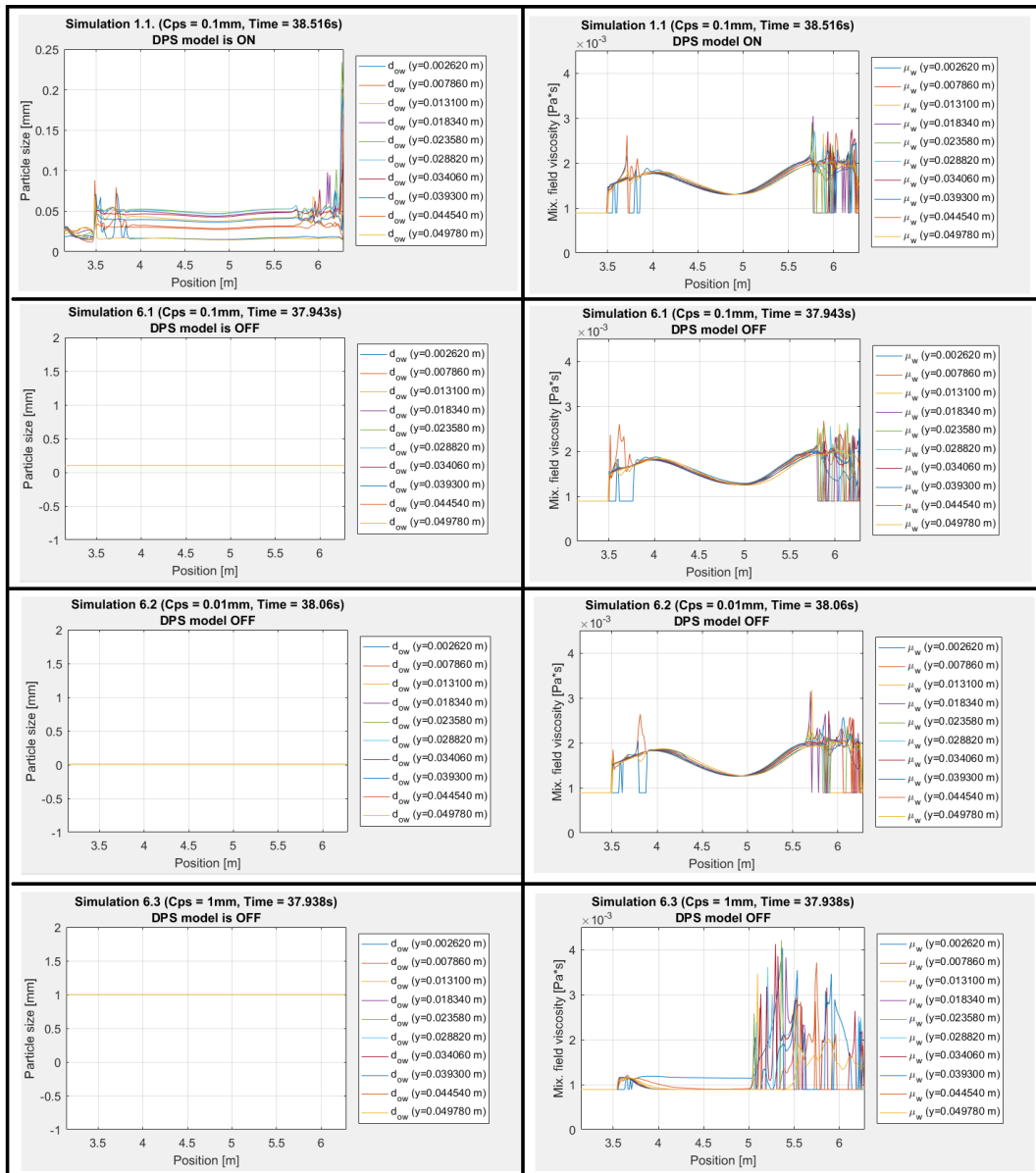


Figure 7.27: “Particle size vs. Position” & “Viscosity vs. Position,” DPS model OFF.

Explanation of the simulation results, for test 6

These observations DPS model make sense. When the DPS model is turned “off,” than the particle sizes will stay constant. Additionally, when the constant particle sizes are increased the viscosity will eventually be affected, and hence the output of torque will be affected as well.

7.5 Comparison of various water cuts

The purpose of test 7

Simulation 7.1 try to emphasize that the phase fractions of the fluid system plays a significant role in the viscosity of the system. This in turn should affect the evolution of torque on the system. Note that we simulate another experiment (different from the wheel flow experiment mentioned in subchapter 5.1, and figure 5.3) when we change the water cut.

Execution method and input parameters, for test 7

Table 7.9 presents the phase fractions of simulation 1.1 and simulation 7.1.

	Phase fractions
Simulation 1.1/Default value	[Gas=0.6], [Oil=0.1], [Water=0.3]
Simulation 7.1	[Gas=0.6], [Oil=0.3], [Water=0.1]

Table 7.9: Phase fractions for simulation 1.1 and simulation 7.1.

Presentation of the simulation results for test 7

Figure 7.26 illustrates the comparison of simulation 1.1 and simulation 7.1, and how changing the water cut affects the evolution of torque in the fluid system.

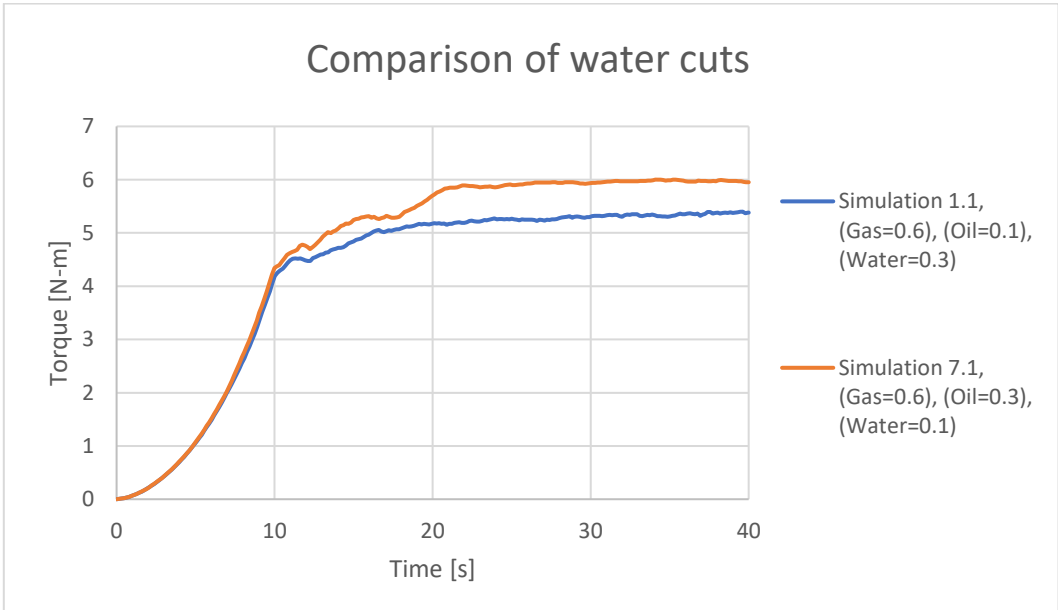


Figure 7.28: Comparison of water cuts – Torque vs. Time.

Figure 7.27 illustrates how the particle size distribution and the mix. field viscosity distribution changed when the water cut is changed.

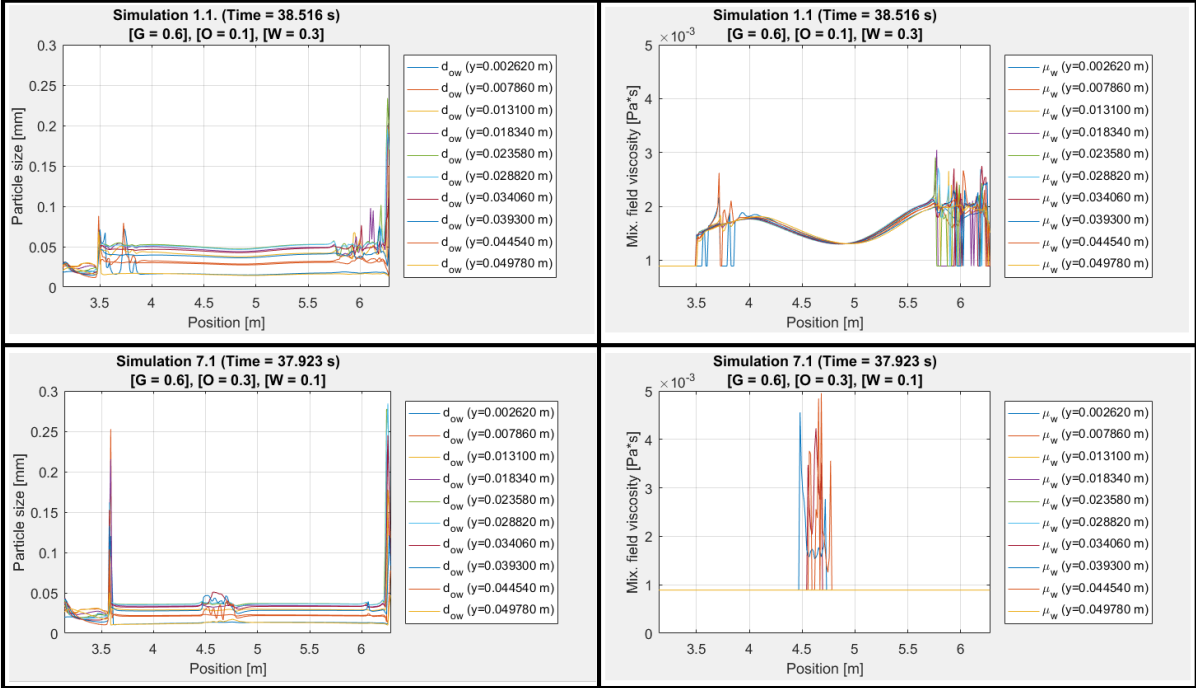


Figure 7.29: “Particle size vs. Position” & “Viscosity vs. Position,” comparing water cuts.

Explanation of the simulation results, for test 7

Test 7 successfully managed to prove that the simulation results (particle size distribution, viscosity distribution and torque) are affected by changing the water cut of the fluid system.

7.6 Tuning simulation cases with wheel velocity of 1 m/s

The purpose of test 8

The adjustment of the “particle size constants, C_1 and C_2 ,” turned out to be very effective in order to tune the simulation results, and both of them successfully managed to match the simulations with the wheel flow experiment (figure 5.3). By using figure 5.3 as a blueprint, representing the results from the wheel flow experiment at SINTEFs multiphase-flow laboratory on Tiller, simulation results were successfully tuned to converge around approximately the same output of torque (4.5 Nm), for a wheel velocity of 2 m/s, when the input value of C_1 was 0.75, and in a separate test, when the input value of C_2 was 0.25.

In the final tests, there was made an attempt to check if the same input parameters that successfully tuned the simulation cases with a wheel velocity of 2 m/s, would work when attempting to tune the simulation cases with a wheel velocity of 1 m/s. If these attempts succeeded, the input parameters for C_1 and C_2 could possibly be used as an approximate blueprint for future simulations (at least for simulations with the same PVT conditions and phase fractions).

Execution method and input parameters, for test 8

From figure 5.3, it is observed that the experiment with the wheel flow simulator gave an output of torque approximately around 1.7 Nm, when the wheel velocity was 1 m/s. Simulation 8.1, 8.2 and 8.3 was then conducted to investigate the outcome of the simulation with default input settings, and how the adjustment of C_1 and C_2 affected the simulation results.

	Wheel velocity [m/s]	C_1	C_2
Simulation 8.1/default values	1	Default	Default
Simulation 8.2	1	0.75	Default
Simulation 8.3	1	Default	0.25

Table 7.10: Final test, with wheel velocity 1 m/s.

Presentation of the simulation results for test 8

Figure 7.29 illustrates that the input parameters that successfully tuned the simulation results to match with the wheel flow experiment, when the wheel velocity was 2 m/s, failed in the attempt to do the same for simulations with a wheel velocity of 1 m/s.

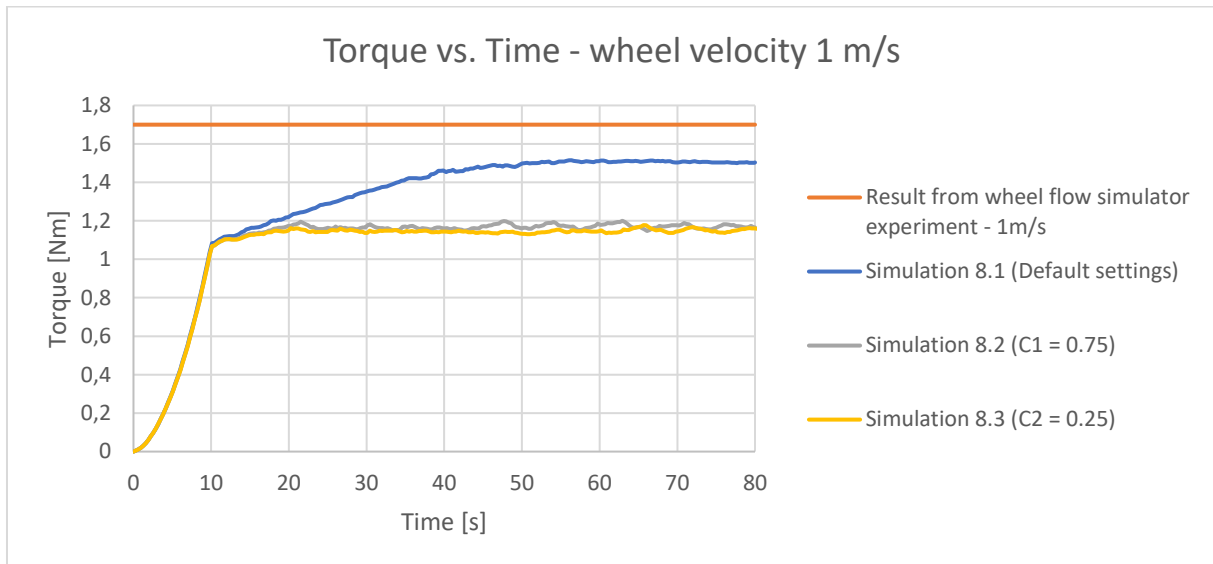


Figure 7.30: Final test – Torque vs. Time.

Explanation of the simulation results, for test 8

There might be many of reasons for why the input values for C_1 and C_2 , which successfully tuned the simulations with wheel velocity of 2 m/s, did not work for simulations with wheel velocity of 1 m/s. Note that as opposed to the simulations in with wheel velocity of 2 m/s, this time the default value had a lower output value of torque than the wheel flow experiment (figure 5.3). The input values of C_1 and C_2 tuned the simulations, but not in the direction towards the same output of torque as from the wheel flow experiment (figure 5.3).

8 Suggestions for future work

Suggestions for further testing:

1. Further testing should be done on all the input parameters, for various wheel velocities, PVT conditions and water cuts. From these tests one may try to look for patterns in the values for the input parameters that successfully manage to tune the simulations.
2. The input parameters only managed to decrease the output of torque while tuning the simulations in this thesis. Further testing should also look for possibilities to tune the simulations by increasing the output of torque.
3. In this thesis, the simulations were only tuned by one input parameter at the time. Further testing could try to adjust several input parameters at the same time, too investigate how this affects the simulations. Multivariable analysis could be included in this particular test.
4. In further work, there should also be more focus on analysing the various graphs from the various simulation cases. If possible, the simulations should be tuned to also match with the measured particle sizes from the wheel flow experiments.

The following results from these tests can be used to obtain an overview or blueprint for which values that should be implemented for each input parameter in future simulations, to create the simulation results as identical as possible to the experimental results with the wheel flow simulator in the laboratory.

By developing a blueprint for the input parameters, which assures that the simulations in LedaFlow Q3D are identical with the results from the wheel flow experiments, this will make the simulation program very useful. Accurate knowledge of the behaviour of oil-water (liquid-liquid) flow in a pipeline is crucial to optimize production, transportation and processing facilities. If LedaFlow is correctly tuned, it can be a useful tool to investigate the evolution of emulsions and viscosity for various water cuts and PVT conditions, and the following output of torque can be linked in conjunction with pressure loss in the pipeline.

9 Summary and conclusion

The simulation work in LedaFlow Q3D resulted in some valuable information about how the program works. First of all, there was acquired some useful information about how to make the simulations more stable. The improvements were in terms of the input values to the simulations, implementing a viscosity model for oil-water emulsions, and to the code itself in the form of bug fixing and added functionality and physics. One of the most effective measures, regarding making the simulations more stable, was to turn off the DPS modelling for the dispersed fields of no interest to the current system, and to reduce the input parameters to 0.1 mm for all the phases in the option flag “Particle size: Constant size.” The default values in the option flag “Particle size: Constant size” was not even close to the normal droplet size distribution for emulsions (figure 2.10), and the reduction of this input parameter should probably be even larger.

The testing of the various input parameters revealed that some had a larger impact on the simulation results than others. For some reason, “the coalescence time constant ($C_{Coalescence}$)” had no impact on the simulation results at all, and “the break up time constant ($C_{breakup}$)” had only a minor effect. In other fluid systems, with different water cuts, it might be possible that “the coalescence time constant ($C_{Coalescence}$)” can be used as a tuning-tool as well, but this need further testing. On the other hand, the adjustment of the “particle size constants, C_1 and C_2 ,” turned out to be very effective in order to tune the simulation results. It might be possible to use the “particle size constants, C_1 and C_2 ,” as the “coarse-tuning tool,” and then optimize the work with “the break up time constant ($C_{breakup}$)” as the “fine-tuning tool.”

Due to the stability problems regarding the simulations, the schedule for the planned simulation work was delayed, and as a consequence, the number of simulations performed with appropriate settings were fewer than if a commercial code was used. However, part of the objective was to determine to what degree the current Leda Q3D could be used to simulate the wheel and match torque values from experiments, and in this case the objective has been met successfully.

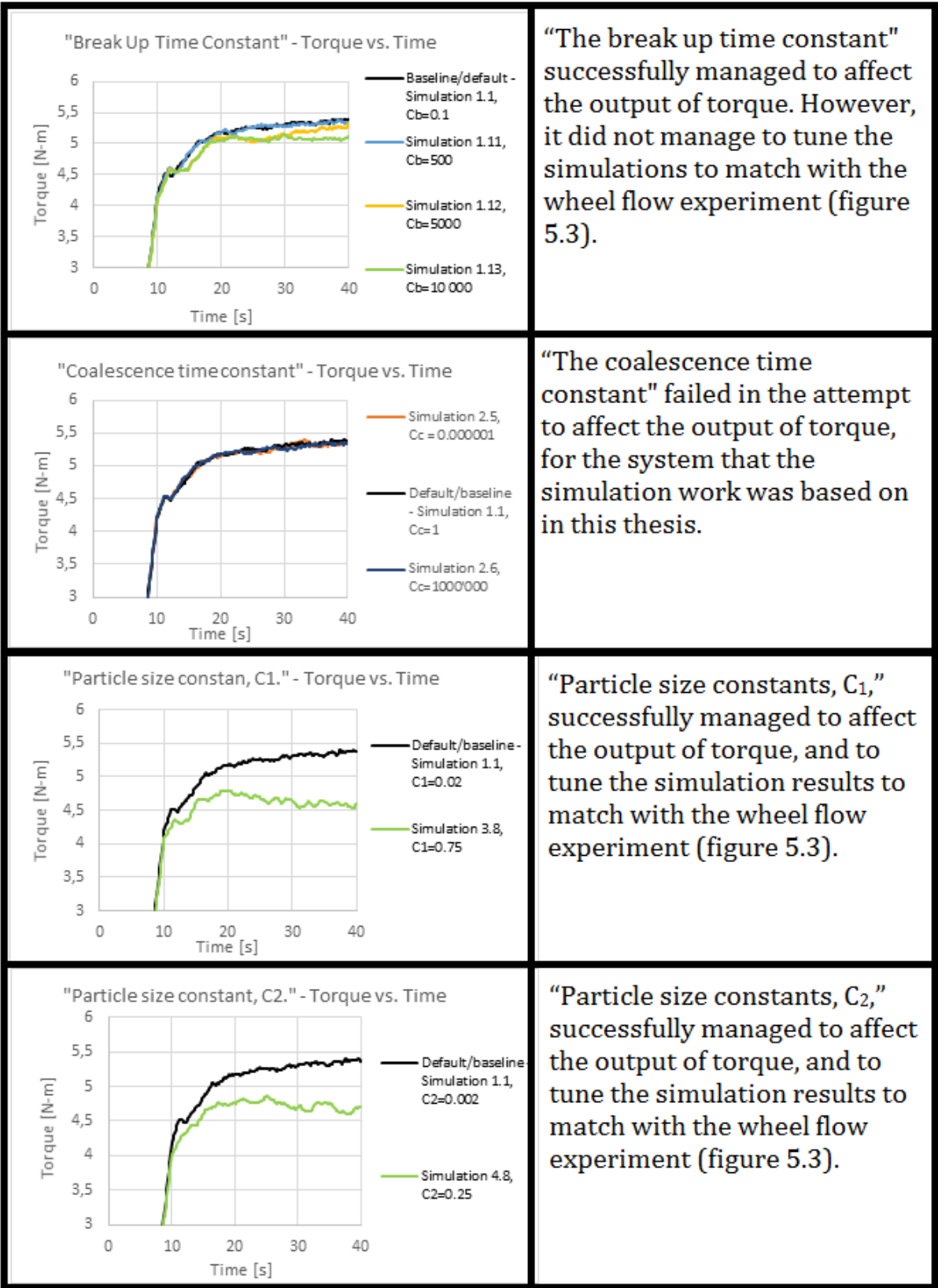


Figure 9.1: Summary of test 1 – 4.

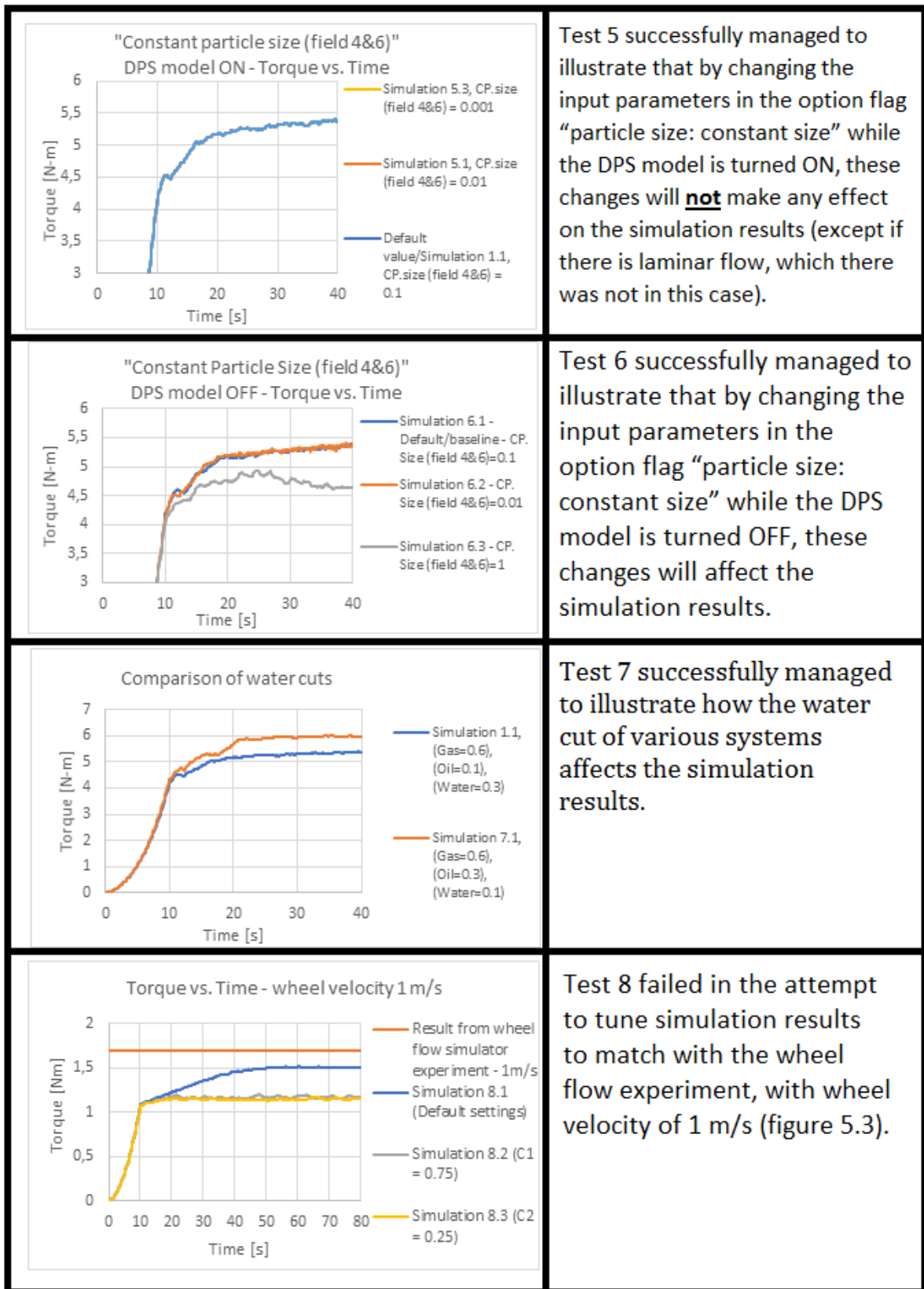


Figure 9.2: Summary of test 5 – 8.

10 Bibliography

1. X.X. Xu, "Study on oil – water two-phase flow in horizontal pipelines," *Journal of Petroleum Science and Engineering*, vol. 59, p. 43 – 58, Mar. 2007.
2. A.S.I. Ismail et al., "Review of oil-water through pipes," *Flow Measurement and Instrumentation*, vol. 45, p. 357 – 374, July 2015.
3. X Amplified Free online Education Resource. *Colloidal dispersions*. Available: <http://www.chemistrylearning.com/colloidal-dispersions/>
Accessed: 26.01.2017
4. L.L. Schramm. "Petroleum Emulsions," *Emulsions*. vol. 231, L.L. Schramm, red. Washington DC, American Chemical Society, 1992, p. 1 - 49.
5. PetroWiki. *Oil emulsions*. Available: [http://petrowiki.org/Oil emulsions](http://petrowiki.org/Oil_emulsions)
Accessed: 30.03.2017
6. J.R. Becker. *CRUDE OIL – Waxes, Emulsions, and Asphaltenes*. Tulsa, Oklahoma: PennWell Books, 1997.
7. S. Kokal, *Crude oil emulsions: Everything you wanted to know but were afraid to ask*. Available: <https://www.onepetro-org.ezproxy.uis.no/download/general/SPE-120500-DL?id=general%2FSPE-120500-DL>.
Accessed: 02.02.2017
8. Wikipedia. *Surfactant*. Available: <https://en.wikipedia.org/wiki/Surfactant>
Accessed: 02.04.2017
9. C. Gupta, M.J. Sverdløve, and N.R. Washburn, "Molecular architecture requirements for polymer – grafted lignin superplasticizers." *Royal Society of Chemistry*, vol. 11, p. 2691 – 2699, 2015. [Online]. Available: <http://pubs.rsc.org/en/content/articlehtml/2015/sm/c4sm02675f>
Accessed: 12.05.2017
10. B. Wolf et al. *Shear thickening of an emulsion stabilized with hydrophilic silica particles*. Available: https://www.researchgate.net/profile/Bettina_Wolf/publication/238994851_Shear_thickening_of_an_emulsion_stabilized_with_hydrophilic_silica_particles/links/00463529861c293335000000/Shear-thickening-of-an-emulsion-stabilized-with-hydrophilic-silica-particles.pdf
Accessed: 14.06.2017
11. N Willenbacher, K. Georgieva, *Rheology of disperse systems*. Available: https://www.mvm.kit.edu/download/Rheology_of_disperse_systems_Buch_Wiley_2013.pdf
Accessed: 14.06.2017
12. PetroWiki. *Stability of oil emulsions*. Available: [http://petrowiki.org/Stability of oil emulsions](http://petrowiki.org/Stability_of_oil_emulsions)
Accessed: 04.04.2017
13. T.F. Tadros. *Emulsion Formation, Stability, and Rheology*. Available: https://application.wiley-vch.de/books/sample/3527319913_c01.pdf
Accessed: 29.03.2017

14. A. Ashrafiyan et al., "Multi-dimensional modeling of stratified wavy three-phase flows," Rio Pipeline Conference & Exposition 2011, Rio de Janeiro, Brazil, Sept. 20-22, 2011.
15. Thermopedia. *Gas-Liquid Flow*. Available: <http://www.thermopedia.com/content/2/>
Accessed: 25.04.2017
16. W.L. Loh and V.K. Premanadhan, "Experimental investigation of viscous oil – water flows in pipeline," *Journal of Petroleum Science and Engineering*, vol. 147, p. 87 – 97, May 2016.
17. J.F. Lea and C.L. Dunham, Artificial Lift Advances Address Challenges, Trends In Gas Well Deliquification, *The Americal Oil&Gas Reporter*, June 2009. [Online].
Available: <http://www.aogr.com/magazine/cover-story/artificial-lift-advances-address-challenges-trends-in-gas-well-deliqumicat>
Accessed: 26.06.2017.
18. Schlumberger *Oilfield Glossary, Slug flow*. Available:
http://www.glossary.oilfield.slb.com/Terms/s/slug_flow.aspx
Accessed: 26.05.2017.
19. Nuclear-power.net. *Two Phase Fluid Flow*. Available: <http://www.nuclear-power.net/nuclear-engineering/fluid-dynamics/two-phase-fluid-flow/>
Accessed: 26.05.2017.
20. A.S.I. Ismail et al., "Experimental investigation of oil – water two – phase flow in horizontal pipes: Pressure losses, liquid holdup and flow patterns," *Journal of Petroleum Science and Engineering*, vol. 127, p. 409 – 420, Feb. 2015.
21. N. Brauner, "Modelling and Control of Two Phase Phenomena: Liquid – Liquid Two Phase Flow Systems," CISM Center, Udine, Italy (2002), p. 1 – 59.
22. C. Hirsch. *Numerical Computation of Internal and External Flows*. Second edition, John Wiley & Sons, 2007.
23. Wikipedia. *Computational fluid dynamics*.
Available: https://en.wikipedia.org/wiki/Computational_fluid_dynamics
Accessed: 26.04.2017
24. Wikipedia. *Navier – Stokes equations*.
Available: https://en.wikipedia.org/wiki/Navier%E2%80%93Stokes_equations
Accessed: 26.04.2017
25. Wikipedia. *Euler equations (fluid dynamics)*.
Available: [https://en.wikipedia.org/wiki/Euler_equations_\(fluid_dynamics\)](https://en.wikipedia.org/wiki/Euler_equations_(fluid_dynamics))
Accessed: 26.04.2017
26. Wikipedia. *Discretization*. Available: <https://en.wikipedia.org/wiki/Discretization>
Accessed: 26.04.2017
27. Wikipedia. *Preprocessor (CAE)*. Available: [https://en.wikipedia.org/wiki/Preprocessor_\(CAE\)](https://en.wikipedia.org/wiki/Preprocessor_(CAE))
Accessed: 26.04.2017
28. LedaFlow. *User Manual LedaFlow v.2.43*. Available: <https://kongsberg.com/en/kongsberg-digital/oil%20and%20gas/flow%20assurance/ledaflow%20software%20-page/>

29. A. Vebenstad and R. Larsen, "Technical specifications SINTEF Rotating Wheel Flow Simulators," *SINTEF Petroleum Research*, Trondheim, Norway, jun. 2005.
30. With courtesy of SINTEF Petroleum AS.
31. Chemeurope.com. *Kolmogorov microscales*. Available:
http://www.chemeurope.com/en/encyclopedia/Kolmogorov_microscales.html
Accessed: 30.05.2017
32. Wikipedia. *Courant-Friedrichs-Lewy condition*. Available:
https://en.wikipedia.org/wiki/Courant%E2%80%93Friedrichs%E2%80%93Lewy_condition
Accessed: 09.06.2017

11 Appendix

A. Set up guide

This section of the appendix will explain the necessary steps to follow when creating a case, edit the initial case settings, update input parameters in “Closures” menu, choosing which formulas to use in “Numerical Parameters Q3D” menu, initializing the case, and finally running the case and plotting the results.

A.1 Creating the case

Go to the **File** menu (upper left corner, figure A.1), and click on **New case**.

Choose **Specific cases**, and **Q3D Wheel case**.

Click **Set up** (figure A.1).

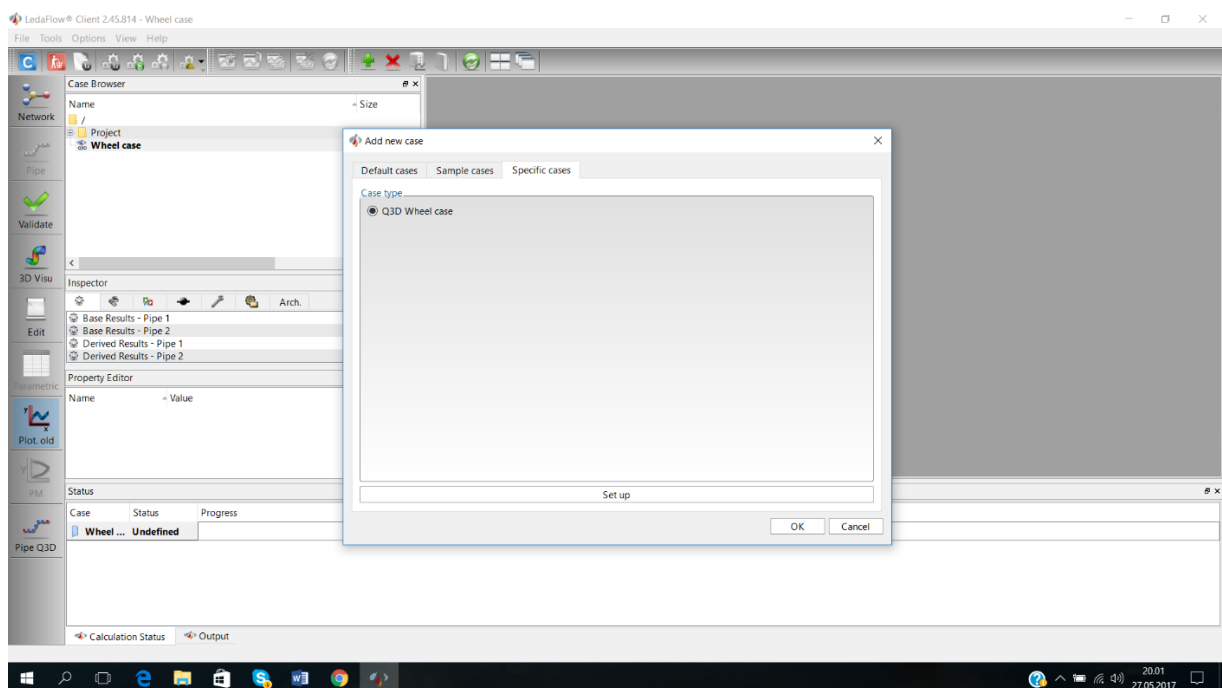
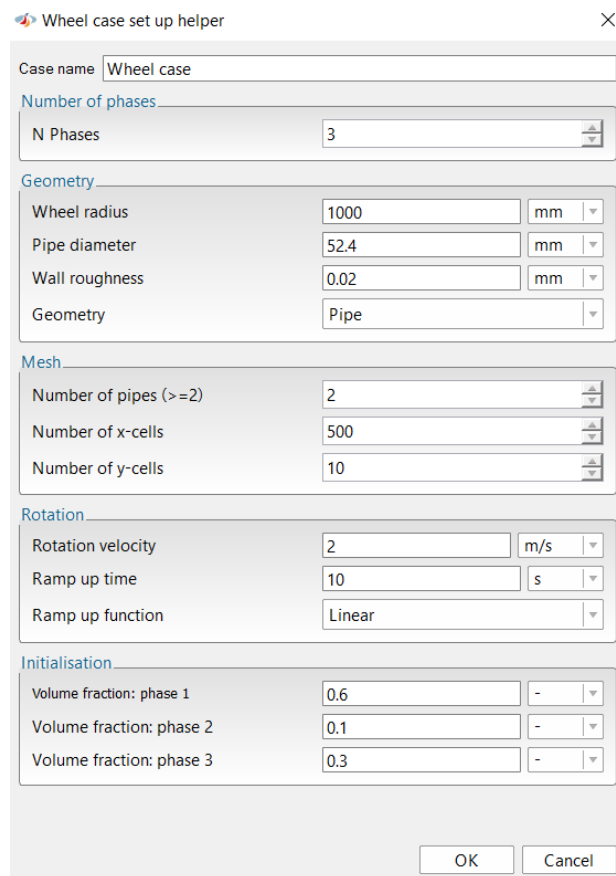


Figure A.1: Overview of overall work window, and “add new case” option menu.

In the **Wheel case set up helper**, fill in the necessary information:

- Case name.
- Number of phases in the fluid system.
- Geometry of the pipe regarding wheel radius, pipe diameter, wall roughness, geometry.
- The simulation mesh size regarding number of pipes, number of x-cells, and number of y-cells.
- Rotation velocity, ramp up time, ramp up function for the wheel.
- The volume fraction of each phase (phase 1 represent gas, phase 2 represent oil, and phase 3 represent water).

Figure A.2 illustrates the **Wheel case set up helper**, with the standard input data used in the simulation work in this thesis.



The screenshot shows the 'Wheel case set up helper' dialog box with the following input fields:

Section	Parameter	Value	Unit
Case name	Case name	Wheel case	
Number of phases	N Phases	3	
	Geometry		
Geometry	Wheel radius	1000	mm
	Pipe diameter	52.4	mm
	Wall roughness	0.02	mm
	Geometry	Pipe	
Mesh	Number of pipes (>=2)	2	
	Number of x-cells	500	
	Number of y-cells	10	
Rotation	Rotation velocity	2	m/s
	Ramp up time	10	s
	Ramp up function	Linear	
Initialisation	Volume fraction: phase 1	0.6	-
	Volume fraction: phase 2	0.1	-
	Volume fraction: phase 3	0.3	-

Buttons: OK, Cancel

Figure A.2: Wheel case set up helper.

When the case is created, it will be located in the **Case browser** (figure A.3).

You can easily create new folders to organise your work by “right click” on the project folder, and click **New folder**.

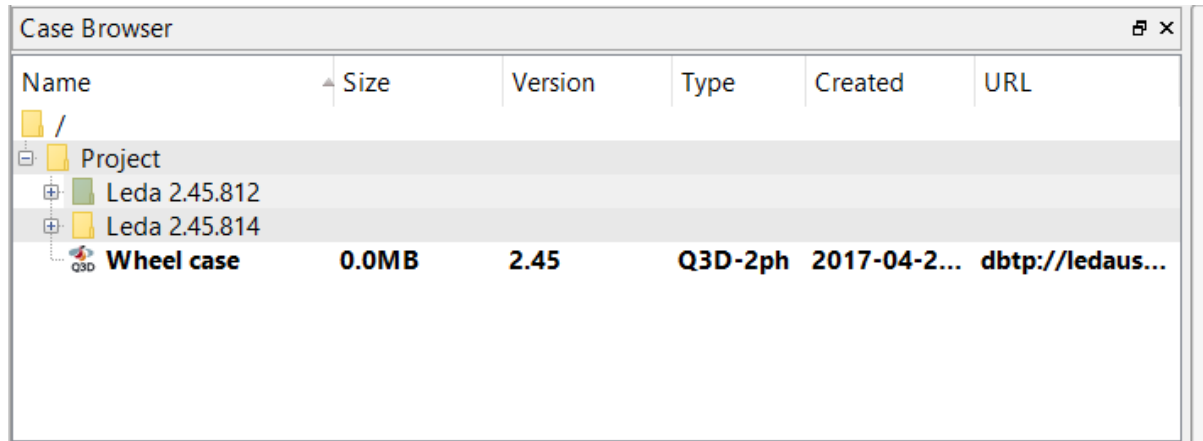


Figure A.3: Case browser.

A.2 Edit case settings

When the case is created, you can start edit the case settings. Click on the **Case settings** button in the upper left corner of the screen (figure A.1) →



In the case settings menu (upper left, figure A.4), you can edit the necessary input parameters:

- **PVT** settings defines the properties of the fluids in the fluid system. Figure A.4 (upper, right) illustrates the PVT settings menu. To enter this menu, click on PVT in the case settings menu, then click on the white sheet on the top of the page. Table A.1 illustrates the standard PVT settings for the simulation work in this thesis.

PVT object	
Gas density [kg/m ³]	1,1347
Gas viscosity [Pa-s]	1,7794*10 ⁻⁵
Gas compressibility [kg/m ³ /bar]	1,1303
Oil density [kg/m ³]	790
Oil viscosity [Pa-s]	0,0018
Oil compressibility [kg/m ³ /bar]	0
Water density [kg/m ³]	997
Water viscosity [Pa-s]	0,00089
Water compressibility [kg/m ³ /bar]	0
Pressure, Pref [bar]	1
Temperature, Tref [C°]	25
Interfacial tension between O&W [N/m]	0,025
Interfacial tension between G/W [N/m]	0,072
Interfacial tension between G/O [N/m]	0,0207

Table A.1: PVT settings.

- In the **Option** menu (lower left, figure A.4) you can choose whether or not to use the dynamic particle size (DPS) model. If you choose not to, then the particle size for the dispersion droplets will stay constant. If the particle size calculation is turned “on”, then the dispersion droplets will change in size during the simulation. The equation used in the DPS model (equation 5.1) is explained in section 5.3. This equation is used to calculate the evolution of the particle sizes, and is a function of several input parameters. The simulation work in this thesis was based on analysing these input parameters, and examine their influence on the simulation results.
- In **Numerical** option menu (lower right, figure A.4), you can edit e.g. time to advance solution, the Courant-Friedrichs-Lewy condition (the CFL-number, also referred to as the Courant number), and solver settings optimized for speed or robustness.

Table A.2 illustrates the standard numerical input settings used in this thesis simulation work.

Numerical	
Time to advance to solution [s]	40
CFL	0,8
Solver settings optimized for:	Robustness
Number of processors:	1

Table A.2: Numerical input settings

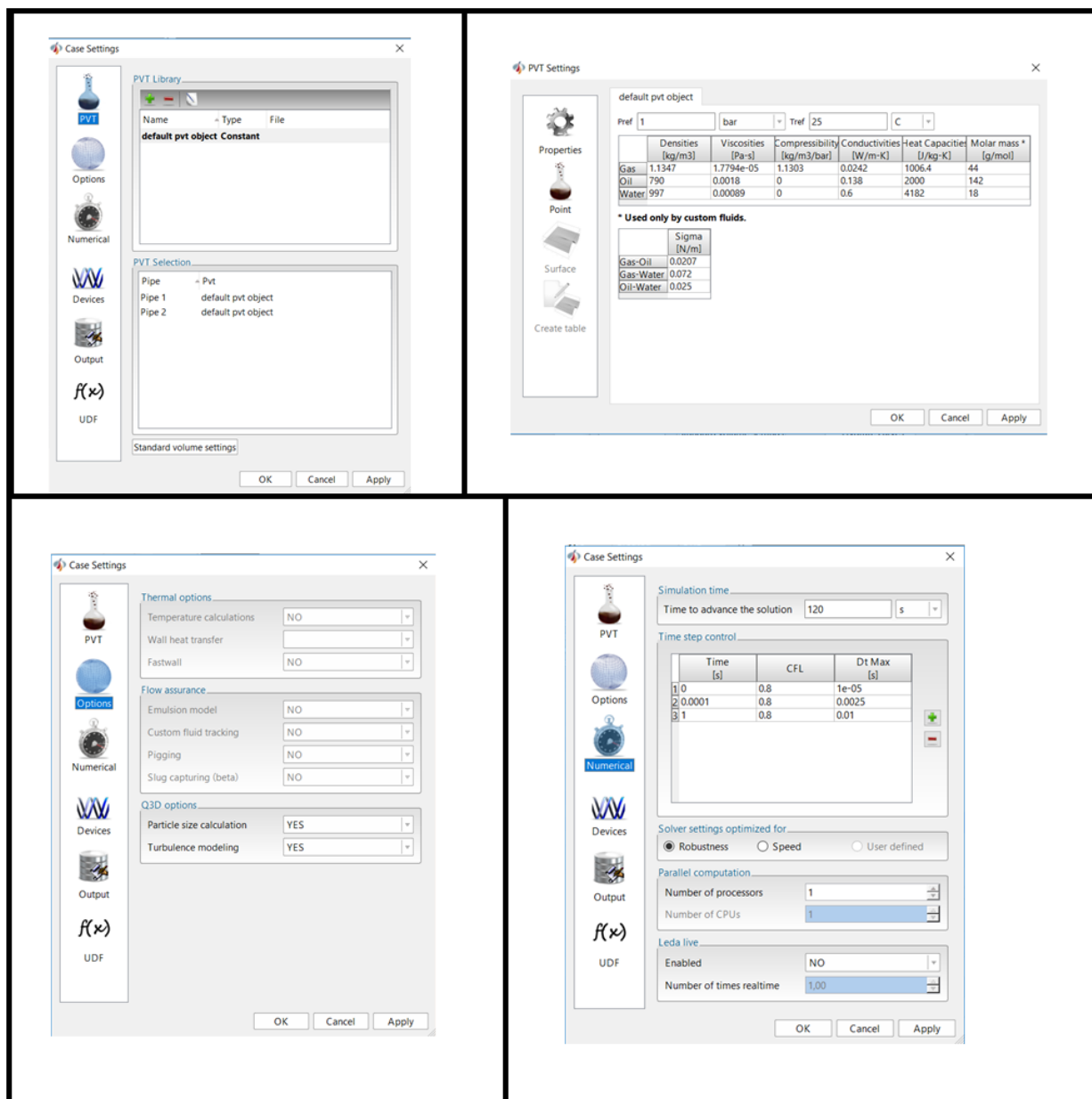


Figure A.4: Case settings menu.

When the correct input parameters are entered in the case settings menu, it is time to edit the **Inspector** window (figure A.5).

In the inspector window, click on **Numerical Parameters Q3D**. In the **Property editor** window below (figure A.5), you can edit which equations you are using for the simulation work. The standard settings are shown in figure A.5. Interpol_ACUTER and Interpol_US1 are intern names in LedaFlow for a higher order convection scheme and first-order upwind (FOU) scheme respectively.

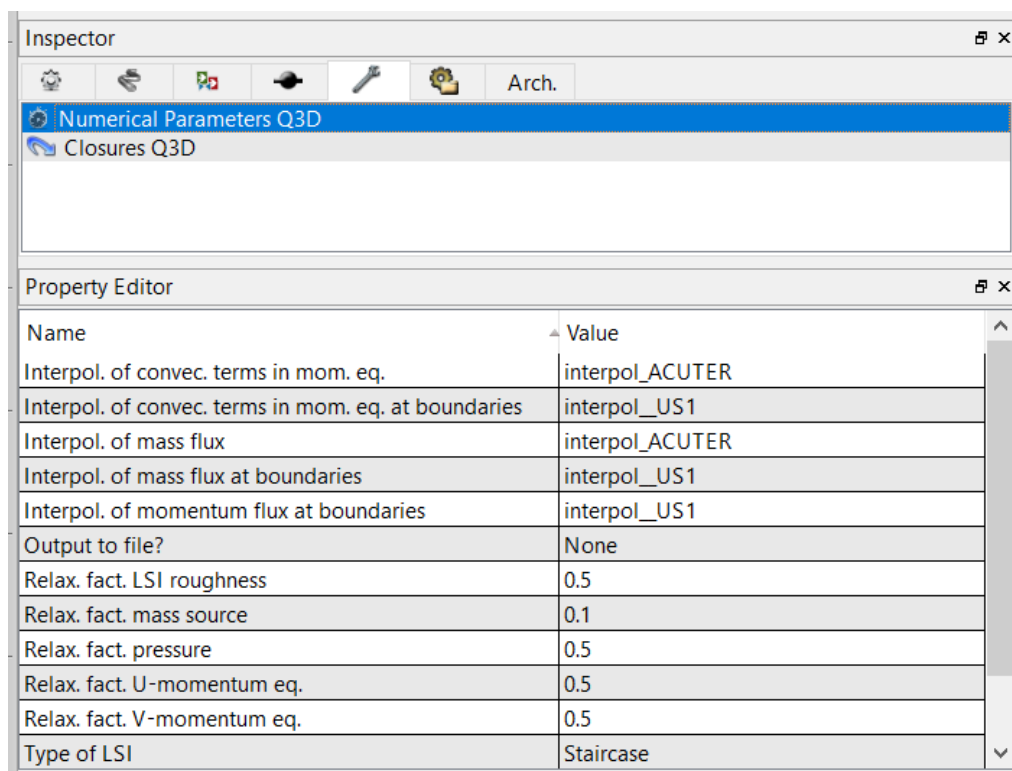


Figure A.5: Numerical Parameter Q3D.

Now click on **Closures Q3D** in the **Inspector** window. In the **Property Editor** window (figure A.6), you can edit several emulsion properties, e.g. turning “on” or “off” DPS model for dispersion/emulsion droplets for individual fields, edit particle break up time constant, edit particle coalescence time constant, turning “on” or “off” emulsion viscosity calculations for individual layers, define the constant particle size for dispersions in phases were the particle size calculation is turned “off” etc. These settings have been explained in chapter 5.3.

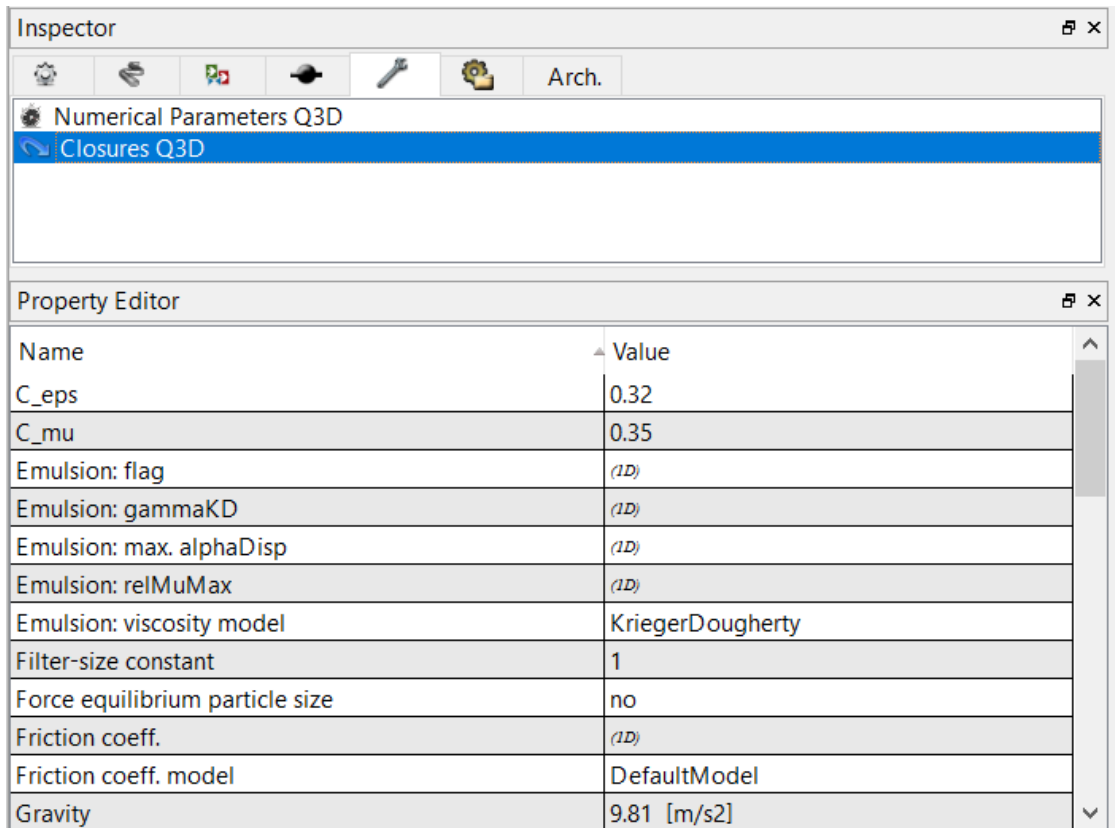


Figure A.6: Closures Q3D

A.3 Initializing the case

When finished editing the case settings, you can start initializing the case.

Press the **Initialize** button in the upper left corner of the screen (figure A.1) →



In the **Initialization** menu (figure A.7), you must update phase fractions of the initial fluid phases, temperature, and pressure. Then, click on **Patches** (figure A.8), and define the coordinates for each fluid phase in the flow wheel simulator. Table A.3 illustrates the input parameters for this section, with phase fractions, test temperature, test pressure, and coordinates for the fluid phases at rest before the rotation of the wheel (figure 5.5).

Initialize	
Friction pressure grad., bar/m	0
Temperature, Kelvin	298,15
Pressure, bar	1
Cont. Gas	0,6
Cont. Oil	0,1
Cont. Water	0,3
Patches - initialization	
Gas (input fraction: 0,6)	Start length: 5,97, stop length: 3,46
Oil left side (input fraction: 0,1)	Start length: 5,65, stop length: 5,97
Oil right side (input fraction: 0,1)	Start length: 3,46, stop length: 3,77
Water (input fraction 0,3)	Start length: 3,77, stop length: 5,65

Table A.3: Input parameters to initialize the case.

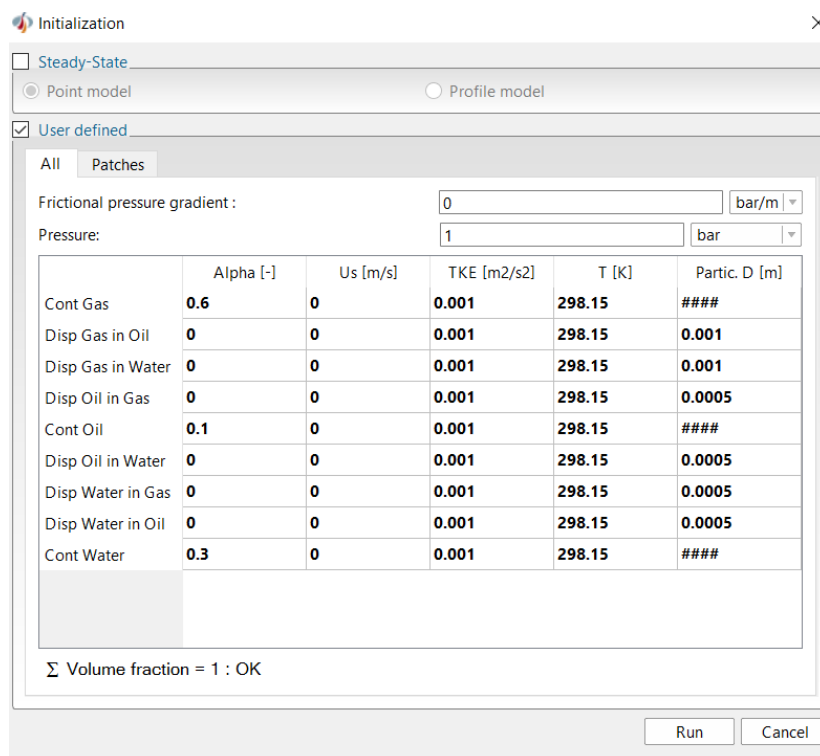


Figure A.7: Initialization menu.

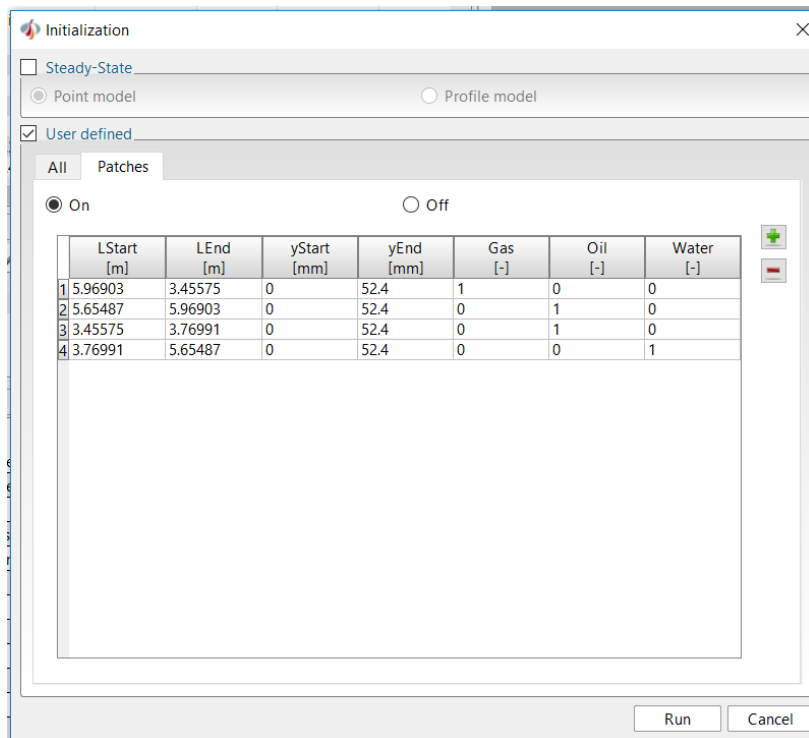


Figure A.8: Patches menu

After specifying the initial conditions, click **Run**, and initialize the case. In the **Status** window, you will see the case initializing (figure A.9).

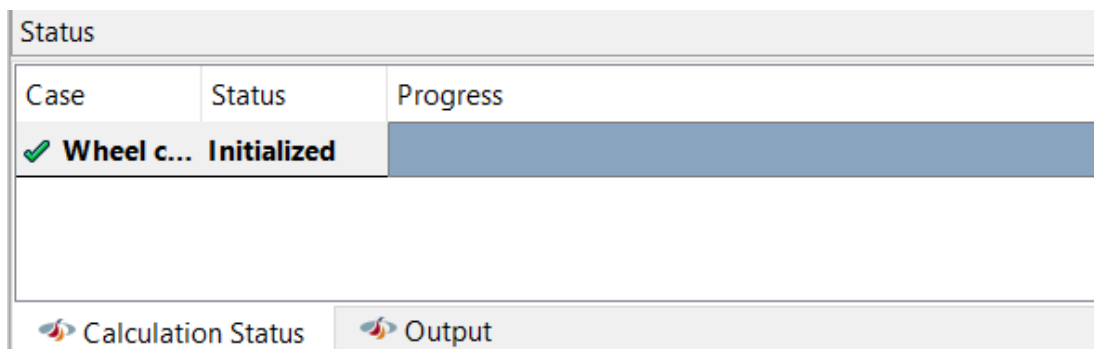


Figure A.9: Initializing the case.

B. Run and plot guide

B.1 Running the case

When finished the initialization of the case, press **Run** → in the upper left corner of the screen (figure A.1).



In the status window, you will now be able to see the running progress of the simulation case (figure B.1). If you press **Output**, in the status window, you can be able to see if there are any warnings or problems occurring during the simulation run of the case (figure B.2).

Status		
Case	Status	Progress
▶ Simula...	Running	<div style="width: 50%;"></div>

▶ Calculation Status ▶ Output

Figure B.1: Status window and simulation running progress.

Status	
LEDAFLOW v.2.47 (2017-04-26 20:45) 0207: Hydrodynamics did not converge (negative volume fractions (min= -0.1084E-02) at index (2 6 232)). Restarting time step (attempt 1). (t= 6.1 sec.; Pipe 2) 0220: Mass balance did not converge. Restarting time step (attempt 1). 0220: Mass balance did not converge. Restarting time step (attempt 1).	

▶ Calculation Status ▶ Output

Figure B.2: Output information of warnings and errors during simulation run.

B.2 Plotting and visualizing the results

When the simulation is finished, you can visualize the results. The flow wheel simulator, mixing the fluid phases (figure B.3), can be visualized by pressing **3D Visu** in the left menu (figure A.1) →

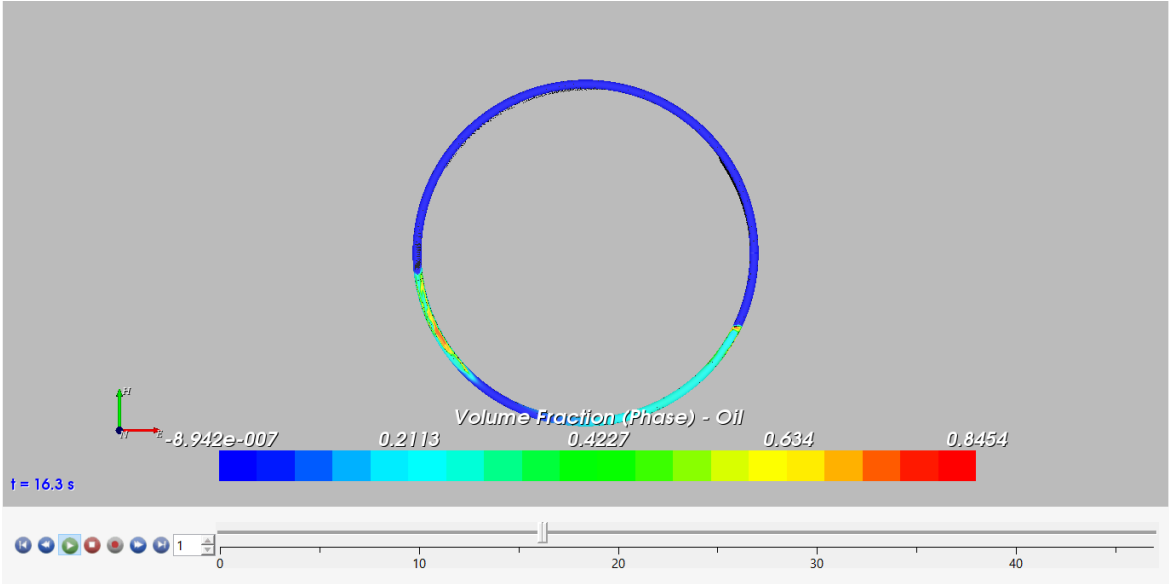


Figure B.3: 3D visualization of the mixing of the fluid phases.

In the upper menu, it is possible to choose what to visualize and which fluid phase to focus on (figure B.4).

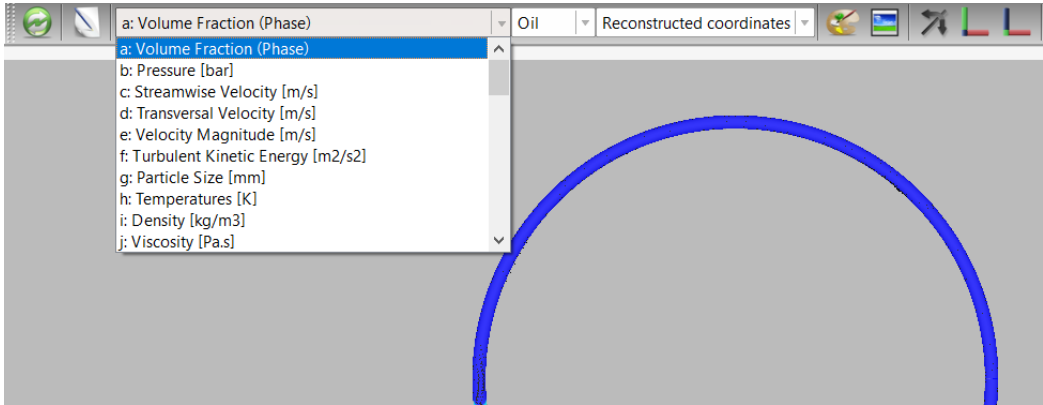


Figure B.4: Visualization options, and selection of which fluid phase to focus on.

By pressing **Plot. Old**



in the left menu (figure A.1), and the green cross



in the upper menu (figure A.1), the **Graph setup** will appear in the work window (figure B.5). In the Graph setup, you can plot several kinds of graphical results from the simulation cases. Matlab codes written by Ivar Eskerud Smith at SINTEF, made it easy to plot graphs illustrating torque, pressure, particle size, mix. field viscosity, mix. field phase fraction and intrinsic phase fraction. By copy and paste the ID number of every simulation case into Matlab, the graphs were quickly produced. This procedure was timesaving, because it eliminated the need to convert the simulation results into excel before using them in the report.

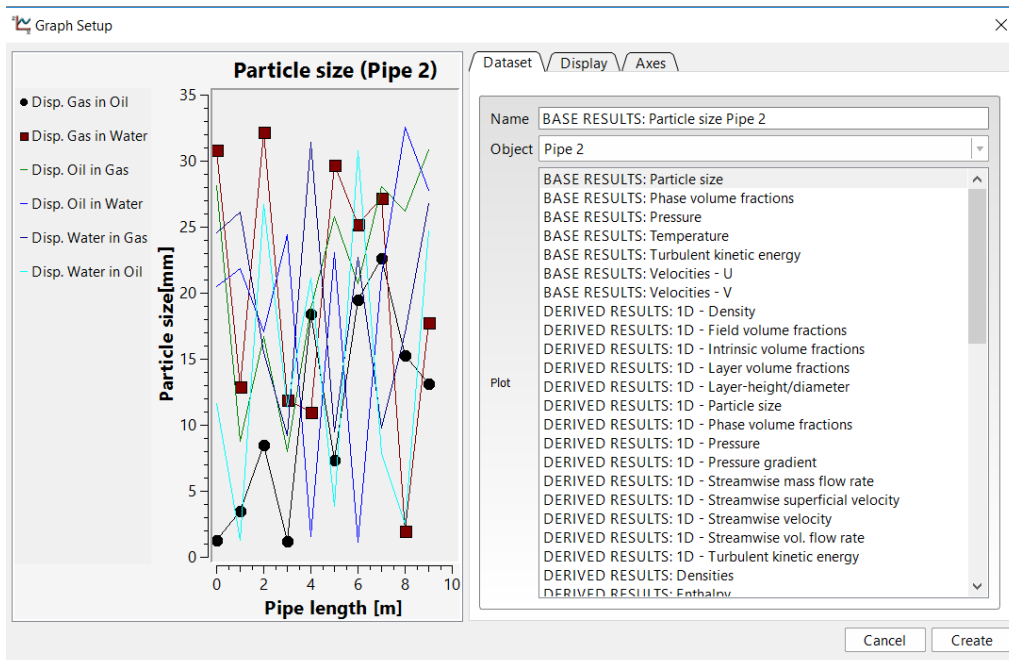


Figure B.5: Graph Setup